

EFFECT OF Cu MODIFIED TiO<sub>2</sub> CATALYSTS PREPARED BY INCIPIENT WETNESS  
IMPREGNATION AND SPUTTERING FOR PHOTOCATALYTIC CO<sub>2</sub> REDUCTION  
IN AQUEOUS SOLUTION



A Thesis Submitted in Partial Fulfillment of the Requirements  
for the Degree of Master of Engineering in Chemical Engineering

Department of Chemical Engineering

Faculty of Engineering

Chulalongkorn University

Academic Year 2018

Copyright of Chulalongkorn University

ผลของตัวเร่งปฏิกิริยาไทเทเนียมที่ดัดแปลงด้วยทองแดงที่เตรียมโดยการเคลือบฝังเปียกแบบพอดี้และ  
การสปีดเตอริงสำหรับปฏิกิริยารีดักชันของคาร์บอนไดออกไซด์ในสารละลายน้ำที่เร่งปฏิกิริยาด้วยแสง



วิทยานิพนธ์นี้เป็นส่วนหนึ่งของการศึกษาตามหลักสูตรปริญญาวิศวกรรมศาสตรมหาบัณฑิต

สาขาวิชาวิศวกรรมเคมี ภาควิชาวิศวกรรมเคมี

คณะวิศวกรรมศาสตร์ จุฬาลงกรณ์มหาวิทยาลัย

ปีการศึกษา 2561

ลิขสิทธิ์ของจุฬาลงกรณ์มหาวิทยาลัย

Thesis Title                      EFFECT OF Cu MODIFIED  
    TiO<sub>2</sub> CATALYSTS PREPARED BY INCIPIENT WETNESS  
    IMPREGNATION AND SPUTTERING FOR PHOTOCATALYTIC  
    CO<sub>2</sub> REDUCTION IN AQUEOUS SOLUTION

By    Miss Nantiya Jantarasorn

Field of Study                      Chemical Engineering

Thesis Advisor                      Professor Piyasan Praserthdam, Ph.D.

---

Accepted by the Faculty of Engineering, Chulalongkorn University in Partial  
Fulfillment of the Requirement for the Master of Engineering

..... Dean of the Faculty of Engineering  
(Professor SUPOT TEACHAVORASINSKUN, Ph.D.)

THESIS COMMITTEE

..... Chairman  
(Associate Professor Anongnat Somwangthanoj, Ph.D.)

..... Thesis Advisor  
(Professor Piyasan Praserthdam, Ph.D.)

..... Examiner  
(Assistant Professor Palang Bumroongsakulsawat, Ph.D.)

..... External Examiner  
(Assistant Professor Okorn Mekasuwandumrong, D.Eng.)

นันทิยา จันทรศร : ผลของตัวเร่งปฏิกิริยาไทเทเนียมที่ดัดแปลงด้วยทองแดงที่เตรียมโดย  
 การเคลือบฝังเปียกแบบพอดีและการสputtering สำหรับปฏิกิริยารีดักชันของ  
 คาร์บอนไดออกไซด์ในสารละลายน้ำที่เร่งปฏิกิริยาด้วยแสง. ( EFFECT OF Cu  
 MODIFIED TiO<sub>2</sub> CATALYSTS PREPARED BY INCIPIENT WETNESS  
 IMPREGNATION AND SPUTTERING FOR PHOTOCATALYTIC CO<sub>2</sub> REDUCTION  
 IN AQUEOUS SOLUTION ) อ.ที่ปรึกษาหลัก : ศ. ดร.ปิยะสาร ประเสริฐธรรม

ในงานวิจัยนี้ศึกษาปฏิกิริยารีดักชันของคาร์บอนไดออกไซด์ในสารละลายน้ำที่เร่ง  
 ปฏิกิริยาด้วยแสงและดำเนินการในถังปฏิกรณ์ชนิดถังกวน โดยใช้ตัวเร่งปฏิกิริยาทองแดงบนตัว  
 รองรับไทเทเนียมเตรียมโดยวิธีเคลือบฝังเปียกแบบพอดีและการสputtering ผลกระทบจากการเติม  
 ทองแดงลงบนตัวรองรับไทเทเนียมจะเพิ่มประสิทธิภาพในการเกิดปฏิกิริยารีดักชันของ  
 คาร์บอนไดออกไซด์ในสารละลายน้ำภายใต้แสงยูวีโดยการเปลี่ยนช่องว่างระหว่างแถบพลังงานที่อยู่  
 ระหว่างแถบวาเลนซ์กับแถบนำไฟฟ้าให้แคบลง อีกทั้งช่วยในการเลือกเกิดสารประกอบ  
 ไฮโดรคาร์บอนซึ่งก็คือมีเทน เมื่อเปรียบเทียบผลของวิธีการเตรียมพบว่าตัวเร่งปฏิกิริยาที่สังเคราะห์  
 ด้วยวิธีเคลือบฝังเปียกแบบพอดีและการสputtering มีการเลือกเกิดของมีเทนเหมือนกัน ตัวเร่ง  
 ปฏิกิริยาที่สังเคราะห์ด้วยวิธีการสputtering มีแนวโน้มการเพิ่มมากขึ้นของการเกิดมีเทนเมื่อเพิ่ม  
 ปริมาณทองแดงบนตัวรองรับไทเทเนียม ในขณะที่ตัวเร่งปฏิกิริยาที่สังเคราะห์ด้วยวิธีเคลือบฝังเปียก  
 แบบพอดีมีแนวโน้มการลดลงของการเกิดมีเทนเมื่อเพิ่มปริมาณทองแดง สรุปผลการสังเคราะห์ด้วย  
 วิธีการสputtering แสดงประสิทธิภาพทางตัวเร่งปฏิกิริยาที่ดีที่สุด เนื่องจากตัวเร่งปฏิกิริยาที่  
 สังเคราะห์ด้วยวิธีการสputtering เมื่อเพิ่มปริมาณการใส่ทองแดงช่องว่างระหว่างแถบพลังงานจะ  
 ลดลงเพียงเล็กน้อย ซึ่งเพิ่มประสิทธิภาพของการเกิดปฏิกิริยา แต่ในกรณีของตัวเร่งปฏิกิริยาที่  
 เตรียมโดยวิธีเคลือบฝังเปียกแบบพอดี เมื่อเพิ่มปริมาณการใส่ทองแดงช่องว่างระหว่างแถบพลังงาน  
 จะลดลงมาก ซึ่งการแคบลงที่มากเกินไปนั้นเป็นการเพิ่มการรวมตัวกันอีกครั้งของอิเล็กตรอนกับ  
 หลุมโฮลทำให้ประสิทธิภาพของปฏิกิริยารีดักชันของคาร์บอนไดออกไซด์ในสารละลายน้ำที่เร่ง  
 ปฏิกิริยาด้วยแสงลดลง

สาขาวิชา วิศวกรรมเคมี  
 ปีการศึกษา 2561

ลายมือชื่อนิสิต .....  
 ลายมือชื่อ อ.ที่ปรึกษาหลัก .....

# # 5970222721 : MAJOR CHEMICAL ENGINEERING

KEYWORD: CO<sub>2</sub> reduction / Cu/TiO<sub>2</sub> / Methane / magnetron sputtering

Nantiya Jantarasorn : EFFECT OF Cu MODIFIED  
TiO<sub>2</sub> CATALYSTS PREPARED BY INCIPIENT WETNESS IMPREGNATION AND  
SPUTTERING FOR PHOTOCATALYTIC CO<sub>2</sub> REDUCTION  
IN AQUEOUS SOLUTION . Advisor: Prof. Piyasan Prasertthdam, Ph.D.

In this work, we investigated the photocatalytic CO<sub>2</sub> reduction in aqueous solution and were carried out in a stirred slurry reactor using Cu/TiO<sub>2</sub> catalysts synthesized by incipient wetness impregnation and sputtering method. Effects of Cu loading onto titania support enhancing efficiency of the photocatalytic CO<sub>2</sub> reduction in aqueous solution under UV irradiation by a band gap energy modification appeared between valence band and conduction band are narrowed. Cu assisted a selective hydrocarbon compound, this is methane. A comparison between Cu/TiO<sub>2</sub> catalysts synthesized by incipient wetness impregnation and sputtering method showed that both methods exhibited similar methane selectivity. Sputtered catalysts are likely to increase methane production when increasing the Cu deposition content onto titania support. While impregnated catalysts are likely to decrease methane production when increasing the Cu loading content. In summary, the synthesis by sputtering method exhibited the best catalytic performance. The sputtered catalysts, increasing the Cu deposition content, the band gap energy slightly decreased, it enhanced the photocatalytic activity. While impregnated catalysts, increasing the Cu loading content, the band gap energy more decreased, limitation of tiny narrow increased electron-hole recombination, the efficiency of the reaction is decreased.

Field of Study: Chemical Engineering

Student's Signature .....

Academic Year: 2018

Advisor's Signature .....

## ACKNOWLEDGEMENTS

I am grateful to my advisor, Professor Piyasan Prasertdam, for his significant support, guidance, and inspiration in this thesis. Furthermore, I would be grateful to Associate Professor Anongnat Somwangthanaroj, as a chairman, Assistant Professor Palang Bumroongsakulsawat and Assistant Professor Okorn Mekasuwandumrong, as the members of the thesis committee and thank you for your correctness and suggestion in my work.

In addition, I am thankful for assistance and experience to the members of Center of Excellence on Catalysis and Catalytic Reaction Engineering, Department of Chemical Engineering, Faculty of Engineering, Chulalongkorn University throughout the study. Besides, I would highly appreciate the Ratchadapisek Sompoch Endowment Fund (2016), Chulalongkorn University (CU-59-006-IC) and Newton Mobility Grants.

Finally, I would like to bestow this thesis to my parent for their support and encouragement throughout my life.

Nantiya Jantarasorn

## TABLE OF CONTENTS

	Page
.....	iv
ABSTRACT (THAI).....	iv
.....	v
ABSTRACT (ENGLISH).....	v
ACKNOWLEDGEMENTS.....	vi
TABLE OF CONTENTS.....	vii
LIST OF TABLES.....	xi
LIST OF FIGURES.....	xii
CHAPTER I	
INTRODUCTION.....	1
1.1 Introduction.....	1
1.2 Objective.....	3
1.3 The scope of research.....	3
1.4 Research methodology.....	5
CHAPTER II	
BACKGROUND AND LITERATURE REVIEWS.....	6
2.1 Photocatalysis.....	6
2.1.1 Semiconductor Photocatalysis.....	6
2.2 Titanium dioxide.....	7
2.2.1 Formation and crystal structure of titanium dioxide.....	7
2.2.2 Application.....	9
2.2.3 Modified and unmodified titanium dioxide.....	10

2.3 Heterogeneous photocatalysts .....	11
2.3.1 Copper catalysts .....	11
2.4 Principles of photocatalysts for Titanium dioxide.....	12
2.5 Mechanism of Photocatalytic CO <sub>2</sub> reduction with H <sub>2</sub> O.....	15
2.6 Preparation method .....	19
2.6.1 incipient wetness impregnation method .....	19
2.6.2 magnetron sputtering method.....	20
2.7 Effect of the copper metal catalyst on photocatalytic CO <sub>2</sub> reduction with H <sub>2</sub> O .....	23
CHAPTER III	
EXPERIMENTAL .....	27
3.1 Materials and chemicals .....	27
3.2 Preparation of catalyst.....	27
3.2.1 Magnetron sputtering method .....	27
3.2.2 Incipient wetness impregnation method .....	28
3.3 Catalyst characterization technique.....	29
3.3.1. X-ray diffraction (XRD).....	29
3.3.2. Surface Area Measurement.....	29
3.3.3. UV-VIS Spectroscopy (UV-VIS).....	30
3.3.4. X-ray photoelectron spectroscopy (XPS).....	30
3.3.5. Scanning electron microscope (SEM-EDX).....	30
3.3.6. Inductively coupled plasma (ICP).....	30
3.3.7. photoluminescence spectroscopy (PL).....	31
3.3.8. transmission electron microscope (TEM).....	31



3.4 Photocatalytic activity reaction on CO <sub>2</sub> reduction and H <sub>2</sub> O .....	31
--	----

#### CHAPTER IV

RESULTS AND DISCUSSION.....	33
-----------------------------	----

4.1 Influence of Cu loading on TiO <sub>2</sub> catalysts synthesized by magnetron sputtering method for photocatalytic reduction of CO <sub>2</sub> and H <sub>2</sub> O into methane.....	35
---	----

4.1.1 Powder X-ray diffraction (XRD).....	35
---	----

4.1.2 Surface Area Measurement.....	38
-------------------------------------	----

4.1.3 UV-vis spectrometer.....	39
--------------------------------	----

4.1.4 photoluminescence (PL).....	42
-----------------------------------	----

4.1.5 X-ray photoelectron spectrometer (XPS).....	44
---	----

4.1.6 Scanning electron microscopy and Energy Dispersive X-ray Spectroscopy (SEM-EDX).....	47
--	----

4.1.7 Inductively coupled plasma (ICP).....	49
---	----

4.1.8 Transmission electron microscopy (TEM).....	50
---	----

4.1.9 Photocatalytic activity of Cu/TiO <sub>2</sub> catalysts for photocatalytic reduction of CO <sub>2</sub> into methane. ....	52
---	----

4.2 Influence of Cu loading on TiO <sub>2</sub> catalysts synthesized by incipient wetness impregnation method for photocatalytic reduction of CO <sub>2</sub> and H <sub>2</sub> O into methane. ....	54
--	----

4.2.1 Powder X-ray diffraction (XRD).....	54
---	----

4.2.2 Surface Area Measurement.....	57
-------------------------------------	----

4.2.3 UV-vis spectrometer.....	58
--------------------------------	----

4.2.4 photoluminescence (PL).....	61
-----------------------------------	----

4.2.5 X-ray photoelectron spectrometer (XPS).....	63
---	----

4.2.6 Scanning electron microscopy and Energy Dispersive X-ray Spectroscopy (SEM-EDX).....	66
--	----

4.2.7 Inductively coupled plasma (ICP).....	68
4.2.8 Transmission electron microscopy (TEM) .....	69
4.2.9 Photocatalytic activity of Cu/TiO <sub>2</sub> catalysts for photocatalytic reduction of CO <sub>2</sub> into methane. ....	71
4.3 Comparison between Cu/TiO <sub>2</sub> catalysts synthesized by magnetron sputtering method and incipient wetness impregnation method.....	74
CHAPTER V	
CONCLUSIONS AND RECOMMENDATIONS.....	76
5.1 Conclusions .....	76
5.2 Recommendations .....	77
APPENDIX.....	78
APPENDIX A	
CALCULATION FOR CATALYST PREPARATION .....	79
APPENDIX B	
CALCULATION OF THE CRYSTALLITE SIZE.....	80
APPENDIX C	
CALCULATION OF THE BAND GAP FROM UV-VIS SPECTRA.....	82
APPENDIX D	
CALCULATION FOR CATALYTIC PERFORMANCE .....	83
REFERENCES .....	84
VITA.....	93

## LIST OF TABLES

	Page
Table 1 Crystal structure properties for various TiO <sub>2</sub> polymorphs. ....	9
Table 2 Chemical used in catalyst preparation. ....	27
Table 3 The specimen designation of the catalysts in this work. ....	34
Table 4 Physical properties of the sputtered catalysts. ....	39
Table 5 Catalyst compositions (%) of sputtered catalysts. ....	46
Table 6 Comparison of Cu doping content on TiO <sub>2</sub> support prepared by magnetron sputtering method. ....	49
Table 7 Physical properties of the incipient wetness impregnated catalysts. ....	58
Table 8 Catalyst compositions (%) of incipient wetness impregnated catalysts. ....	65
Table 9 Comparison of Cu doping content on TiO <sub>2</sub> support prepared by magnetron sputtering method. ....	68

## LIST OF FIGURES

	Page
Figure 1 Unit cells of different structural phases of anatase, rutile and brookite. ....	8
Figure 2 Schematic illustration of the photoexcitation process in a semiconductor particle. ....	14
Figure 3 Schematic illustration for mechanism of photocatalytic CO <sub>2</sub> reduction on Cu-modified TiO <sub>2</sub> . ....	18
Figure 4 The total pathways for production of the main products of photocatalysis of CO <sub>2</sub> . ....	19
Figure 5 Diagram of the DC Magnetron Sputtering Process. ....	23
Figure 6 Schematic diagram of the band structure of the pure TiO <sub>2</sub> and metal-doped TiO <sub>2</sub> . ....	24
Figure 7 P25-TiO <sub>2</sub> in magnetron sputtering chamber and the location of Cu target. ..	28
Figure 8 Schematic of incipient wetness impregnation method for preparation of Cu/TiO <sub>2</sub> nanoparticles. ....	29
Figure 9 Schematic diagram of the experimental system for photocatalytic reduction of CO <sub>2</sub> . ....	32
Figure 10 XRD patterns of Cu/P25 (SP) catalysts. ....	36
Figure 11 XRD patterns of Cu/Ana (SP) catalysts. ....	37
Figure 12 XRD patterns of Cu/Rut (SP) catalysts. ....	37
Figure 13 The UV-Vis absorption spectra of Cu/P25 (SP) catalysts. ....	40
Figure 14 The UV-Vis absorption spectra of Cu/Ana (SP) catalysts. ....	41
Figure 15 The UV-Vis absorption spectra of Cu/Rut (SP) catalysts. ....	41
Figure 16 The PL emission spectra of Cu/P25 (SP) catalysts. ....	42
Figure 17 The PL emission spectra of Cu/Ana (SP) catalysts. ....	43

Figure 18 The PL emission spectra of Cu/Rut (SP) catalysts. ....	43
Figure 19 The X-ray photoelectron spectra of SP3-P25 catalyst is simulated by Gaussian equation; XPS spectra of Ti2p (a), XPS spectra of O1s (b), and XPS spectra of Cu2p. ....	45
Figure 20 The X-ray photoelectron spectra of SP3-Ana catalyst is simulated by Gaussian equation; XPS spectra of Ti2p (a), XPS spectra of O1s (b), and XPS spectra of Cu2p. ....	45
Figure 21 The X-ray photoelectron spectra of SP3-Rut catalyst is simulated by Gaussian equation; XPS spectra of Ti2p (a), XPS spectra of O1s (b), and XPS spectra of Cu2p. ....	46
Figure 22 SEM of sputtered catalysts. ....	48
Figure 23 %Wt. of Cu-adhered onto P25-TiO <sub>2</sub> , Ana-TiO <sub>2</sub> , and Rut-TiO <sub>2</sub> supports prepared by magnetron sputtering method. ....	50
Figure 24 TEM and average Cu nanoparticle sizes of SP3-P25 catalyst. ....	51
Figure 25 TEM and average Cu nanoparticle sizes of SP3-Ana catalyst. ....	51
Figure 26 TEM and average Cu nanoparticle sizes of SP3-Rut catalyst. ....	52
Figure 27 CH <sub>4</sub> production yield of sputtered catalysts. ....	53
Figure 28 The stability of SP3-P25 catalyst. ....	53
Figure 29 XRD patterns of Cu/P25 (IM) catalysts. ....	55
Figure 30 XRD patterns of Cu/Ana (IM) catalysts. ....	56
Figure 31 XRD patterns of Cu/Rut (IM) catalysts. ....	56
Figure 32 The UV-Vis absorption spectra of Cu/P25 (IM) catalysts. ....	59
Figure 33 The UV-Vis absorption spectra of Cu/Ana (IM) catalysts. ....	60
Figure 34 The UV-Vis absorption spectra of Cu/Rut (IM) catalysts. ....	60
Figure 35 The PL emission spectra of Cu/P25 (IM) catalysts. ....	61
Figure 36 The PL emission spectra of Cu/Ana (IM) catalysts. ....	62

Figure 37 The PL emission spectra of Cu/Rut (IM) catalysts.....	62
Figure 38 The X-ray photoelectron spectra of IM3-P25 catalyst is simulated by Gaussian equation; XPS spectra of Ti2p (a), XPS spectra of O1s (b), and XPS spectra of Cu2p. ....	64
Figure 39 The X-ray photoelectron spectra of IM3-Ana catalyst is simulated by Gaussian equation; XPS spectra of Ti2p (a), XPS spectra of O1s (b), and XPS spectra of Cu2p. ....	64
Figure 40 The X-ray photoelectron spectra of IM3-Rut catalyst is simulated by Gaussian equation; XPS spectra of Ti2p (a), XPS spectra of O1s (b), and XPS spectra of Cu2p. ....	65
Figure 41 SEM of incipient wetness impregnated catalysts.....	67
Figure 42 %Wt. of Cu-adhered onto P25-TiO <sub>2</sub> , Ana-TiO <sub>2</sub> , and Rut-TiO <sub>2</sub> supports prepared incipient wetness impregnation method. ....	69
Figure 43 TEM and average Cu nanoparticle sizes of IM3-P25 catalyst. ....	70
Figure 44 TEM and average Cu nanoparticle sizes of IM3-Ana catalyst. ....	70
Figure 45 TEM and average Cu nanoparticle sizes of IM3-Rut catalyst.....	71
Figure 46 CH <sub>4</sub> production yield of incipient wetness impregnated catalysts. ....	72
Figure 47 Stability of IM3-P25 catalyst.....	73
Figure 48 The PL emission spectra of TiO <sub>2</sub> catalysts.....	75
Figure 49 UV-visible absorption characteristics of TiO <sub>2</sub> (P25). ....	82
Figure 50 The calibration curve of methane. ....	83

# CHAPTER I

## INTRODUCTION

### 1.1 Introduction

Energy is the most important thing that everyone has used in the present and tend to use more in the future. It may find many ways but fossil fuels are the most popular for users to create energy through combustion (burning) of the fuel. During fossil fuels combustion processes can emit chemical pollution due to uncompleted burn such as carbon dioxide ( $\text{CO}_2$ ), Carbon monoxide (CO), chlorofluorocarbon (CFCs), Sulphur oxides ( $\text{SO}_x$ ), Nitrogen oxides ( $\text{NO}_x$ ), Heavy metals, and so on[1]. These products become environmental issues, quality of human life, and the main cause of the greenhouse effect. The  $\text{CO}_2$  gas is the most emitted to atmosphere due to human activates such as fossil fuels combustion, chemical industrial processes, agricultural processes and vehicle engine leading to climate change (increment of winter/summer temperature), natural disaster (flood, drought, avalanche, forest fire, and so on) [2]. In order to decrease the emission of  $\text{CO}_2$  into the atmosphere,  $\text{CO}_2$  is used as a substance for production useful chemical products by the direct and indirect process. Direct process, it is widely used in the cooler system[3], extinguisher[4], dry ice[5] and so on. In the indirect process, it is used for generating chemical commercial such as urea[6], polycarbonate[7], methanol[8], acetic acid[9], formaldehyde[10] and so on.

This research will study another way to reduce emission  $\text{CO}_2$  by using them as a substrate for chemicals synthesis by photoreaction. The photochemical reaction is one of the attractive technology due to its low cost, the environmentally friendly, non-generation of pollution, easy for control process, non-consumption of thermal energy. In the photoreaction is just using irradiation from light for activating the

substrate to create chemical products such as Methane ( $\text{CH}_4$ ), Methanol ( $\text{CH}_3\text{OH}$ ), Carbon Monoxide ( $\text{CO}$ ), Formaldehyde ( $\text{HCHO}$ ) and Formic Acid ( $\text{HCOOH}$ ).

For this experimental research, photocatalytic  $\text{CO}_2$  reduction in aqueous suspension as a substrate contained with semiconductor powders, irradiation under UV light at room temperature and atmospheric pressure [11, 12]. Semiconductor materials are used as photocatalyst and extensively studied such as  $\text{TiO}_2$ ,  $\text{SnO}_2$ ,  $\text{ZrO}_2$ ,  $\text{ZnO}$ ,  $\text{SiC}$ ,  $\text{WO}_3$ ,  $\text{CeO}_2$ ,  $\text{GaP}$ ,  $\text{SrTiO}_3$ , etc. [13]. Among various semiconductor materials, the most extensively studied photocatalysts are  $\text{TiO}_2$ , because of its high stability, high photosensitivity, non-toxic, convenience for use and low cost [14]. However,  $\text{TiO}_2$  has a high recombination rate of electron-hole pairs due to the wide bandgap, weak  $\text{CO}_2$  adsorption of  $\text{TiO}_2$ , and very low photocatalytic activity. In order to improved efficiency of  $\text{TiO}_2$  for photocatalytic  $\text{CO}_2$  reduction in the water. There are several pathways for adjusting the photocatalytic property of  $\text{TiO}_2$  such as extending lifetime of charge carrier, inhibition of electron-hole recombination probability by doping with metals or non-metals onto  $\text{TiO}_2$  [15]. Some of the metal such as platinum ( $\text{Pt}$ )[16], silver ( $\text{Ag}$ )[17], copper ( $\text{Cu}$ )[18], nickel ( $\text{Ni}$ )[19] or a metal oxide such as a copper oxide ( $\text{Cu}_x\text{O}$ )[20], nickel oxide ( $\text{NiO}$ )[21] were used as co-catalyst for enhance lifetime of electrons and hole pairs by trapping electrons and increasing production yield [22].

In several studies, Cu species are deposited on the  $\text{TiO}_2$  surface enhance the photocatalytic efficiency of  $\text{TiO}_2$  by reduced the band gap energy. It made an energy level between the conduction and valence bands narrow. Moreover, shifted an absorption edge from the UV edge to the visible edge, separation of photoexcited electron-hole pairs by trapped electrons for prevented recombination probability that showed effectiveness in  $\text{CO}_2$  photoreduction. Besides Cu nanoparticles is selected due to its result in a high yield of methane formation [23].



For the surface modification techniques, the conventional impregnation method is widely used as the metal deposition method. In preparation required a lot of procedure such as dropping of metal precursor solution, drying, calcination which generates waste. The magnetron sputtering method which is the new direct metal deposition method is offered for catalyst preparation due to its convenient procedure and no waste generated [24]. In this research, for compared efficiency of Cu/TiO<sub>2</sub> catalyst from preparation, Cu/TiO<sub>2</sub> catalysts were synthesized by both a conventional impregnation method and a magnetron sputtering method. The photocatalytic activities were observed from the photoreduction of CO<sub>2</sub> with water under UV irradiation for methane production.

## 1.2 Objective

To investigate effects of Cu dopant content modified TiO<sub>2</sub> which have different phases such as anatase, rutile, and Degussa P25 (a mixture of 80% anatase and 20% rutile) have been prepared by incipient wetness impregnation method and magnetron sputtering method for photocatalytic CO<sub>2</sub> reduction in aqueous solution.



## 1.3 The scope of research

1. Effects of preparation of Cu/TiO<sub>2</sub> catalysts for photocatalytic reduction of CO<sub>2</sub> and H<sub>2</sub>O into methane.

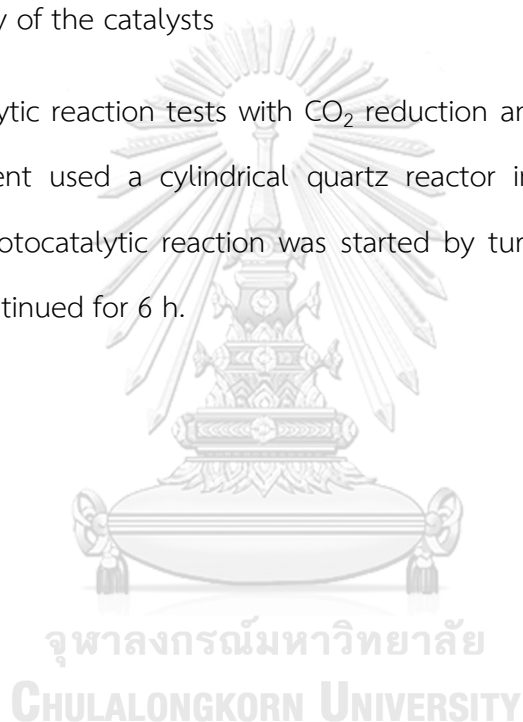
Synthesis of Cu supported on TiO<sub>2</sub> by various loadings of Cu dopant via incipient wetness impregnation and a magnetron sputtering method. TiO<sub>2</sub> is used as a support in the experiment have various phase consist of anatase, rutile, and Degussa P25 (a mixture of 80% anatase and 20% rutile).

## 2. Characterization of the catalysts

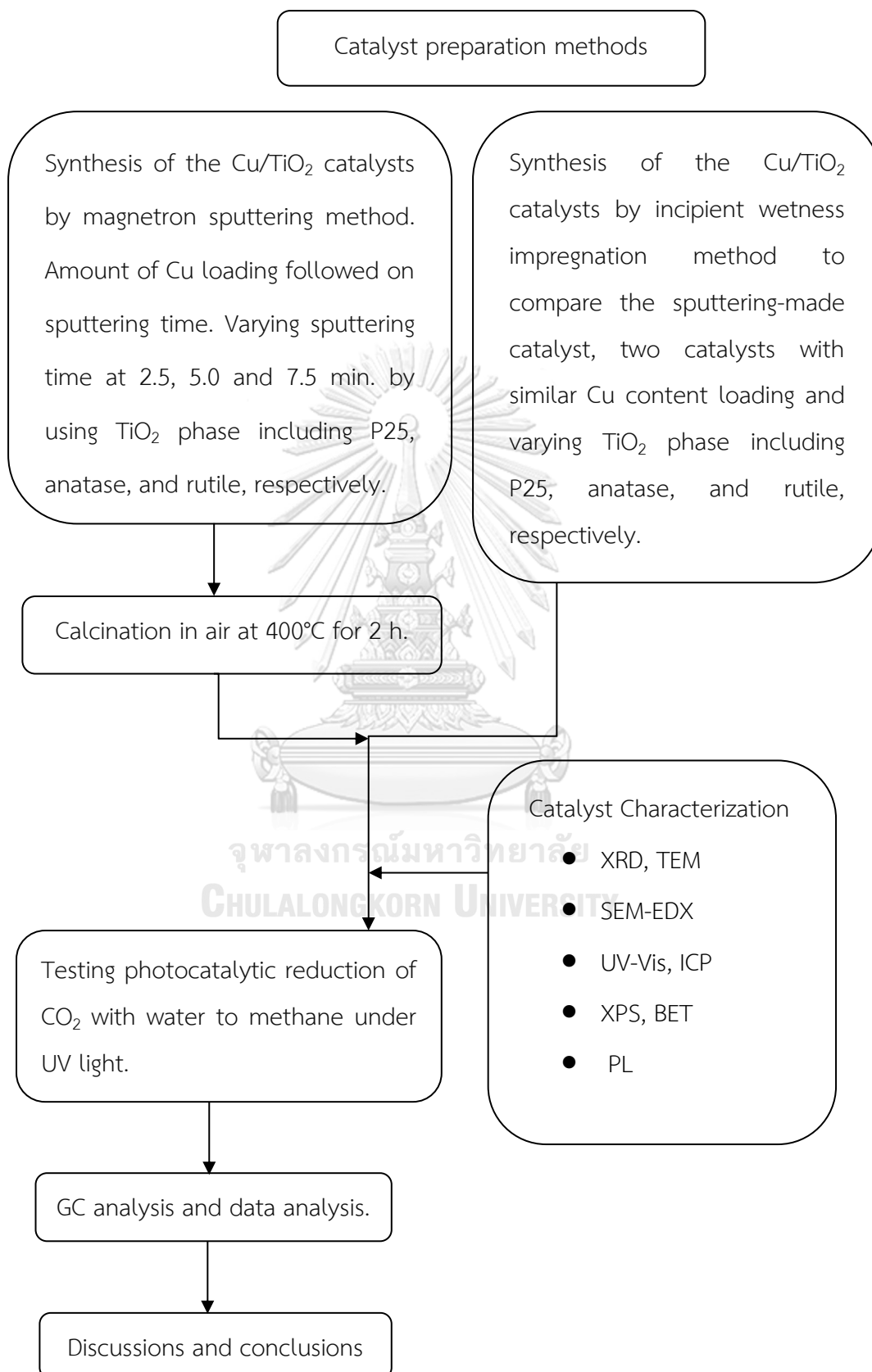
The obtained Cu/TiO<sub>2</sub> catalysts were characterized by using X-ray diffraction (XRD), N<sub>2</sub> temperature programmed desorption (BET), UV-VIS Spectroscopy (UV-VIS), X-ray photoelectron spectroscopy (XPS), Inductively coupled plasma (ICP), Transmission electron microscopy (TEM), Scanning electron microscope-Energy dispersive X-ray Spectrometer (SEM-EDX) and photoluminescence (PL),

## 3. Efficiency of the catalysts

Photocatalytic reaction tests with CO<sub>2</sub> reduction and water into hydrocarbon fuels. In experiment used a cylindrical quartz reactor install with UV-light bulbs around it. The photocatalytic reaction was started by turning on the UV light, and irradiation was continued for 6 h.



## 1.4 Research methodology



## CHAPTER II

### BACKGROUND AND LITERATURE REVIEWS

The purpose of this chapter provides the fundamental concept and literature review for this thesis. The first section of the chapter describes the photocatalytic principle. Next section describes the fundamental information about the properties of  $\text{TiO}_2$  and applications. Then describes the modified  $\text{TiO}_2$  supports. After that, the fundamental of photocatalytic  $\text{CO}_2$  reduction was described.

#### 2.1 Photocatalysis

Photocatalysis can be defined as the acceleration of a photoreaction by the presence of a catalyst. The semiconductor material was used in a reaction as photocatalysts that are present as follows:

##### 2.1.1 Semiconductor Photocatalysis.

Semiconductor photocatalysis is a critical substance for photocatalytic reaction due to it can be chemically activated by light irradiation. In the field of heterogeneous photocatalysis is interesting as shown by the number of publication and the most extensively studied due to a broad range of its application. A knowledge of chemistry such as crystal structure, electronic conductivity, light-absorption properties and excited state lifetimes are important, especially the structures, morphology and the electronic properties of surfaces. The adsorption and bonding of particles on surfaces are tried to understand the mechanisms in heterogeneous photocatalysis [25, 26].

Photosensitive semiconductor materials are used such as  $\text{TiO}_2$ ,  $\text{ZnO}$ ,  $\text{ZrO}_2$ ,  $\text{CeO}_2$ ,  $\text{WO}_3$ ,  $\text{SnO}_2$ ,  $\text{Fe}_2\text{O}_3$ ,  $\text{SrTiO}_3$ , etc. [27-29]. They may be used as pure metal oxide or doped oxides. Among various semiconductor materials, the most extensively used photocatalyst is  $\text{TiO}_2$ , because of its high stability, high photosensitivity, non-toxic, wide availability and low cost. However,  $\text{TiO}_2$  has a wider band gap, high

recombination rate of electron-hole pairs limit and weak CO<sub>2</sub> adsorption [30]. So, it is interesting to modify several properties to enhance efficiency.

## 2.2 Titanium dioxide

Titanium dioxide is the naturally occurring oxide of titanium, also known as titanium (IV) oxide or titania, and the chemical formula is TiO<sub>2</sub>. Normally titania used as a pigment, it has a white color. The most widely used in a variety of applications, including self-cleaning glass, air, and water purification systems, electronic systems and photoelectrochemical reaction. In industrials, titania is usually used as a catalyst support in the chemical reaction such as hydrogenation, oxidation and photoreaction, due to it has a lot of advantages such as high thermal stability, high chemical stability, excellent electrical properties, non-toxicity, non-corrosive, inexpensive semiconductor, an inert chemical and biological[31, 32]. In environmental applications, titania is an excellent photocatalyst application, it was used for produced alternative fuel from the photochemical reaction, which is the photocatalytic transformation of CO<sub>2</sub> into hydrocarbon fuel[33]. Titania is established as three different crystalline phases such as anatase, rutile, and brookite. More information is present as follows:

### 2.2.1 Formation and crystal structure of titanium dioxide

There are three main types of titania crystalline phases consist of anatase, rutile and brookite phases, that are plentifully found in nature[34]. In **Table 1** both of anatase and rutile phases have a tetragonal crystal structure, while the brookite phase has an orthorhombic crystal structure [35, 36]. The unit-cell structure of the titanium dioxide phases showed in **Figure 1** Polymorphs of TiO<sub>2</sub> structure, titania is in octahedral coordination, which contains 6 oxygen atoms per unit cell. However, the number of the edges-sharing octahedral structure increases from two in rutile, to three in brookite, to four in anatase. The rutile phase is stable at high temperatures and pressures, while anatase and brookite phase can transform to the rutile phase at

temperature upon 600 °C. Two main types of titanium dioxide are used industrially, rutile and anatase, while brookite is not often used for experiment due to it has a complex structure and difficult synthesis.

Among them, anatase and rutile phases have efficiency under light radiation. Anatase and rutile phases presented band gap energy at around 3.20 eV and 3.02 eV, respectively. The rutile phase can absorb under the visible light region with an absorption edge at 410 nm because of its narrow band gap energy, while the anatase phase only presented its response to UV irradiation with an absorption edge at 384 nm because of its broad band gap energy[34]. Both anatase and rutile phases are photocatalytic but anatase is the most reactive form. So, the rutile phase is not widely used due to its incapability photoactivity. The best way for improving effective photoactivity is by combining anatase with a slight amount of rutile such as Commercial Degussa P25, it is found P25 the most active than only anatase or rutile phases[37-39].

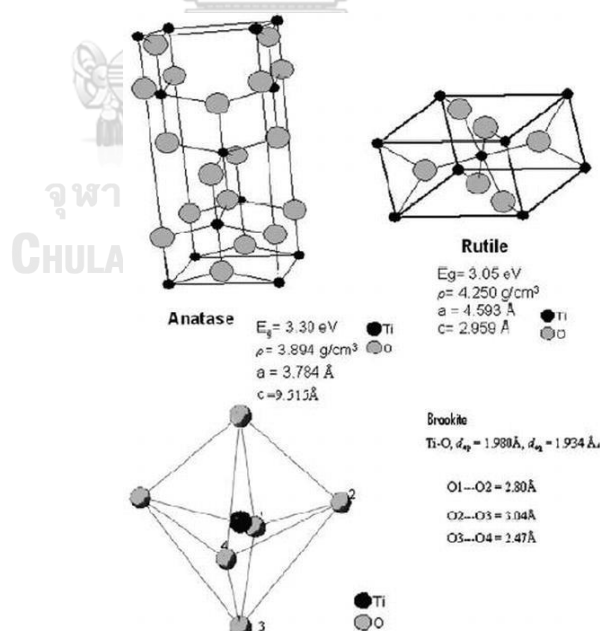


**Figure 1** Unit cells of different structural phases of anatase, rutile and brookite.

**Table 1** Crystal structure properties for various TiO<sub>2</sub> polymorphs.

Phase	Anatase	Rutile	Brookite
Crystal structure	Tetragonal	Tetragonal	Orthorhombic
Density, kg/m <sup>3</sup>	3830	4240	4170
Atoms per unit cell (Z)	4	2	8
Space group	I4 <sub>1</sub> /amd	P4 <sub>2</sub> /mnm	e Pbca
Lattice constant (Å)			
A	3.785	4.593	9.182
B	-	-	5.456
C	9.514	2.959	5.143

### 2.2.2 Application

Titanium dioxide is widely used in applications which exhibited its high chemical stability and non-toxicity in many works that are present as follows:

#### 1. Purification facilities.[40]

Titanium dioxide is used in a lot of systems such as purification systems for water treatment and air conditioners.

#### 2. Destruction of microorganism.[41]

Titanium dioxide particles can disinfect a lot of bacterias and viruses.

#### 3. Interior furnishing materials.[42]

Titanium dioxide is part of materials for interior decoration such as wallpaper, window blinds, indoor paints, and indoor tiles.

#### 4. Exterior construction materials.[43]

Titanium dioxide is part of materials for exterior construction such as plastic films, coating, glass, tile, and curtain.

#### 5. Road-construction materials.[44]

Titanium dioxide particles and films for the photocatalytic destruction of gaseous organic pollutants is applied for photodestruction and self-cleaning photofilms. That is used to tunnel walls panels, road coating and roadblocks.

#### 6. Household goods.[45]

Titanium dioxide particles are applied to one part of the component in manufacturing such as textiles, clothes, fabric, and fibers for its self-cleaning property.

#### 7. Catalysis.[46]

Titanium dioxide particles are used as catalysts in a lot of reaction such as photocatalysis for photoreaction because its capability to generate photo-excited electron ( $e^-$ ) and hole ( $h^+$ ) pairs which are an oxidizing and reducing agent in the process.



### 2.2.3 Modified and unmodified titanium dioxide

In the present, Titanium dioxide is widely used as a support of the catalyst because of their high chemical stability, high photosensitivity and economical. There are many types of research about titanium dioxide used as a support of the photocatalyst. However, unmodified-TiO<sub>2</sub> has a disadvantage for using such as wider band gap energy, high electron-hole recombination rate, and weak CO<sub>2</sub> adsorption. So, it is interesting to modify the several properties for enhancing efficiency for the photochemical reduction of CO<sub>2</sub> to carbon fuel such as CO, HCOOH, HCHO, CH<sub>3</sub>OH. From the most extensively studied, Modified-TiO<sub>2</sub> with various elements such as metals, metal oxides, non-metal and sensitizers, in photocatalyst both metal acted



as electron ( $e^-$ ) traps prevented the recombination of a electron ( $e^-$ ) and a hole ( $h^+$ ), therefore extend the lifetime of the photogenerated charge carrier ( $e^-$ ). Sometimes modified-TiO<sub>2</sub> with various elements such as non-metal (N, S, and C) cause the band gap is reduced [47, 48].

### 2.3 Heterogeneous photocatalysts

In the photocatalytic CO<sub>2</sub> reduction, heterogeneous photocatalysts are the most widely used. There are two main types of heterogeneous photocatalysts, are bulk semiconductor photocatalysts and matrix-dispersed photocatalysts [49]. Matrix-dispersed photocatalysts are the highest activity for photoreduction of CO<sub>2</sub>, due to high adsorption capacity and large surface area. And bulk semiconductor photocatalysts are one of the heterogeneous photocatalysts, consist of metal oxide, sulphides, nitrides, and oxynitrides [50]. Metal oxide is widely used as a support of the catalyst in photocatalytic CO<sub>2</sub> reduction, the most acceptable and broadly metal oxide is Titanium dioxide, due to photocatalytic activity can enhance by doping noble metal act as co-catalysts with suitable ratio, usually noble metals are doped on titania consist of Pt, Au, Ag, Pd, Cu, Ni, NiO, Cu<sub>x</sub>O, etc.[51].

#### 2.3.1 Copper catalysts

In this research, noble metals are selected for modification TiO<sub>2</sub> is Copper. Copper is a chemical element with the symbol Cu, atomic number 29, and melting point at 1084 °C. It is a reddish-gold metal that occurs naturally in the environment and reflects red and orange light, due to its band structure can absorb light in the visible light region. Its properties are a soft, flexible, and ductile metal with very high thermal and electrical conductivity. Copper has been one of the metals used to make a conductor of heat and electricity. It also has uses in electrical equipment such as electrical wires due to its good conductivity, and industrial machinery such as heat exchangers due to its good heat conductivity. Moreover, it is used as a component of various metal alloys, such as sterling silver used in jewelry,

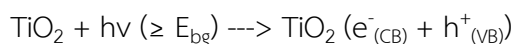
cupronickel used to make coins and constantan used in thermocouples for temperature measurement. The commonly encountered copper forms are copper(I) and copper(II) with oxidation states +1 and +2, respectively. There are two the principal oxides of copper, one is Copper(I) oxide with the formula  $\text{Cu}_2\text{O}$  and Copper(II) oxide with the formula  $\text{CuO}$ .  $\text{Cu}_2\text{O}$ , which often yellow or red colors have been used commonly as a pigment, a fungicide, and an antifouling agent for marine paints.  $\text{Cu}_2\text{O}$  is widely studied as semiconductor, due to its photochemical properties is a p-type semiconductor, it has the narrowest bulk excited energy, the direct band gap around 2.0 eV, the wavelength is 620 nm [52]. In part of  $\text{CuO}$ , which often black color has been used commonly as a pigment in ceramics to produce blue, red, and green colors, production wood preservatives, and production dry cell batteries.  $\text{CuO}$  is widely studied as semiconductor, due to its photochemical properties is a p-type semiconductor, it has the direct band gap around 1.2eV-1.8 eV, the wavelength is 1,033-689 nm [53]. In photocatalysts, doping copper metal is widely used as co-catalyst semiconductor due to its narrowed band gap energy, it can reduce band gap energy of  $\text{TiO}_2$  for enhancing photocatalytic activity.



#### 2.4 Principles of photocatalysts for Titanium dioxide

Titanium dioxide has electronic structure, so it is semiconductor. In the photocatalytic process, semiconductor is activated by photons ( $h\nu$ ) from light source with sufficient energy, which is equal to, or greater than band gap value of semiconductor photocatalyst. The electronic structure of a semiconductor is characterized by a valence band (VB) and a conduction band (CB), space between us is an energy band gap ( $E_{bg}$ ), a band gap energy of titania around 3.2 eV. Absorption of photons on surface, irradiation have to higher than 3.2 eV, in order to excite electrons from the valence band (VB) promotes to the conduction band (CB),

generating electron-hole pairs. Negative charges exist at conduction band, while generating positive hole ( $h^+$ ) causes of losing an electron at the valence band. this step is expressed as:



The electron-hole pairs or charge carriers are necessary to initiate the photocatalysis process. The oxidizing and reducing agent participate in reduction and oxidation reaction is shown in **Figure 2**. The reaction takes place on the surface of titania, normally absence of trapping sites of electron and hole pairs lead to recombination at the surface or bulk of photocatalyst in a short time, and releasing thermal energy. If titania has suitable trapping sites for electron and hole pairs can occur reduction and oxidation reaction. The photocatalytic process onto a semiconductor particle can be summarized in four steps:

1. Absorption of light with energy over  $E_{bg}$  followed by the generation and separation of the electron hole pairs;
2. Adsorption of the substrate;
3. reduction and oxidation reaction (redox reaction);
4. Desorption of the products.

The redox reaction depends on the energy levels of the photocatalyst and substrate species adsorbed on the photocatalyst surface. The potentials of the redox couple which is adsorbed substrate ( $E_1, E_2$ ) are cooperative with both the potential of conduction band (CB) and the potential of valence band (VB). These can be successful when the potential of CE should be more negative than the redox potential of the species to be oxidizing agent ( $E_1$ ) for the reduction reaction, so the electrons charge ( $e^-$ ) can reduce the oxidized form of this species ( $ox_1 / red_1$ , see

**Figure 2).** At the same time, an oxidation reaction may appear if the potential of the VB be more positive than the redox potential of the species to be reducing agent ( $E_2$ ), so that the positive charge holes ( $h^+$ ) can oxidize the reduced form of this species ( $red_2 / ox_2$ , see **Figure 2**). When both conditions are revealed, both reduction and oxidation are thermodynamically favored, and the overall photocatalytic process takes place [54, 55].

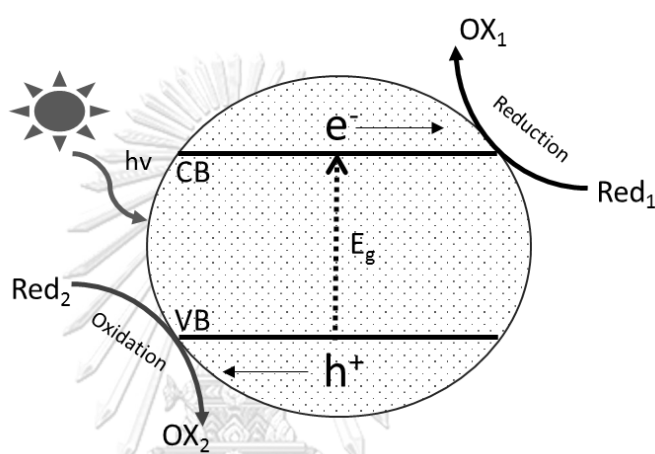
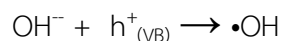
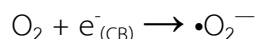


**Figure 2** Schematic illustration of the photoexcitation process in a semiconductor particle.

For the photocatalytic water/ air purification and photocatalytic hydrogen production system. The basic mechanisms of the redox reactions take place onto the semiconductor catalyst surface which show oxidation of hydroxyl groups by photo-generated holes into hydroxyl radical in the aqueous system:



In degradation process, hydroxyl radicals are mostly used as the primary oxidants the break the substrates by reducing them to their elemental form. Molecular oxygen dissolved in the aqueous phase is reduced by electrons charge from CB to superoxide radical.

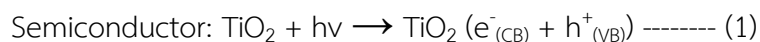


Reduction of a proton donor by electrons charge generated  $\bullet\text{H}$  radicals, which are used in two processes: combination for  $\text{H}_2$  production or hydrogenation of adsorbed substrate:

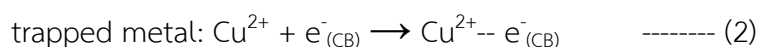


## 2.5 Mechanism of Photocatalytic $\text{CO}_2$ reduction with $\text{H}_2\text{O}$

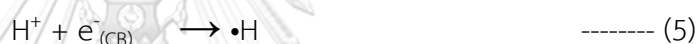
**Figure 3** show mechanism of photocatalytic reduction of  $\text{CO}_2$  in the aqueous water solution. Beginning, Photocatalysis will be occurred when absorption of photons energy from light equal to or higher than the band gap energy ( $E_{\text{bg}}$ ) of a semiconductor, and this time electron charge ( $e^-$ ) generated at conduction band (CB), while an empty valence band (VB) area became to hole ( $h^+$ ) due to losing of electron. The photocatalytic activity depends on the capability of the catalyst to generate charge carriers, which is used in formation of free radicals (e.g. hydroxyl radicals:  $\bullet\text{OH}$ , hydrogen radical:  $\bullet\text{H}$ ) carried out secondary reactions. Activated semiconductor reactions show in Eqs.(1) [54]. These charge carriers will be used in redox reaction as follows.



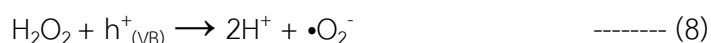
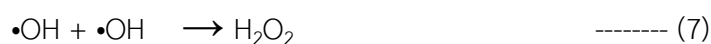
Eqs.(2) show trapping by metals prevent electron-hole pairs recombination and enhance the lifetime of charges. So, photocatalytic activity will improve in the process.



On the photocatalyst surface, holes act as primary oxidizing species in oxidation reaction.  $\text{H}_2\text{O}$  is trapped on active surface hole and react with it for production of hydroxyl radicals ( $\bullet\text{OH}$ ), which is commonly produce via direct oxidation of  $\text{OH}^-$  (Eqs.(3-4)) [55]. For protons ( $\text{H}^+$ ) is used to produce hydrogen radical ( $\bullet\text{H}$ ), which is initial substance for association of hydrogen (Eqs.(5-6)). The most significance of hydrogen radical is necessary for hydrocarbon chemical products. In this process,  $\text{H}_2\text{O}$  is an available and inexpensive substance, which is used as source of hydrogen make up for  $\text{H}_2$  consumption.

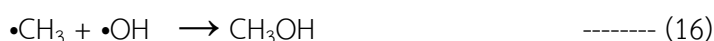


The hydroxyl radicals are a main substance using in produce hydrogen peroxide ( $\text{H}_2\text{O}_2$ ) (Eqs.(7)). Oxygen generate via oxidation reaction of Superoxide ( $\bullet\text{O}_2^-$ ) by valence band hole (Eqs.(9)).  $\bullet\text{O}_2^-$  radical anion is main product from oxidation of hydrogen peroxide by a trapped hole (Eqs.(8)).  $\bullet\text{O}_2^-$  radical anion is extrinsic in oxidation reaction due to it is poor oxidizing species so productions of  $\text{O}_2$  hardly reveal in the process.



In reaction of photocatalytic reduction of  $\text{CO}_2$  in the aqueous water solution,  $\text{CO}_2$  is used as source of carbon radical ( $\bullet\text{C}$ ) by breaking C—O bonds then, add

hydrogen radical ( $\bullet\text{H}$ ) will be new C–H bonds formation for useful chemical fuel production. In order to receive hydrocarbon products,  $\text{H}_2\text{O}$  is used as a reducing agent for provide source of hydrogen. So, the compositions for photocatalytic reduction of  $\text{CO}_2$  reaction are completely. Eqs.(10-16) show pathway of hydrocarbon compounds such as methane and methanol. The overall formation summarizes  $\text{CO}_2$  to form methane and methanol via a series of reactions;  $\text{CO}_2 \rightarrow \text{CO} \rightarrow \text{CH}_4, \text{CH}_3\text{OH}$  as follows [56]. The initial,  $\text{CO}_2$  is adsorbed onto a semiconductor photocatalyst surface and it receive an electron charge from the conduction band of a photocatalyst for  $\bullet\text{CO}_2^-$  anion radical formation, which is reactant captured with  $\bullet\text{H}$  generated from  $\text{H}_2\text{O}$  reductants to give carbon monoxide (CO) (Eqs.(10-11)). CO is the first product is desired due to it can be formed to  $\bullet\text{C}$  radical via combination of  $\bullet\text{CO}^-$  anion radical and  $\bullet\text{H}$  radical (Eqs.(12-13)).  $\bullet\text{C}$  radical is basic element lead to the formation of C–H bonds product. It can be seen that an associate formation of  $\bullet\text{C}$  radical by  $\bullet\text{H}$  radical is the major reaction to give hydrocarbon compound (Eqs.(14)). Methane is known as the product of formation between  $\bullet\text{CH}_3$  radical and  $\bullet\text{H}$  radical, while methanol can be formed from  $\bullet\text{CH}_3$  radical and  $\bullet\text{OH}$  radical (Eqs.(15-16)).



Water is by produced from association of hydroxyl radical ( $\bullet\text{OH}$ ) and hydrogen radical ( $\bullet\text{H}$ ). The production of hydroxyl radical reveal from oxidation of hydroxide ion ( $\text{OH}^-$ ) by a trapped hole.



So, the product of methanol and methane are fact follows to Eqs.(19-20) and other hydrocarbon product show in **Figure 4**. Using 6-8 electrons and protons for reduction of  $\text{CO}_2$  to hydrocarbon compounds[57].

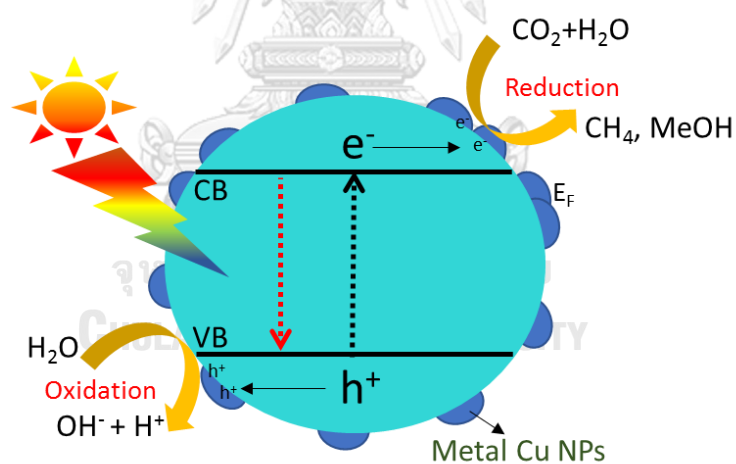
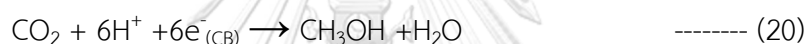
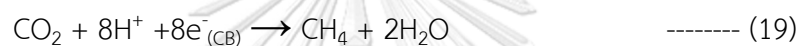


**Figure 3** Schematic illustration for mechanism of photocatalytic  $\text{CO}_2$  reduction on Cu-modified  $\text{TiO}_2$ .



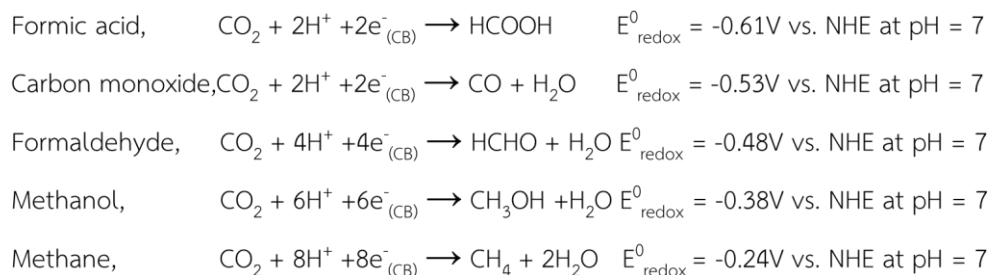


**Figure 4** The total pathways for production of the main products of photocatalysis of  $\text{CO}_2$ .

## 2.6 Preparation method

### 2.6.1 incipient wetness impregnation method

In other words, the incipient wetness impregnation method is called capillary impregnation or dry impregnation, is the most common method of catalyst preparation for heterogeneous catalysts. This method is popular because of its simple preparation, low costs and generates less waste. In the procedure, the certain metal precursor is dissolved in an aqueous or organic solution. The volume of the metal precursor solution is sufficient with the pore volume of the support. The metal loading depended on the concentration of metal ions in solution due to calculation from the number of metal ions excluded salts solution. Generally, metal salts used as a metal precursor consist of nitrate, chloride, acetate, complexes, etc. In many cases, nitrates precursor is very attractive because it is inexpensive, dissolve in polar solvents (aqueous) and facile disintegration. Then the metal solution is slowly impregnated on a catalyst support, the solution is drawn into the pores of support by capillary action, so this is physisorption. After that impregnated support is dried and activated by heat treatment (e.g. calcination and/or reduction) to discharge contaminant in solution, the catalyst obtained.

This method is least adsorption controlled, because of depositing the concentration of metal ions species are uncontrolled on the catalyst surface. The solution volume is enough used with capacity of the pore volume. Sometimes, excess of precursor solution is added in pore volume causes the solution transfer from a capillary action process to a diffusion process.

The precursor salts such as nitrate salt have the poor performance for catalyst include the low dispersion of metal on powders. Due to this preparation methods, the precursor solution is redistributed during drying. And one of the reason is sintering during calcination causes the low dispersion of impregnated catalyst [58], sintering is the process of heat treatment using temperature is below the melting point of the main component of the powder material, after removal of residual liquid by evaporation, nearing powder particles are agglomerated. Poels, E., et al. (1991) [59] reported the nickel on alumina catalysts occurred sintering due to the nitrate decomposition products (nitrogen oxides and water).

### **2.6.2 magnetron sputtering method**

Usually, synthesis of deposited metal nanoparticle catalysts for photoreaction used a complicated method such as incipient wetness impregnation method, sol-gel method, deposition precipitation method, and photo-deposition method. There were several procedures for preparation such as filtration, drying, and calcination and generated waste products to the environment. In order to solve the problem, magnetron sputtering is the one of method for metal deposition onto the surface of  $\text{TiO}_2$ . Magnetron sputtering preparation is surface modification methods prevented from contamination due to a catalyst is controlled in vacuum chamber [24].

Sputtering is one of the surface modification techniques for metal deposition onto powder by producing thin-film covered on the surface. This technique is Physical Vapor Deposition (PVD) used to deposit solid coatings which operate in

gaseous state processes. In the deposited process, metal materials are deposited on an atomic level using a charged plasma stream of electrons and ions under a vacuum environment. **Figure 5** shows the basic structure of a magnetron sputtering coating system is the target material or source material (negative cathode) to be used as a coating is installed in a vacuum chamber and the substrate (positive anode) to be coated is loaded into sample vessel which is installed parallel to the target, at sputtering cathode a permanent magnet array is installed behind the cathode.

The sputtering process starts on a substrate is contained in a vacuum chamber. Then, the vacuum chamber is evacuated to a base pressure for removing almost every molecule from the chamber such as  $H_2O$ , Air and then backfilled with a high purity inert gas. Normally argon gas (Ar) is used in the process due to its ability to create the gas ions that are the primary driving force for sputtering process. Inside of vacuum chamber is controlled under low pressures range from 0.5mTorr to 100mTorr. After that, a negative electrical potential from a DC electrical current is applied to a target material become to negatively charged target material which generates a free electrons flow. The partial ionization of a neutral argon gas occurs from collision with free electrons flow in the plasma environment, these electrons getting out from the outer electronic shell of the argon gas atoms, the inert gas atoms lose electron become positively charged ions. These positively charged ions bombarded to the target material with a very high velocity for “Sputters off” or eject atomic sputtered particle from the target material. When sputtered particles are ejected from a target material these particles cross the vacuum chamber and are deposited on the surface of the substrate as a thin layer. During the process, the light of the plasma is generated from recombination of free electrons and positively charged ions into a lower energy state and discharged that light.

Due to DC Sputtering usually has low deposition rates and the substrate is damaged from a bombardment of ion currents due to it create overheating. Improving the efficiency of deposition rates by installing a magnet array behind the cathode that is called DC Magnetron sputtering. DC Magnetron sputtering installs magnets behind the negative cathode for creates the magnetic field in tunnel form to trap electrons above the surface of the target. In order to enhance the efficiency of the deposition rate electron trapping is used to protect bombardment of free electrons on a substrate. Moreover, the magnetic field is used to control the velocity and direction of the positively charged ions.

The most common sputter deposition inert gas types have been used in the process is argon gas. But in a special case, a non-inert gas such as oxygen or nitrogen is used to produce oxide and nitride component. In the process, a non-inert gas is added to the vacuum chamber and become ionized which is reactive with atomic sputtered particle by a chemical reaction and produce a molecular compound before deposition. For example, a copper target reactively sputtered with oxygen gas can produce a copper oxide layer.

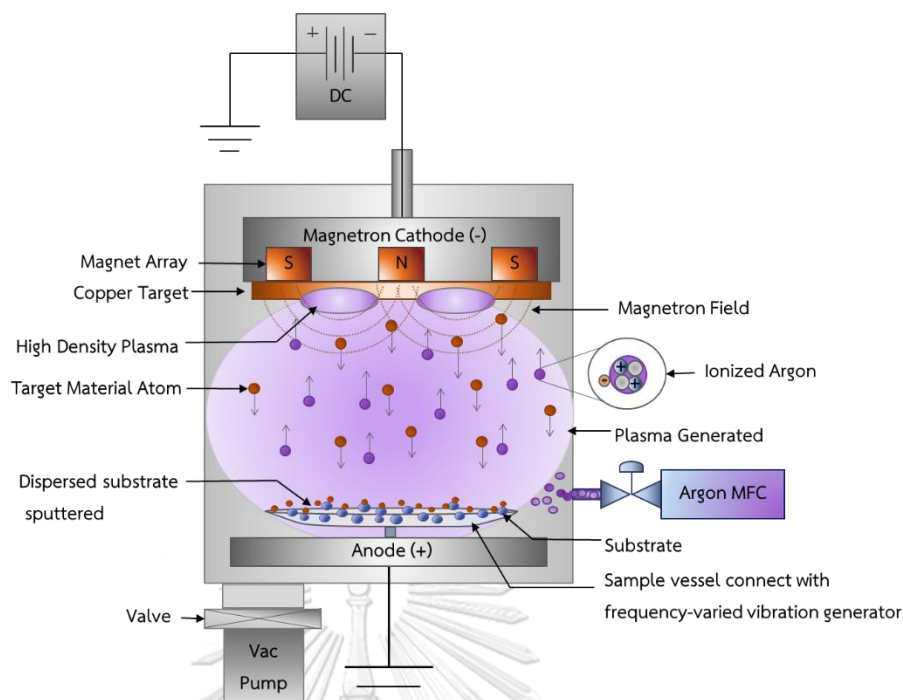


**Figure 5** Diagram of the DC Magnetron Sputtering Process.

## 2.7 Effect of the copper metal catalyst on photocatalytic CO<sub>2</sub> reduction with H<sub>2</sub>O

The surface modification method is one of the most widely applied techniques for enhancing photocatalytic CO<sub>2</sub> reduction with H<sub>2</sub>O. The best one is doping which have been applied for improvement efficiency of TiO<sub>2</sub> support. Limitation of the practical application of TiO<sub>2</sub> for activating photocatalytic reaction is it responded to UV light irradiation and recombination rate of electron-hole pairs is fast due to its wide bandgap (3.2 eV). In order to prevent recombination of charge carriers, doping with metal or non-metal is good arrangement for extension of the light absorption range of TiO<sub>2</sub> from UV region to visible region as a result of reduced the bandgap of semiconductor. Usually, metal doping is more excellent than doping with non-metal. The metal elements such as Cu is commonly used due to it able to prevent the rearward recombination of a negative charge electron (e<sup>-</sup>) and a hole (h<sup>+</sup>) by trapping electron charge. For the capability of reducing the band gap energy

of semiconductor, it takes place in the crystal lattice structure of  $\text{TiO}_2$  atoms Cu can substitute in it and create an empty energy state below the conduction band of  $\text{TiO}_2$  that show in **Figure 6**. The new energy level of band gap presented visible light response. So, it confidently effect the photocatalytic activity of  $\text{TiO}_2$ .

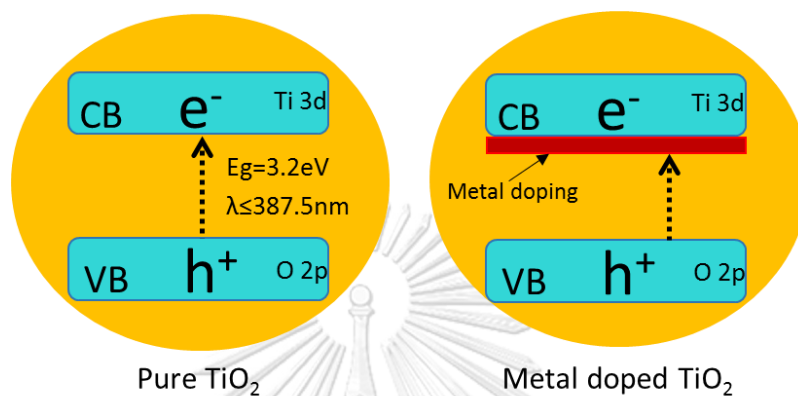


**Figure 6** Schematic diagram of the band structure of the pure  $\text{TiO}_2$  and metal-doped  $\text{TiO}_2$ .

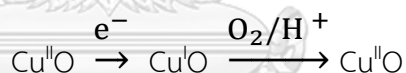
Li, Y., et al. (2010) [60] reported the photocatalytic reaction was carried out under irradiation of a Xe lamp using  $\text{Cu}/\text{TiO}_2\text{-SiO}_2$  as a catalyst system. The preparation of silica supported  $\text{Cu}/\text{TiO}_2$  catalysts was based on a sol-gel method. Photocatalytic experiments, using  $\text{CO}_2$  and water vapor as the reactants in a continuous-flow reactor. Begin with catalyst was loaded in the reactor and purged with the mixture of  $\text{CO}_2$  and water vapor at 100 mL/min for 45 min and then reduced the flow rate to 3.0 mL/min for 30 min in order to stabilize the process. The Xe lamp was turned on and the concentrations of gases within the reactor were recorded every hour. The  $\text{CO}_2$  photoreduction of  $\text{TiO}_2\text{-SiO}_2$  catalysts produces only CO and higher than  $\text{TiO}_2$  catalysts due to the high surface area of silica substrate ( $>300\text{ m}^2/\text{g}$ ) enhanced adsorption of  $\text{CO}_2$  and  $\text{H}_2\text{O}$  and dispersion  $\text{TiO}_2$  on the catalyst. For doping Cu on  $\text{TiO}_2\text{-SiO}_2$  catalysts promoted  $\text{CH}_4$  production rates and enhanced the efficiency of  $\text{CO}_2$  photoreduction because Cu species inhibited the electron-hole

recombination by trapping electron charge. From investigation by varying the Cu loading from 0.2% to 3%, it found the optimum Cu loading content on TiO<sub>2</sub>-SiO<sub>2</sub> catalyst is 0.5%wt. which produced the highest production rates for CO and CH<sub>4</sub> at 60 and 10 μmol g-cat<sup>-1</sup> h<sup>-1</sup>, respectively. But in case of a Cu loading content higher than the optimum, Cu species became to recombination centers and reduce the catalytic activity because it covered on the illuminated TiO<sub>2</sub> surface.

Liu, D., et al. (2012) [61] reported the preparation of Cu/TiO<sub>2</sub> catalysts was prepared using a sol-gel method. Photocatalytic experiments using a stirred batch annular reactor under irradiation of a four 8-watt UVA lamp. In flat-bottomed quartz reactor, 1 g of catalyst powder was suspended in 200 ml of deionized water by a magnetic stirrer throughout the reaction. Then, CO<sub>2</sub> was bubbled into the reactor for 20 min to purge air. After that, the reactor was pressurized with CO<sub>2</sub> at 1 bar and held for 15 min to saturate the water with gaseous CO<sub>2</sub>. The UVA lamp was turned on and irradiation was continued for 1.5 h. Product from the CO<sub>2</sub> photoreduction was only methane. The Cu/TiO<sub>2</sub> catalyst exhibited higher the CO<sub>2</sub> photoreduction performance than undoped TiO<sub>2</sub> catalysts for CH<sub>4</sub> production. Because Cu acted as co-catalyst, capturing the electron charge inhibited the electron-hole recombination. From XPS result, it shows the peak of the Cu 2p<sub>3/2</sub> binding energy at ~932.4 eV indicative copper (I) species. The optimum Cu loading content on TiO<sub>2</sub> catalyst is 0.03 wt.% which produced the optimum CH<sub>4</sub> production at 24 nmol g-cat<sup>-1</sup> h<sup>-1</sup>. The Cu loadings higher than the optimum possibly promoted electron-hole recombination.

Nasution, H. W., et al. (2005) [62] synthesized the Cu/TiO<sub>2</sub> catalyst in the different copper species copper (0), copper (I), copper (II) by an improved-impregnation method via reduction-oxidation steps. Photocatalytic experiments using a stirred batch reactor under irradiation of UV black light lamps. Within a reactor, 0.3 g of catalyst was suspended in 300 ml of 1 M KHCO<sub>3</sub> solution by a

magnetic stirrer. Then, CO<sub>2</sub> was bubbled into the reactor for 30 min to purge air and to saturate the solution with CO<sub>2</sub>. After that, the reactor was closed during the reaction, the UV lamp was turned on and irradiation was continued for 6 h. The CO<sub>2</sub> photocatalytic reduction of CO<sub>2</sub> produced the only methanol. 3%CuO/TiO<sub>2</sub> catalyst is optimum for methanol production. It found that copper(II) species has the highest catalytic activity compared with other copper species and copper species acted as a trap for capturing the electrons inhibited electron-hole recombination. In case of copper(I) species, its highest positive redox potential value created stronger interaction between TiO<sub>2</sub> and Cu species, Cu dopant extremely catches electrons, electrons difficultly transferred to catches with the adsorbed species on the catalyst surface and acted as electron-hole recombination center. While copper(II) species have lower positive redox potential value which is suitable for capturing the electrons. Moreover, copper species on TiO<sub>2</sub> surface can change between Cu<sup>2+</sup> and Cu<sup>1+</sup> species due to redox reaction as follows:



The Cu(II) species can change to Cu(I) species via reduction reaction by trapped electrons. While Cu(I) species can become to Cu(II) species via oxidation reaction by H<sup>+</sup> and/or O<sub>2</sub>.



## CHAPTER III

### EXPERIMENTAL

This chapter provides the details of chemicals, catalyst preparation, characterization, and catalytic reaction test.

#### 3.1 Materials and chemicals

**Table 2** Chemical used in catalyst preparation.

Chemicals	Chemicals name	Purity (%)	Suppliers
TiO <sub>2</sub> (Degussa, P-25)	Titanium(IV) oxide	100	Aeroxide
Cu(NO <sub>3</sub> ) <sub>2</sub> ·3H <sub>2</sub> O	Copper(II) nitrate trihydrate	99.5	Aldrich
Cu target	Copper Metal	100	-

#### 3.2 Preparation of catalyst

There are two preparations method for Cu/TiO<sub>2</sub> catalysts were the magnetron sputtering method and the incipient wetness impregnation method. The details of the preparation method for Cu/TiO<sub>2</sub> catalysts are present as follows:

##### 3.2.1 Magnetron sputtering method

**Figure 7** shown the Cu/TiO<sub>2</sub> catalysts were prepared by a magnetron sputtering method. The Cu target was installed in the sputtering chamber, 2 g of TiO<sub>2</sub> support was loaded in a sample vessel. Before synthesis begins, the sputtering chamber was vacuumed by vacuum pumps. The condition for coating Cu onto TiO<sub>2</sub> consist of power 200W, voltage 350V, current 0.57A, and frequency 200kHz were used. The uniform Cu coating on the TiO<sub>2</sub> is made by the vibration generator. A magnetron sputtering of Cu target was done under argon atmosphere. The P25-TiO<sub>2</sub> support was

coated with Cu particles and varied time at 2.5, 5, 7.5 min, respectively. The other phase of TiO<sub>2</sub> support including anatase and rutile were used respectively.

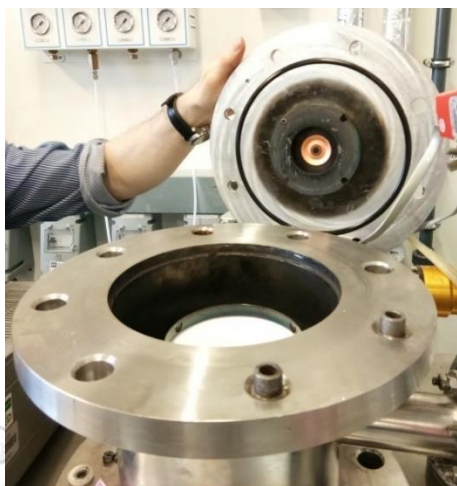


**Figure 7** P25-TiO<sub>2</sub> in magnetron sputtering chamber and the location of Cu target.

### 3.2.2 Incipient wetness impregnation method

**Figure 8** shown the Cu/TiO<sub>2</sub> catalysts were prepared by incipient wetness impregnation methods. A Copper (II) nitrate trihydrate (Cu(NO<sub>3</sub>)<sub>2</sub>·3H<sub>2</sub>O) was used as a precursor of Cu metal. The Copper(II) nitrate trihydrate was dissolved in aqua. The precursor solution was dropped into 2 g of P25-TiO<sub>2</sub> support. Then, the Cu/TiO<sub>2</sub> catalyst was dried at ambient temperature for 3h and dried in an oven at 110 °C overnight in air. After that, the Cu/TiO<sub>2</sub> catalyst was calcined in air at 400 °C, heating rate 10 °C/min for 2 h. The Cu/TiO<sub>2</sub> catalysts were obtained. The other phase of TiO<sub>2</sub> support including anatase and rutile were used respectively.

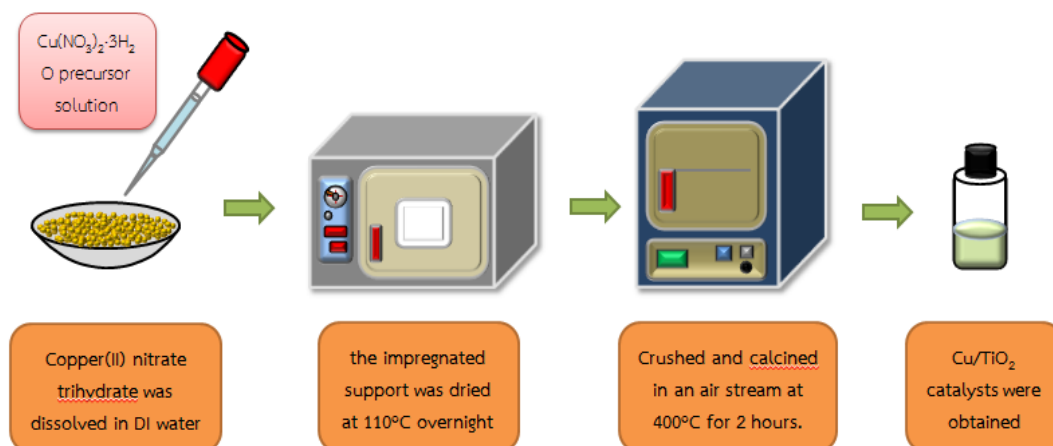


**Figure 8** Schematic of incipient wetness impregnation method for preparation of Cu/TiO<sub>2</sub> nanoparticles.

### 3.3 Catalyst characterization technique

The characterization technique was used to verify the characteristic of catalyst structure and texture properties.

#### 3.3.1. X-ray diffraction (XRD)

The X-ray diffraction (XRD) patterns were analyzed by X-ray diffractometer (Bruker D8 Advance) using Cu K $\alpha$  irradiation at a range between 20° and 80° with a step of 0.05° s<sup>-1</sup>. The lattice parameter and d-spacing were calculated based on Bragg's law. Crystallite size was calculated by the Scherrer equation.

#### 3.3.2. Surface Area Measurement

The surface area of the catalyst was determined by N<sub>2</sub>-TPD using a BEL-SORP automated system. 50 mg of catalysts were packed in a cell of sample and treated in N<sub>2</sub> at 200 °C for 1 h for removed moistness before cooling down to 30 °C. For adsorption, 15 mL/min of N<sub>2</sub> was applied through the sample. Then, added liquid nitrogen in the basin which cell of the sample was installed and waited until baseline stable. Push peak area button, the adsorption area was obtained. After that,

put out of the basin and waited until the baseline stable. Push peak area button, the desorption area was obtained.

### **3.3.3. UV-VIS Spectroscopy (UV-VIS)**

The band gap of the catalyst was determined by UV-VIS Spectroscopy using LAMDA 650 UV/Vis spectrophotometer. The spectrophotometer was scanned around a wavelength of 200–900 nm and obtained by UV Win Lab software from Perkin-Elmer. 1 g of catalysts were analyzed. Measures the absorption of light across the ultraviolet and visible light wavelengths through a sample. After that, UV-VIS shows diffuse reflectance spectra of catalysts. Its exhibited the absorption edge was assigned to the intrinsic band gap.

### **3.3.4. X-ray photoelectron spectroscopy (XPS)**

XPS was used to investigate the binding energy and surface composition of catalysts by using an AMICUS photoelectron spectrometer equipped with Mg K $\alpha$  X-ray source as a primary excitation. XPS elemental spectra were acquired with a 0.1 eV energy step at a pass energy of 75 eV. The binding energy was calibrated by the C 1s peak at 285.0 eV. The computer controlled by using the KRATOS VISION2 software.

### **3.3.5. Scanning electron microscope (SEM-EDX)**

The elemental distribution on a surface of the catalysts was investigated with SEM-EDX using Link Isis series 300 program SEM (JEOL model JSM-5800LV). Generally, SEM will connect with energy dispersive X-ray spectroscopy (EDX). Which measured the number of metal particles on the surface of sample.

### **3.3.6. Inductively coupled plasma (ICP)**

The amount of elements in the bulk of the catalyst was analysed by Inductively coupled plasma using Perkin Elmer Optima 7000DV. It can analyze many elements simultaneously. Liquid samples were prepared by dissolved 80 mg of

catalysts in sulfuric acid solution. The ICP operated by energy from inductively coupled plasma, it made an atom of elements changed from ground state to excited state or to be ions. When it returned to a ground state, ions emitted light at different characteristic wavelengths which can measure quantitative analysis by comparing with a standard solution.

### 3.3.7. photoluminescence spectroscopy (PL)

photoluminescence spectroscopy used for the identification of impurities that produce radiative recombination by using FluoroMax 4+ Model. Using a laser beam to irradiate a substance after that light discharged from a substance during it drops from the excited state to ground state was captured by a laser beam. By measuring the luminescence spectrum, it used to observe electron-hole combination rate.

### 3.3.8. transmission electron microscope (TEM)

The morphology of catalysts on a surface of the catalysts was investigated with the transmission electron microscope (TEM) using a JEOL-JEM 2010. TEM using energy-dispersive X-ray detector operated at 200kV. TEM might connect with energy dispersive X-ray spectroscopy (EDX). Which measured the number of metal particles on the surface of sample for confirmation types of elemental.

## 3.4 Photocatalytic activity reaction on CO<sub>2</sub> reduction and H<sub>2</sub>O

The photocatalytic reaction experiment on the photocatalytic reduction of CO<sub>2</sub> with water was carried in a photoreactor system as shown in **Figure 1**. UV-light bulbs (Philips' Germicidal Ozone UV Quartz Glass UVC Bulb: 16 watt, 6 bulbs) were installed around a cylindrical quartz reactor. Cu/TiO<sub>2</sub> catalyst 0.5 g was suspended into a stirred batch reactor by a magnetic stirrer which contained 150 mL of deionized water. Then, ultra-pure gaseous CO<sub>2</sub> was bubbled into the cylindrical

quartz reactor at  $100 \text{ ml min}^{-1}$  for 30 min to purge air and saturate the water with  $\text{CO}_2$ . After that, the reactor was pressurized with  $\text{CO}_2$  at 1 bar and closed during the reaction throughout the experiment. The photocatalytic reaction was started by turning on the UV light, and irradiation was continued for 6 h.

The resultant gas samples were analyzed every 6 hours by using an on-line GC-14B (Shimadzu) gas chromatograph equipped with a flame-ionization detector (FID) and a shincarbon column for hydrocarbon analysis.

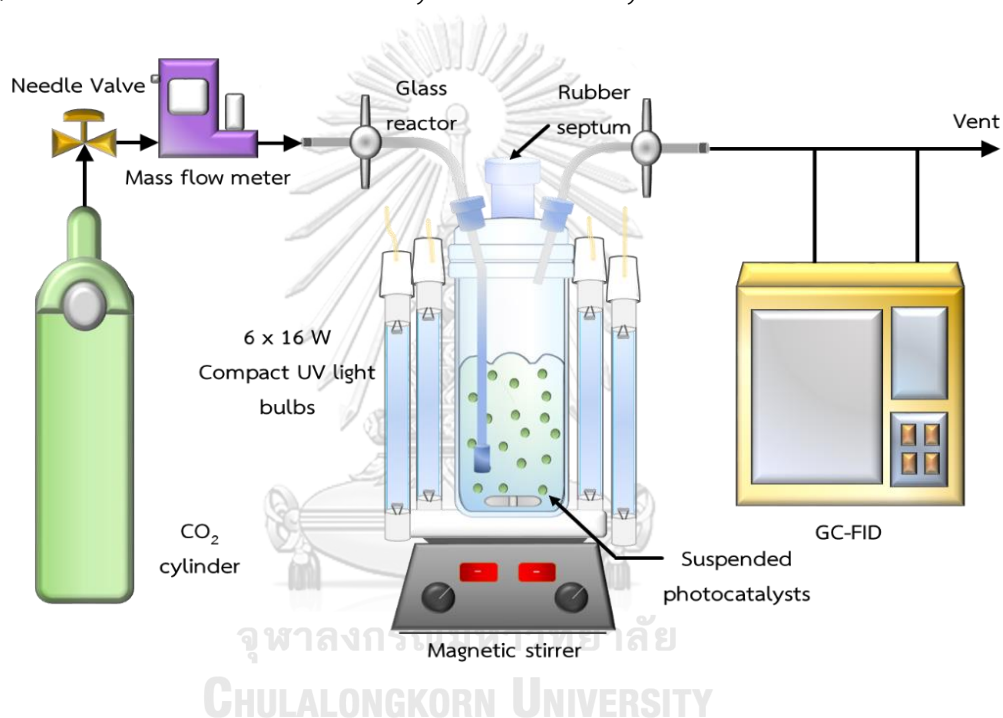


**Figure 9** Schematic diagram of the experimental system for photocatalytic reduction of  $\text{CO}_2$ .

The calculation of hydrocarbon production is determined by using the following equation which is the production rate of methane.

$$\text{Yield of methane} = \left[ \frac{\text{Mole fraction of methane}}{(\text{hour of testing})(\text{amount of catalyst})} \times \text{Volume of CH}_4 \right]$$

## CHAPTER IV

### RESULTS AND DISCUSSION

This chapter discusses the characteristics and photocatalytic properties of unmodified TiO<sub>2</sub> and Cu-modified TiO<sub>2</sub> catalysts prepared by the incipient wetness impregnation method and the magnetron sputtering method. The results and discussions in this chapter are separated into three sections. The first section describes the influence of Cu loading on TiO<sub>2</sub> catalysts synthesized by incipient wetness impregnation method for photocatalytic reduction of CO<sub>2</sub> and H<sub>2</sub>O into methane. The second section describes the influence of Cu loading on TiO<sub>2</sub> catalysts synthesized by magnetron sputtering method. Finally, the tertiary section compared the photocatalytic activity of Cu/TiO<sub>2</sub> catalysts for photocatalytic reduction of CO<sub>2</sub> and H<sub>2</sub>O into methane with both preparations. All catalysts were analyzed by XRD, N<sub>2</sub>-physisorption, ICP, XPS, PL emission spectra, UV-vis, SEM-EDX, and TEM. To convenient for discussion, the specimen designation of catalysts were given in **Table 3**.

**Table 3** The specimen designation of the catalysts in this work.

Sign	Detail of sign
P25-TiO <sub>2</sub>	The TiO <sub>2</sub> commercial catalyst P25 (Degussa).
Ana-TiO <sub>2</sub>	The TiO <sub>2</sub> commercial catalyst in Anatase phase.
Rut-TiO <sub>2</sub>	The TiO <sub>2</sub> commercial catalyst in Rutile phase.
SP1-P25	Sputtered Cu/P25 catalyst at 2.5 min.
SP2-P25	Sputtered Cu/P25 catalyst at 5.0 min.
SP3-P25	Sputtered Cu/P25 catalyst at 7.5 min.
SP1-Ana	Sputtered Cu/Anatase catalyst at 2.5 min.
SP2-Ana	Sputtered Cu/Anatase catalyst at 5.0 min.
SP3-Ana	Sputtered Cu/Anatase catalyst at 7.5 min.
SP1-Rut	Sputtered Cu/Rutile catalyst at 2.5 min.
SP2-Rut	Sputtered Cu/Rutile catalyst at 5.0 min.
SP3-Rut	Sputtered Cu/Rutile catalyst at 7.5 min.
IM1-P25	Impregnated Cu/P25 catalyst at 1.00 wt%
IM2-P25	Impregnated Cu/P25 catalyst at 2.12 wt%
IM3-P25	Impregnated Cu/P25 catalyst at 3.25 wt%
IM1-Ana	Impregnated Cu/Anatase catalyst at 0.47 wt%
IM2-Ana	Impregnated Cu/Anatase catalyst at 1.00 wt%
IM3-Ana	Impregnated Cu/Anatase catalyst at 1.69 wt%
IM1-Rut	Impregnated Cu/Rutile catalyst at 0.72 wt%
IM2-Rut	Impregnated Cu/Rutile catalyst at 1.64 wt%
IM3-Rut	Impregnated Cu/Rutile catalyst at 2.65 wt%



#### 4.1 Influence of Cu loading on TiO<sub>2</sub> catalysts synthesized by magnetron sputtering method for photocatalytic reduction of CO<sub>2</sub> and H<sub>2</sub>O into methane

The purpose of this section was to describe the physiochemical and photocatalytic properties of nanocrystalline TiO<sub>2</sub> powder varied Cu loading contents. In addition, we also investigated the effects of TiO<sub>2</sub> support including anatase, rutile, and Degussa P25 to the photocatalytic reduction of CO<sub>2</sub> and H<sub>2</sub>O into methane.

In order to describe correlation of catalytic efficiency with the catalytic properties, the catalysts were detected by various characterization techniques such as the X-ray diffraction (XRD), N<sub>2</sub>-physisorption, UV-Vis spectroscopy (UV-vis), Transmission electron microscopy (TEM), X-ray photoelectron spectrometer (XPS), PL emission spectra, Scanning electron microscopy (SEM), and Energy dispersive X-ray spectroscopy (EDX).

The Cu/TiO<sub>2</sub> catalysts synthesized by magnetron sputtering method were referred to as SP. This method was one of the preparations, which catalyst have a specific characteristic effect to a reaction as follows.

##### 4.1.1 Powder X-ray diffraction (XRD)

The XRD diffraction pattern of Cu deposited on P25-TiO<sub>2</sub> catalysts are shown in **Figure 10** All Cu/P25(SP) catalysts prepared by magnetron sputtering method exhibited the main characteristic peak of anatase phase that located at  $2\theta = 25.3$  (101), 37.8 (004), 48.0 (200), 54.5, (105 and 211), and 62.8 (213) and the rutile phase located at  $2\theta = 27.5(110)$ , 36.1(101), 54.4(211). The main diffraction peak of the anatase (101) and rutile (110) located at  $2\theta = 25.3$  and 27.5, respectively. In the case of Cu deposited on Ana-TiO<sub>2</sub> catalysts shown in **Figure 11**, only the characteristic peaks of the anatase phase were observed. In addition, the peaks of the rutile phase were only observed for Cu deposited on Rut-TiO<sub>2</sub> catalysts as shown in **Figure 12** XRD patterns of all Cu/TiO<sub>2</sub> (SP) catalysts after loading with Cu did not show any

peak of Cu/CuO phases. This is perhaps due to the slight Cu loading content, the extremely small Cu clusters and/or high dispersion of Cu/CuO on the TiO<sub>2</sub> supports.

The average crystallite sizes of the TiO<sub>2</sub> samples were determined from the full-width at half maximum of the anatase (101) and rutile (110) peaks calculated by the Scherrer's equation. The Cu/P25 (SP) samples exhibited the same patterns with an average crystallite size of anatase phase and rutile phase in the range of 19-20 nm and 23-25 nm, respectively. The Cu/Ana (SP) samples exhibited the same patterns with an average crystallite size of the anatase phase in the range of 18-20 nm. The Cu/Rut (SP) samples exhibited the same patterns with an average crystallite size of the rutile phase in the range of 15-23 nm. The crystallite size of the anatase phase and rutile phase of TiO<sub>2</sub> support are shown in **Table 4**. This demonstrated that the preparation methods did not affect the crystal structure, crystallite size of TiO<sub>2</sub>(SP) catalysts even after prolonging the sputtering time.

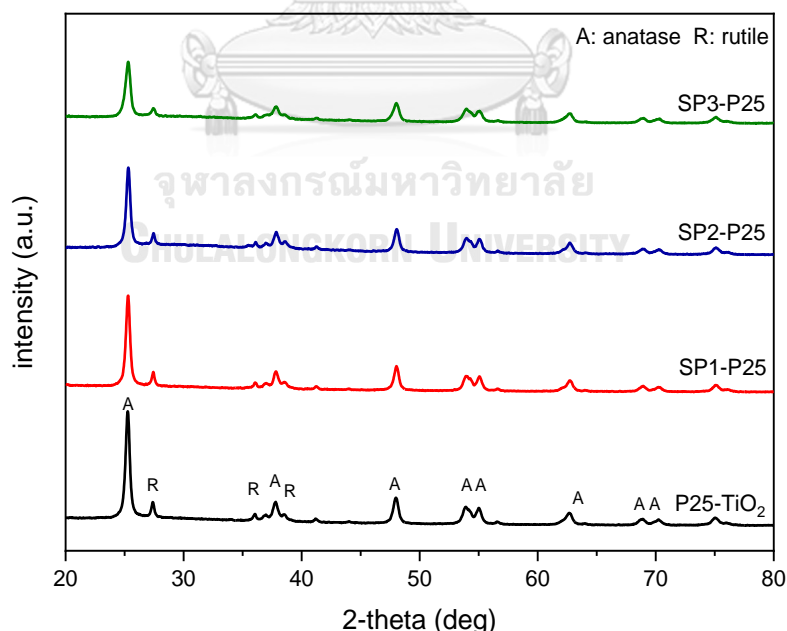


**Figure 10** XRD patterns of Cu/P25 (SP) catalysts.

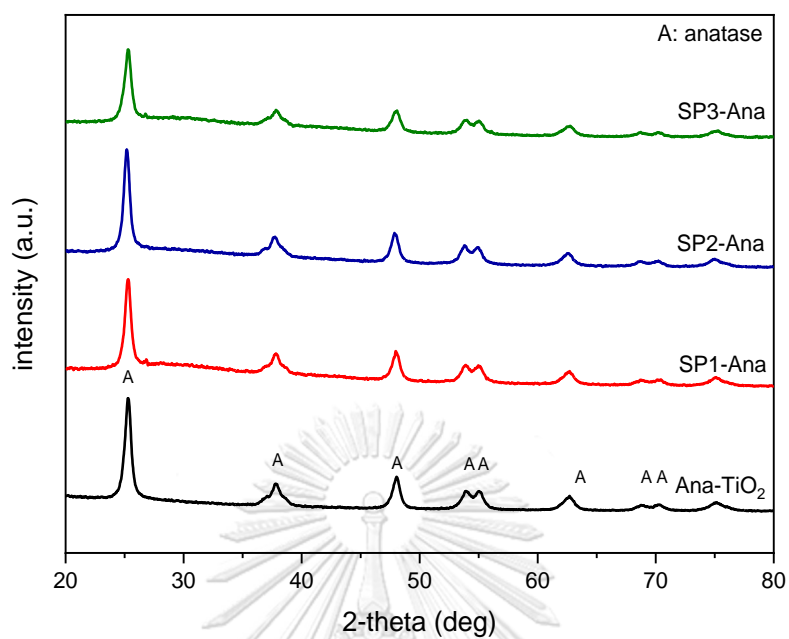


Figure 11 XRD patterns of Cu/Ana (SP) catalysts.

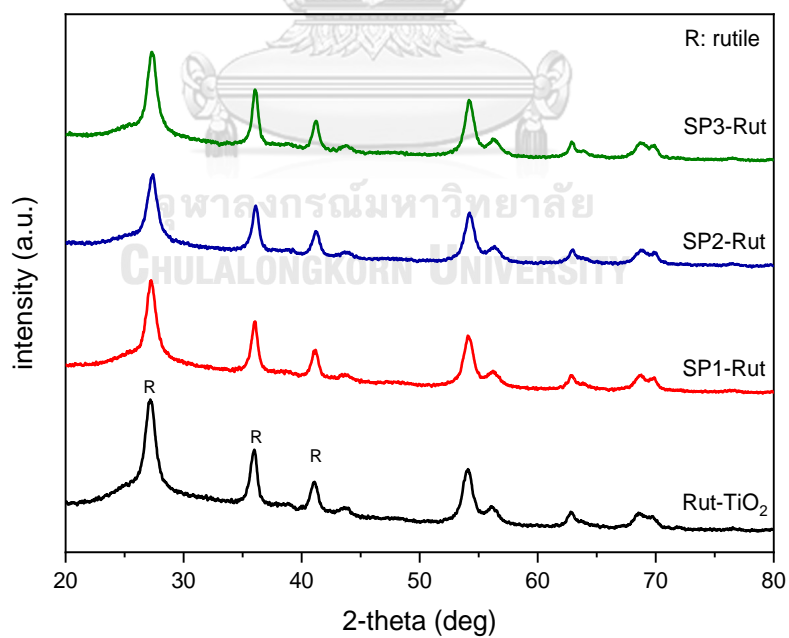
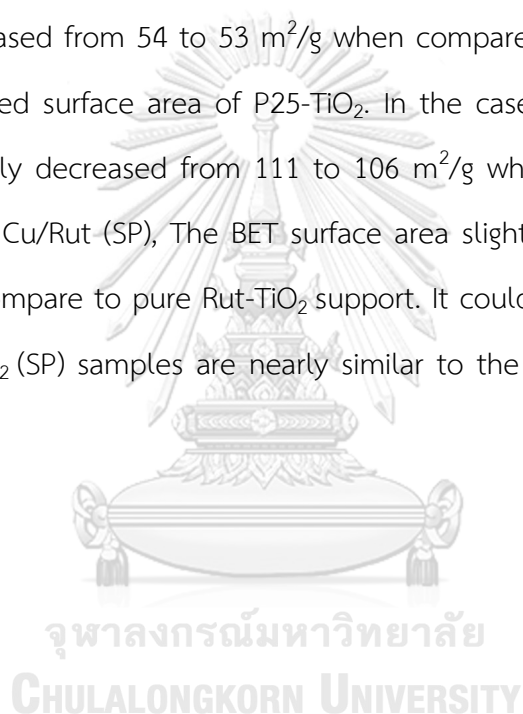


Figure 12 XRD patterns of Cu/Rut (SP) catalysts.

#### 4.1.2 Surface Area Measurement

This characterization techniques were to describe the specific surface area, pore volume, and pore size. The specific surface area refers to the activity of the photocatalysts due to photocatalytic reactions occur at the surface of the photocatalyst, when the high specific surface areas of photocatalysts will promote the activity of reaction which increased the production rate of methane.

The specific surface area of TiO<sub>2</sub> support and Cu deposited on TiO<sub>2</sub> prepared by magnetron sputtering method exhibited in **Table 4** The BET surface area of Cu/P25 (SP) slightly decreased from 54 to 53 m<sup>2</sup>/g when compare to pure P25-TiO<sub>2</sub> support because Cu blocked surface area of P25-TiO<sub>2</sub>. In the case of Cu/Ana (SP), The BET surface area slightly decreased from 111 to 106 m<sup>2</sup>/g when compare to pure Ana-TiO<sub>2</sub> support. And Cu/Rut (SP), The BET surface area slightly decreased from 171 to 169 m<sup>2</sup>/g when compare to pure Rut-TiO<sub>2</sub> support. It could be seen that the surface area of all Cu/TiO<sub>2</sub> (SP) samples are nearly similar to the surface area of pure TiO<sub>2</sub> support.



**Table 4** Physical properties of the sputtered catalysts.

Catalyst	<sup>a</sup> Crystallite size (nm)		<sup>b</sup> Surface area (m <sup>2</sup> /g)	<sup>c</sup> band gap energy (eV)
	Anatase	Rutile		
P25-TiO <sub>2</sub>	20	23	54	3.21
SP1-P25	19	25	53	3.09
SP2-P25	18	24	54	3.04
SP3-P25	19	23	54	3.01
Ana-TiO <sub>2</sub>	20	-	111	3.23
SP1-Ana	18	-	110	3.21
SP2-Ana	20	-	110	3.2
SP3-Ana	19	-	106	3.16
Rut-TiO <sub>2</sub>	-	23	171	3.17
SP1-Rut	-	21	169	3.14
SP2-Rut	-	17	170	3.09
SP3-Rut	-	15	169	3.06

<sup>a</sup> Average crystalline size was determined by XRD using Scherrer equation.

<sup>b</sup> The BET surface area was determined by single point BET method.

<sup>c</sup> band gap energy was calculated by UV-visible absorption spectra.

#### 4.1.3 UV-vis spectrometer

The UV-vis absorption spectra of all the sputtered catalysts compare with pure TiO<sub>2</sub> supports are presented in **Figure 13-15** respectively. The absorption spectra of Cu modified TiO<sub>2</sub> catalysts can separate into three phases, including the sharp absorption band at wavelengths less than 400 nm, which were associated with the band structure of the original TiO<sub>2</sub> supports, the absorption band in 700–800 nm region, due to the Cu d-d transition, and an absorption tail in the 400–500 nm region, which was associated with the interfacial charge transfer (IFCT) phenomenon between TiO<sub>2</sub> valence band electrons and Cu(II) species.

The sputtered catalysts obviously appeared of typical adsorption bands of TiO<sub>2</sub> and Cu nanoparticles but the absorption tail between 400 and 500 nm presented to IFCT was much less evident. That indicated the formation between Cu nanoparticles and the TiO<sub>2</sub> support were less interaction.

The band gap energy ( $E_{bg}$ ) of all the Cu/TiO<sub>2</sub> catalysts were obtained from the extrapolation of Tauc plots of  $(h\nu\alpha)^{1/2}$  as a function of photon energy ( $h\nu$ ) and the obtained results are also shown in **Table 4** It was investigated that increasing of Cu doping content also slightly reduced the band gap energy. The lowering of  $E_{bg}$  leads to Fermi level reducing, improving the photosensitivity of the catalysts and improving an absorption edge in the visible light region (400–700 nm).

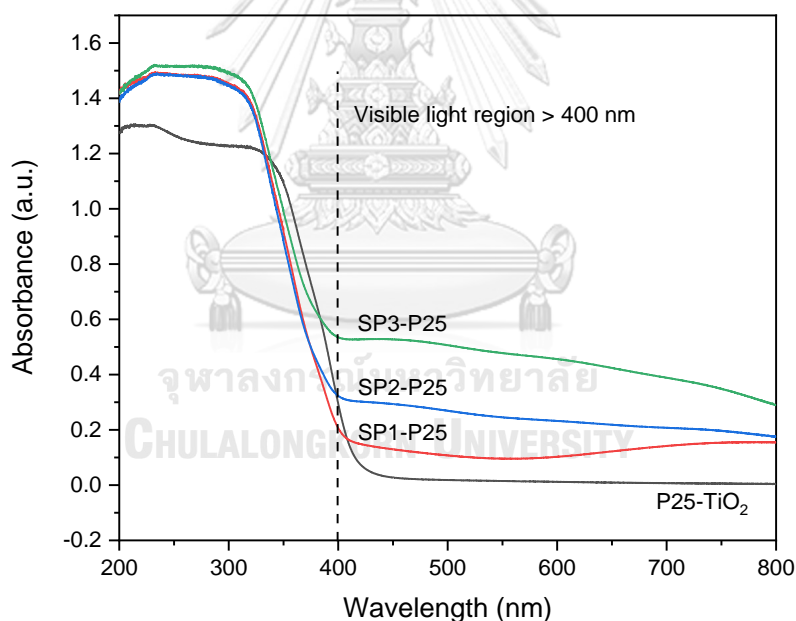


**Figure 13** The UV-Vis absorption spectra of Cu/P25 (SP) catalysts.

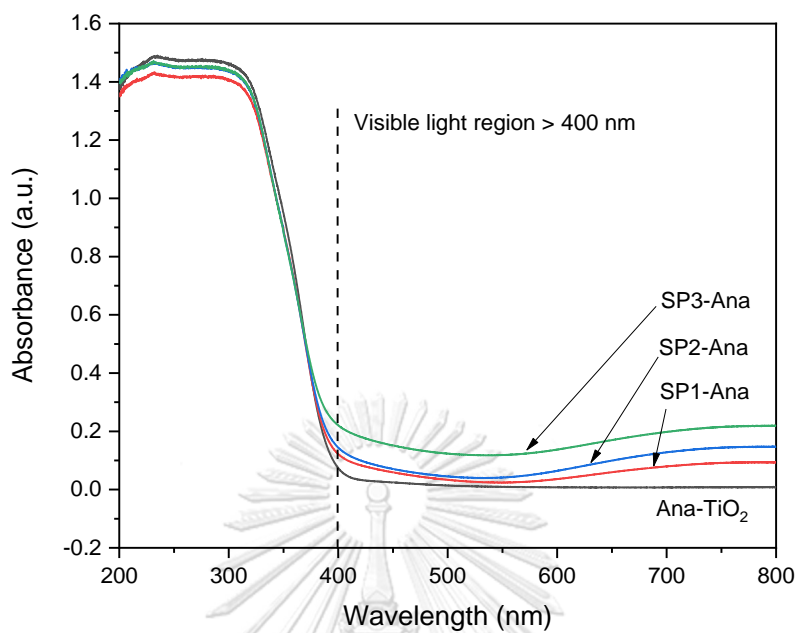


Figure 14 The UV-Vis absorption spectra of Cu/Ana (SP) catalysts.

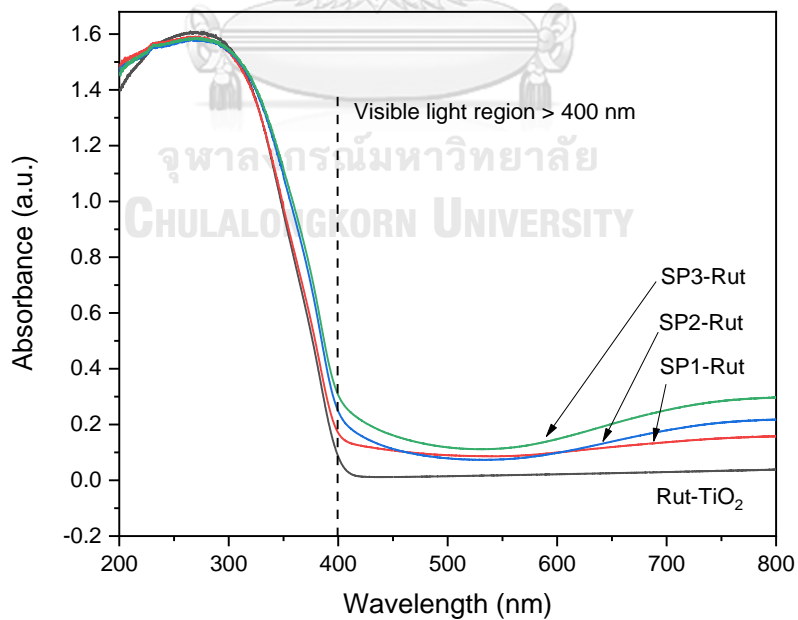
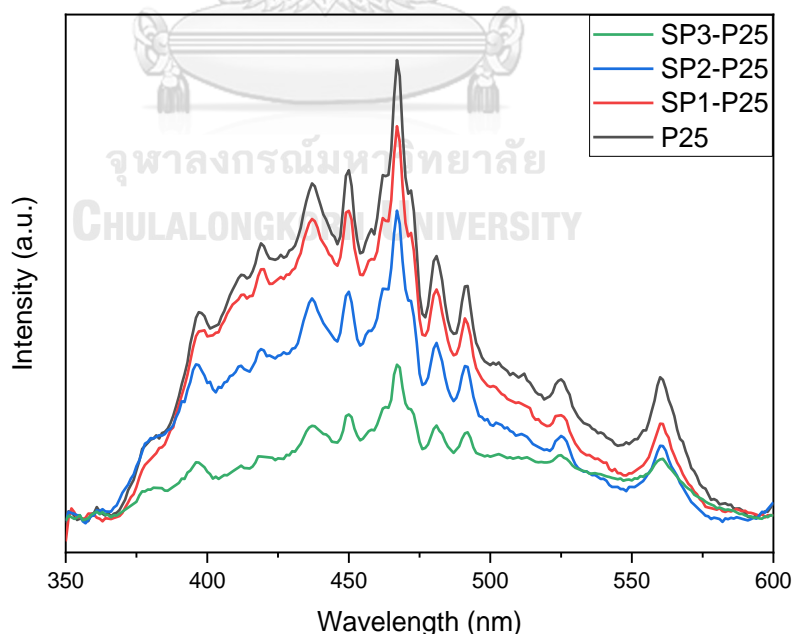


Figure 15 The UV-Vis absorption spectra of Cu/Rut (SP) catalysts.

#### 4.1.4 photoluminescence (PL)

photoluminescence (PL) is a technique for measured the electronic properties of semiconductor to determine the efficiency of photocatalysts such as charge carrier trapping, carrier lifetime and recombination of  $e^-h^+$  pairs. The PL emission spectra of all Cu/TiO<sub>2</sub> catalysts prepared by magnetron sputtering method are shown in **Figure 16-18** respectively.

There are many peaks can be detected from PL consist of the signals at 436 nm was corresponded to the self-trapped electron localized on TiO<sub>6</sub> octahedral complex[63], and peaks at 469, 484, 492 nm was corresponded to the oxygen vacancies with two trapped electrons on TiO<sub>2</sub> surface [64, 65]. The emission spectra of the Cu modified TiO<sub>2</sub> was observed after Cu deposition, PL emission spectra decreased as Cu loading content increased. The lower emission intensity due to the Cu nanoparticles trapped photoelectron from the conduction band of TiO<sub>2</sub> and retarded recombination of charge carrier process.



**Figure 16** The PL emission spectra of Cu/P25 (SP) catalysts.



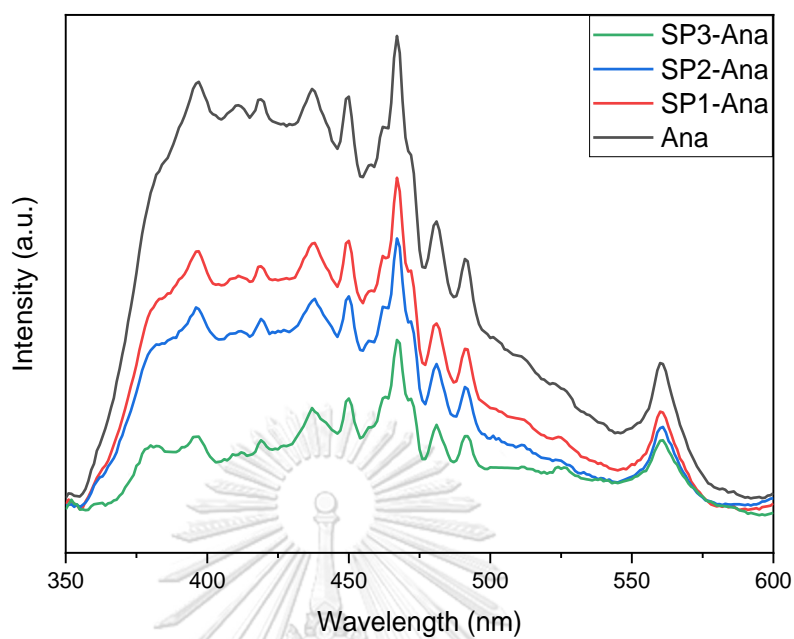


Figure 17 The PL emission spectra of Cu/Ana (SP) catalysts.

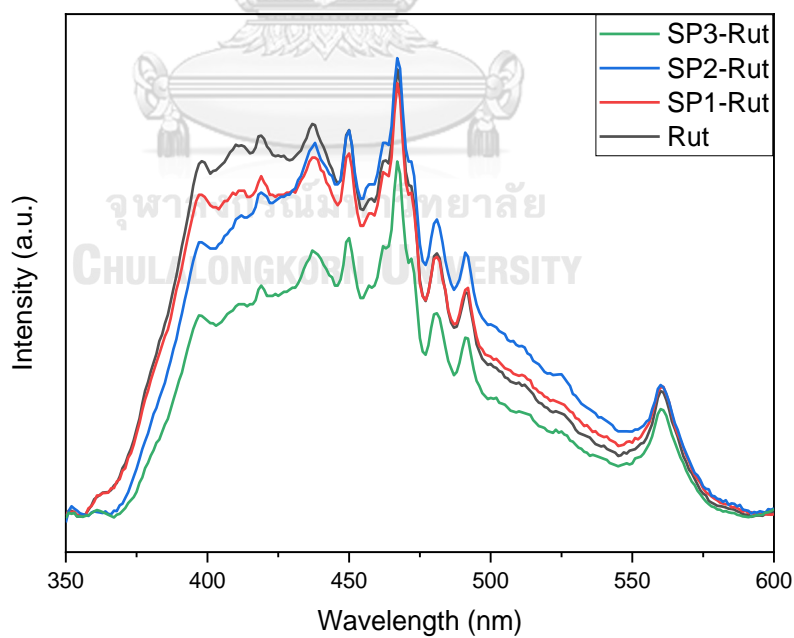
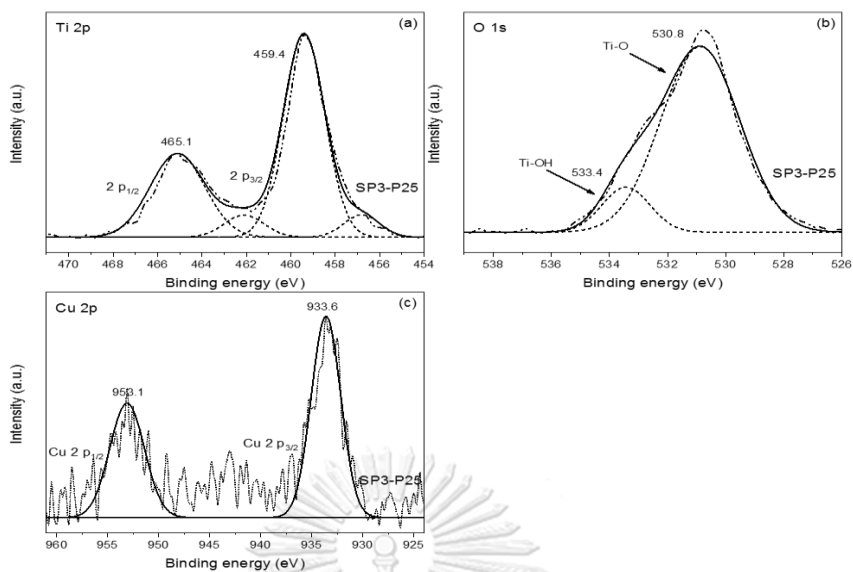


Figure 18 The PL emission spectra of Cu/Rut (SP) catalysts.

#### 4.1.5 X-ray photoelectron spectrometer (XPS)

X-ray photoelectron spectrometer (XPS) is a technique to determine the composition of the element on surface and electronic state. The XPS spectra of Ti 2p, O1s, and Cu2p of all Cu/TiO<sub>2</sub> catalysts prepared by magnetron sputtering method are shown in **Figure 19-21** respectively. For Cu/P25 (SP) catalysts, the peaks located at around 456.8 and 462.1eV have corresponded to the Ti<sup>3+</sup> 2p<sub>3/2</sub> and Ti<sup>3+</sup> 2p<sub>1/2</sub>, respectively [66, 67], the other peaks at around 459.4 and 465.1 eV have corresponded to Ti<sup>4+</sup> 2p<sub>3/2</sub> and Ti<sup>4+</sup> 2p<sub>1/2</sub>, respectively [68-70]. In XPS spectra of O1s, the peak at 530.8 and 533.4 eV is corresponded as the Ti-O and OH-[71]. And XPS spectra of Cu2p, there are two peaks at around 933.6 and 953.1 eV, it is suggested that the Cu peaks around this area indicated to CuO [72].

For all Cu/TiO<sub>2</sub> (SP) catalysts, it is assigned that the characteristic peaks of Ti2p and O1s did not different after modified with Cu doping with magnetron sputtering method. However, catalyst compositions (%) of sputtered catalysts are shown in **table 5** It presented the amount of Cu increased in the order of P25 > anatase > rutile phase.



**Figure 19** The X-ray photoelectron spectra of SP3-P25 catalyst is simulated by Gaussian equation; XPS spectra of Ti2p (a), XPS spectra of O1s (b), and XPS spectra of Cu2p.

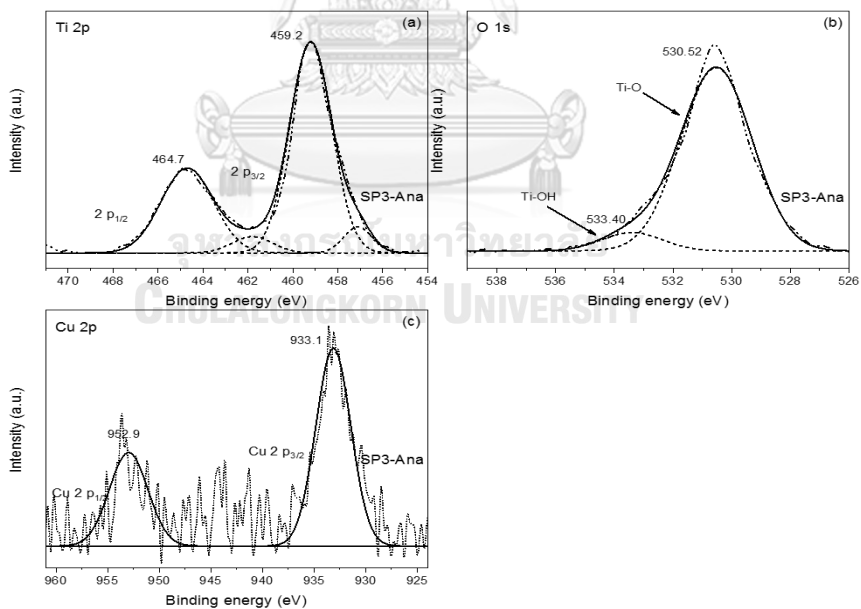


**Figure 20** The X-ray photoelectron spectra of SP3-Ana catalyst is simulated by Gaussian equation; XPS spectra of Ti2p (a), XPS spectra of O1s (b), and XPS spectra of Cu2p.

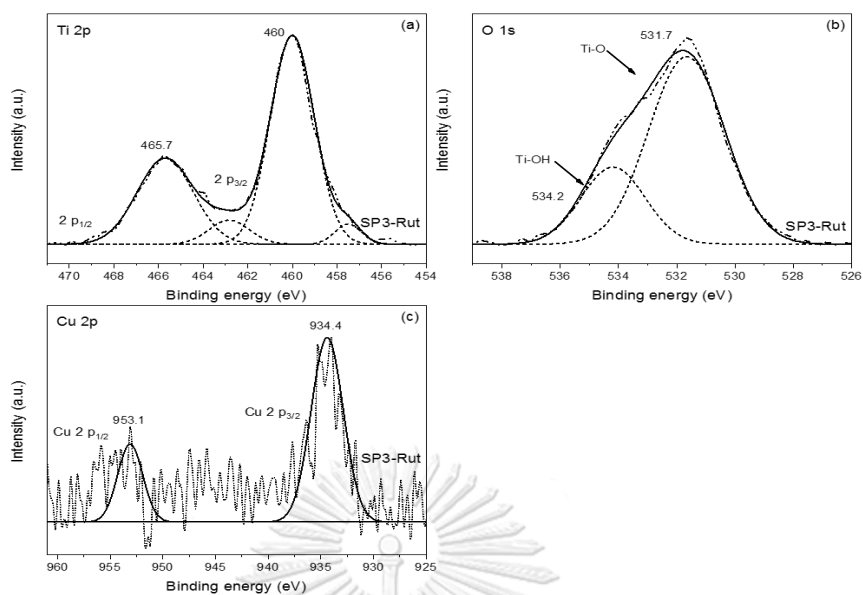


**Figure 21** The X-ray photoelectron spectra of SP3-Rut catalyst is simulated by Gaussian equation; XPS spectra of Ti2p (a), XPS spectra of O1s (b), and XPS spectra of Cu2p.

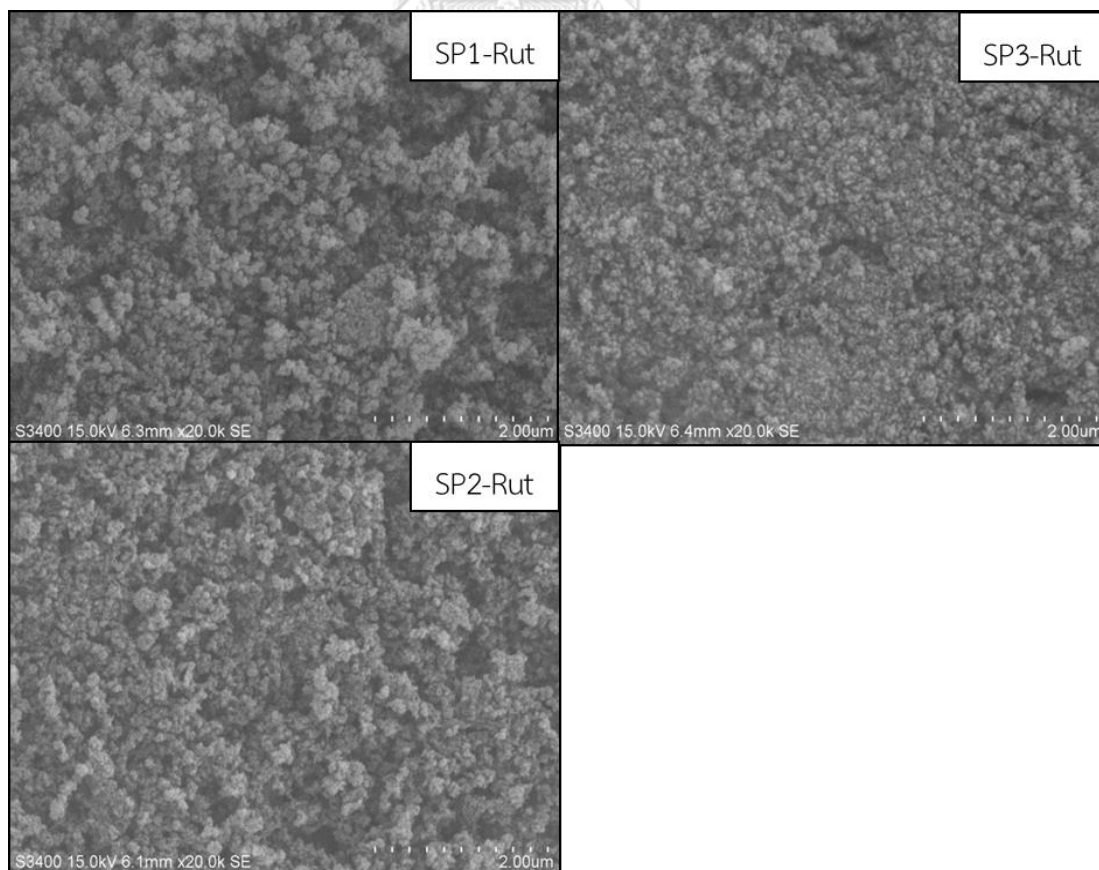
**Table 5** Catalyst compositions (%) of sputtered catalysts.

Catalyst	Catalyst compositions (%)			Catalyst compositions of Ti (%)	
	Cu	Ti	O	Ti <sup>3+</sup>	Ti <sup>4+</sup>
SP3-P25	5.05	74.89	20.06	8.71	91.29
SP3-Ana	3.69	72.92	23.39	7.76	92.24
SP3-Rut	2.50	82.33	15.17	5.49	94.51

#### 4.1.6 Scanning electron microscopy and Energy Dispersive X-ray Spectroscopy (SEM-EDX)

**Figure 22** presented the morphology of Cu particles adhered onto all types of  $\text{TiO}_2$  support. The micrographs exhibited dispersion of Cu nanoparticles on Cu/P25 (SP), Cu/Ana (SP), and Cu/Rut (SP) respectively. It distinctly showed the agglomeration of spherical nanoparticles and the form of P25- $\text{TiO}_2$  supports is not much difference from modified with Cu nanoparticles and each other support, which prepared by magnetron sputtering method.

In addition, the EDX technique was used to reveal the amount of %wt. Cu covered on  $\text{TiO}_2$  surface are shown in **Table 6** Amount of %wt. Cu on Cu-adhered onto  $\text{TiO}_2$  sample presented increasing of the Cu loading content, it is linearly with sputtering time. The amount of Cu increased in the order of P25 > rutile > anatase phase.



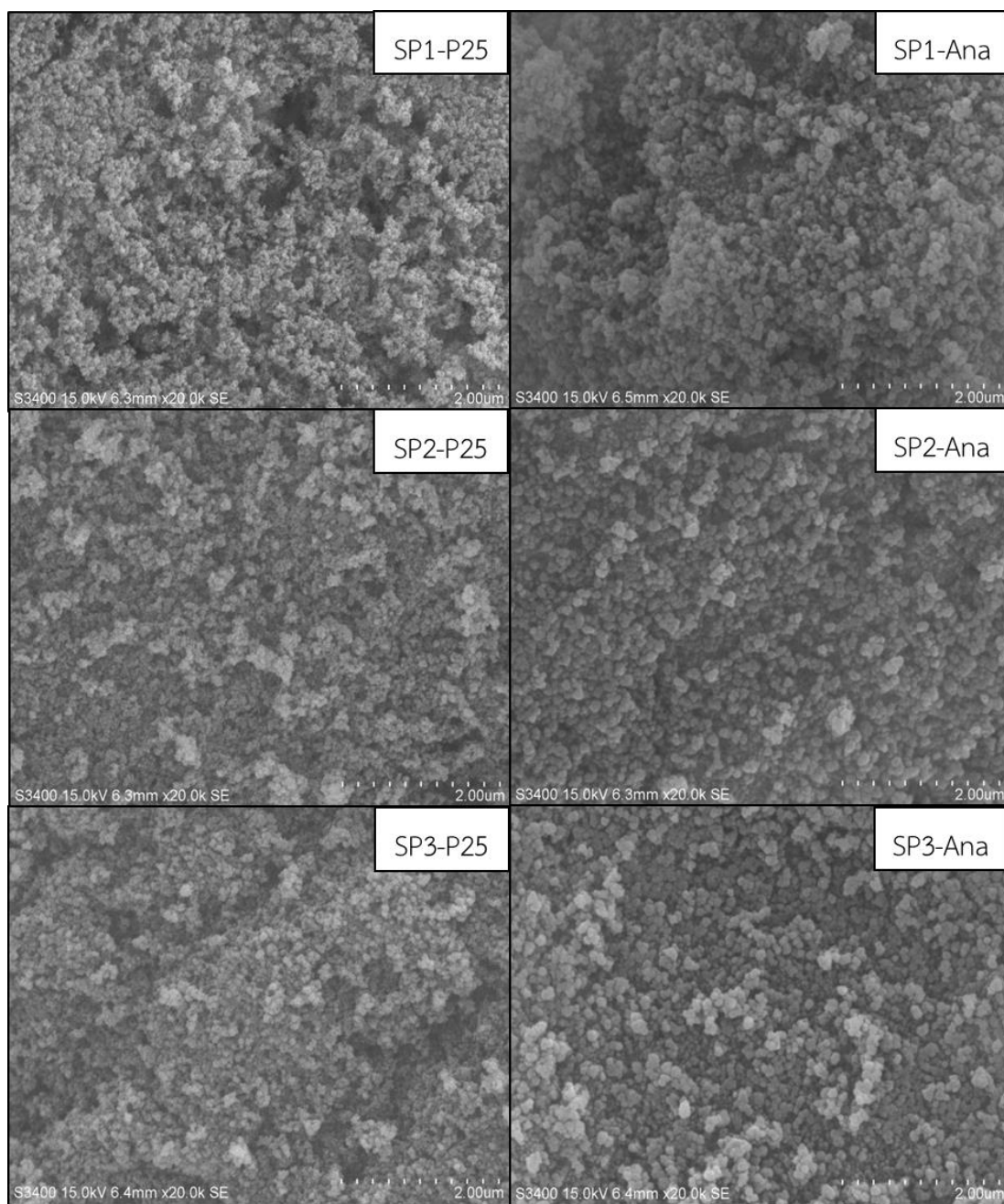


Figure 22 SEM of sputtered catalysts.

#### 4.1.7 Inductively coupled plasma (ICP)

The Cu doping content was measured by ICP techniques. ICP technique was used to reveal the amount of %wt. Cu in TiO<sub>2</sub> modified with Cu bulks. **Figure 23** clearly showed the amount of %wt. Cu in P25-TiO<sub>2</sub> modified with Cu samples higher was higher than those modified on other supports, including Rut-TiO<sub>2</sub> and Ana-TiO<sub>2</sub> respectively. And the Cu loading content increased linearly with increasing of the sputtering time.

Moreover, comparison of Cu doping content on all TiO<sub>2</sub> support measured by the ICP and EDX techniques shown in **Table 6** It can be seen that the Cu loading content measured by EDX technique was higher than the ICP technique. It demonstrated that Cu doping content covered on TiO<sub>2</sub> surfaces more than absorbed in TiO<sub>2</sub> pores.

**Table 6** Comparison of Cu doping content on TiO<sub>2</sub> support prepared by magnetron sputtering method.

Catalyst	Wt% of Cu	
	ICP	EDX
SP1-P25	0.73	4.89
SP2-P25	1.44	5.96
SP3-P25	2.21	7.77
SP1-Ana	0.33	2.06
SP2-Ana	0.65	4.17
SP3-Ana	1.18	5.50
SP1-Rut	0.52	3.45
SP2-Rut	1.18	5.13
SP3-Rut	1.91	6.52

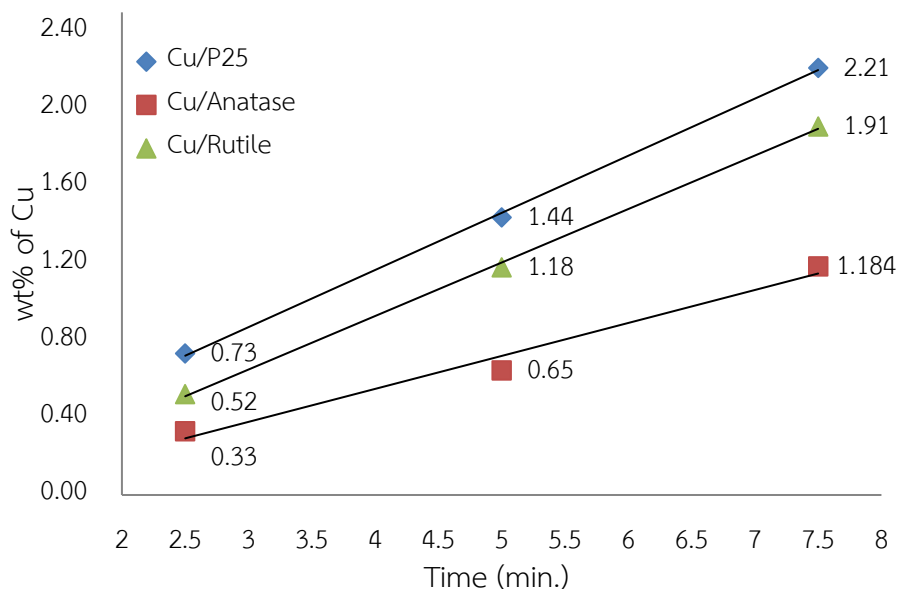


**Figure 23** %Wt. of Cu-adhered onto P25-TiO<sub>2</sub>, Ana-TiO<sub>2</sub>, and Rut-TiO<sub>2</sub> supports prepared by magnetron sputtering method.

#### 4.1.8 Transmission electron microscopy (TEM)

The morphology and metal particles size of all the Cu/TiO<sub>2</sub> catalysts was determined by transmission electron microscopy. The TEM images of the Cu/TiO<sub>2</sub> (SP) catalysts are presented in **Figure 24-26**. The Cu/TiO<sub>2</sub> (SP) exhibited an irregular shape and well dispersion. The irregular metal particles were the specific structure of the deposited metal prepared by using the magnetron sputtering method. An average Cu particles size of Cu/P25 (SP) equals 3.75 nm, Cu/Ana (SP) equals 3.21 nm and Cu/Rut (SP) equals 3.44 nm [73, 74].



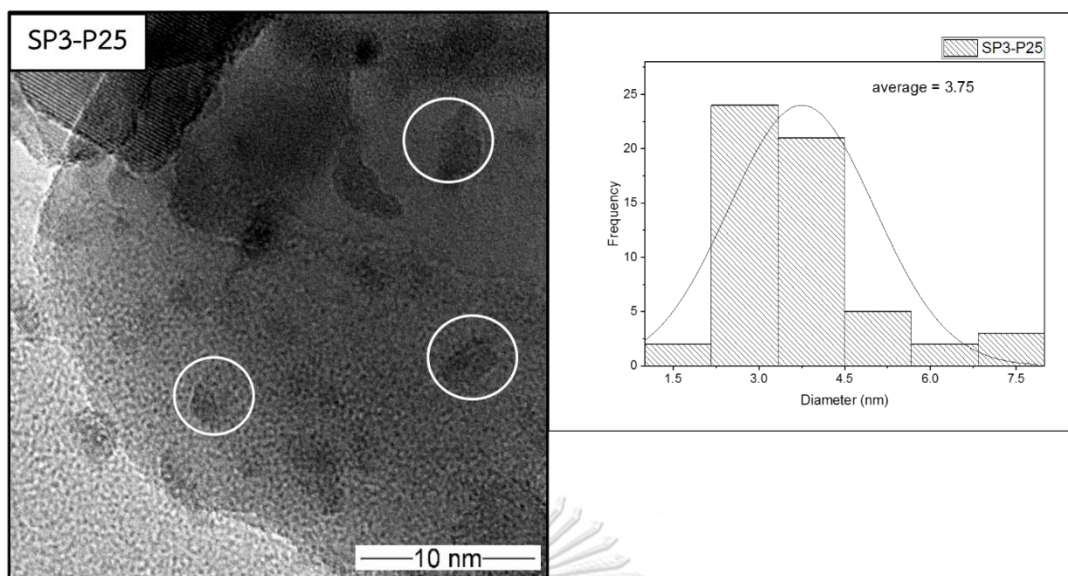


Figure 24 TEM and average Cu nanoparticle sizes of SP3-P25 catalyst.

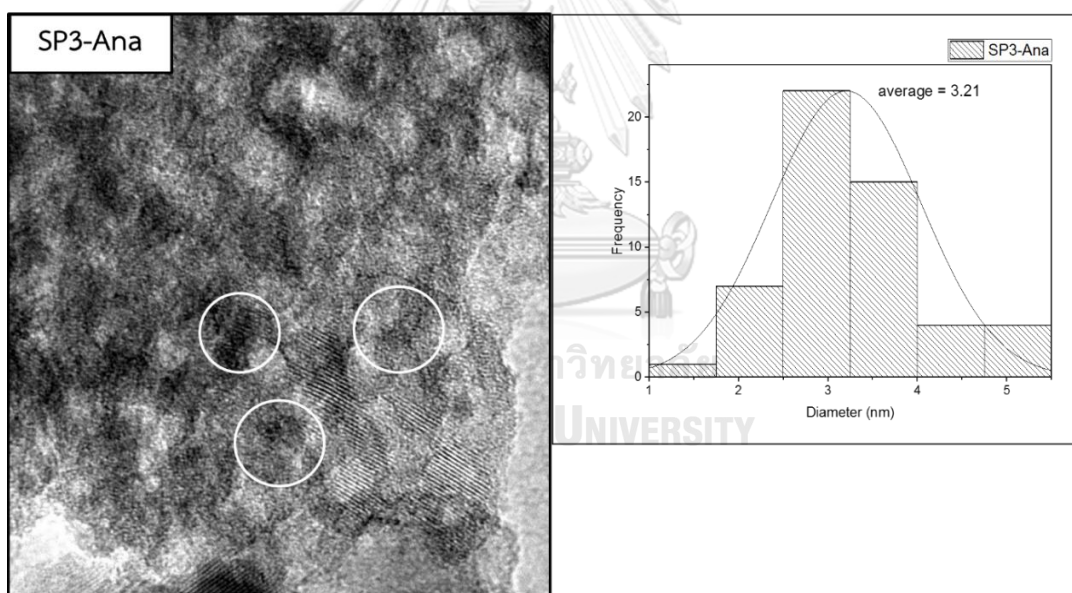
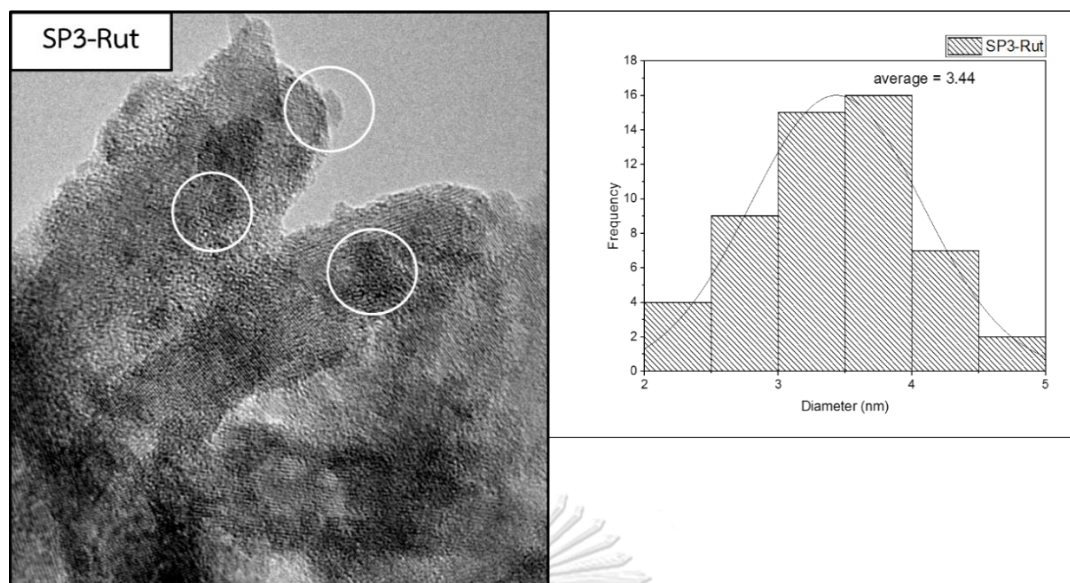


Figure 25 TEM and average Cu nanoparticle sizes of SP3-Ana catalyst.



**Figure 26** TEM and average Cu nanoparticle sizes of SP3-Rut catalyst.

#### 4.1.9 Photocatalytic activity of Cu/TiO<sub>2</sub> catalysts for photocatalytic reduction of CO<sub>2</sub> into methane.

The photocatalytic activity of all catalysts for photocatalytic reduction of CO<sub>2</sub> into methane under UV light is shown in **Figure 27**. For this experiment, methane was the main product obtained from all Cu/TiO<sub>2</sub> catalysts. The pure TiO<sub>2</sub> support showed relatively low activity under UV light irradiation. After doping with Cu on TiO<sub>2</sub> support, the photocatalytic activity of all sputtered catalysts are likely to increase the CH<sub>4</sub> production yield. Cu deposition can improve the photocatalytic performance of TiO<sub>2</sub> due to Cu clusters trapped photoelectron and retarded recombination of charge carrier process. The CH<sub>4</sub> production of Three types of support increased in the order of rutile > P25> anatase phase.

**Figure 28** showed the stability of SP3-P25 catalyst. The first round of the experiment showed the CH<sub>4</sub> production yield at 1.89. The stability of SP3-P25 catalyst slightly decreased after the second round and third round at 1.53 and 1.55, respectively.

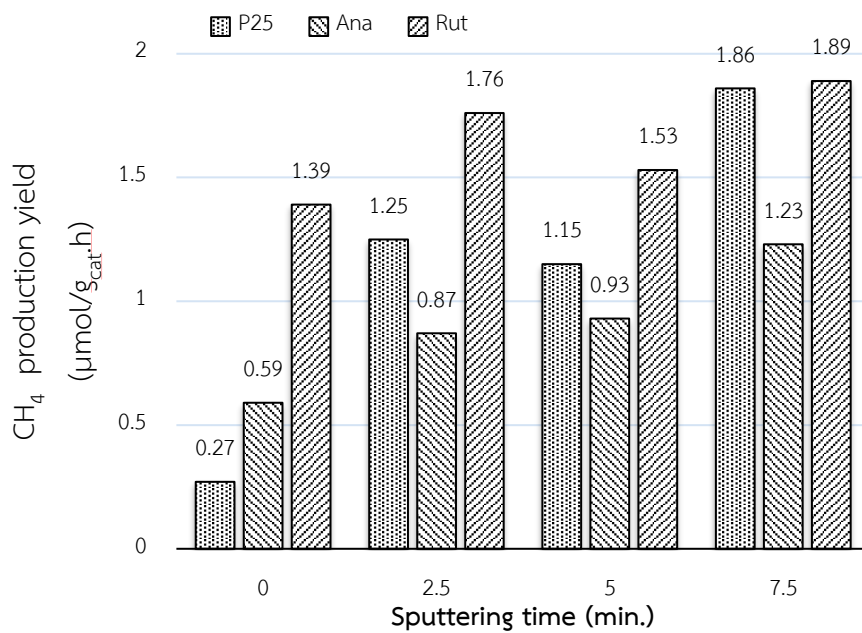


Figure 27 CH<sub>4</sub> production yield of sputtered catalysts.

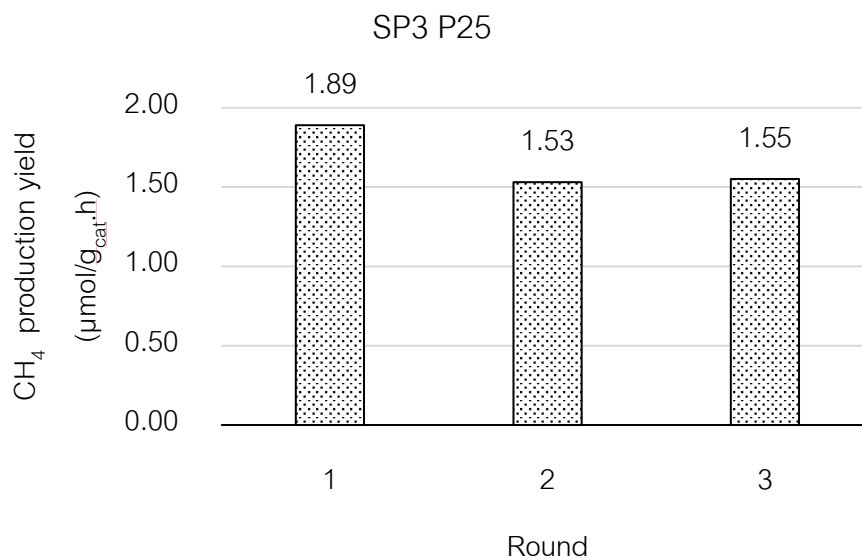


Figure 28 The stability of SP3-P25 catalyst.

## 4.2 Influence of Cu loading on TiO<sub>2</sub> catalysts synthesized by incipient wetness impregnation method for photocatalytic reduction of CO<sub>2</sub> and H<sub>2</sub>O into methane.

From part 4.1 results, the purpose of this section was to compare the effect of preparations. The Cu/TiO<sub>2</sub> catalysts with similar Cu loading content of sputtered catalysts were prepared by using incipient wetness impregnation method by the amount of %wt. Cu based on ICP measurement.

In order to describe correlation of catalytic efficiency with the catalytic properties, the catalysts were detected by various characterization techniques such as the X-ray diffraction (XRD), N<sub>2</sub>-physisorption, UV-Vis spectroscopy (UV-vis), Transmission electron microscopy (TEM), X-ray photoelectron spectrometer (XPS), PL emission spectra, Scanning electron microscopy (SEM), and Energy dispersive X-ray spectroscopy (EDX).

The Cu/TiO<sub>2</sub> catalysts synthesized by incipient wetness impregnation method were referred to as IM. This method was one of the preparations, which catalyst have a specific characteristic effect to the reaction as follows.

### 4.2.1 Powder X-ray diffraction (XRD)

The XRD diffraction pattern of Cu deposited on P25-TiO<sub>2</sub> catalysts shown in **Figure 29**. All Cu/P25(IM) catalysts were prepared by incipient wetness impregnation method exhibited the main characteristic peak of anatase phase that located at  $2\theta = 25.3$  (101), 37.8 (004), 48.0 (200), 54.5, (105 and 211), and 62.8 (213) and the rutile phase located at  $2\theta = 27.5$ (110), 36.1(101), 54.4(211). The main diffraction peak of the anatase (101) and rutile (110) located at  $2\theta = 25.3$  and 27.5, respectively. In the case of Cu deposited on Ana-TiO<sub>2</sub> catalysts shown in **Figure 30**, only the characteristic peaks of the anatase phase were observed. In addition, the peaks of the rutile phase were only observed for Cu deposited on Rut-TiO<sub>2</sub> catalysts shown in **Figure 31**. XRD

patterns of all Cu/TiO<sub>2</sub>(IM) catalysts after loading with Cu did not observe a peak of Cu/CuO phase, this is perhaps due to the slight Cu loading content, the extremely small Cu clusters and/or high dispersion of Cu/CuO on the TiO<sub>2</sub> supports.

After modified TiO<sub>2</sub> supports with Cu, anatase, and rutile phases were observed on the samples. The average crystallite sizes of the TiO<sub>2</sub> samples were determined from the full-width at half maximum of the anatase (101) and rutile (110) peaks calculated by the Scherrer's equation. The Cu/P25 (IM) samples exhibited the same patterns with an average crystallite size of the anatase phase and rutile phase in the range of 20-17 nm and 23-21 nm, respectively. The Cu/Ana (IM) samples exhibited the same patterns with an average crystallite size of the anatase phase in the range of 20-17 nm. The Cu/Rut (IM) samples exhibited the same patterns with an average crystallite size of rutile phase in the range of 23-18 nm. The crystallite size of the anatase phase and rutile phase of TiO<sub>2</sub> support as shown in **Table 7**. This demonstrated preparations did not affect the crystal structure, crystallite size of Cu/TiO<sub>2</sub> (IM) catalysts even after increasing of Cu loading content.

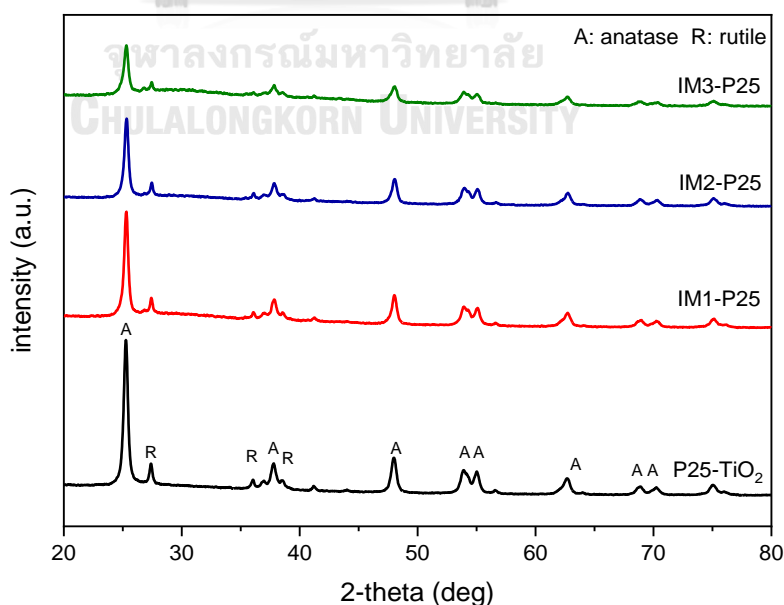


**Figure 29** XRD patterns of Cu/P25 (IM) catalysts.

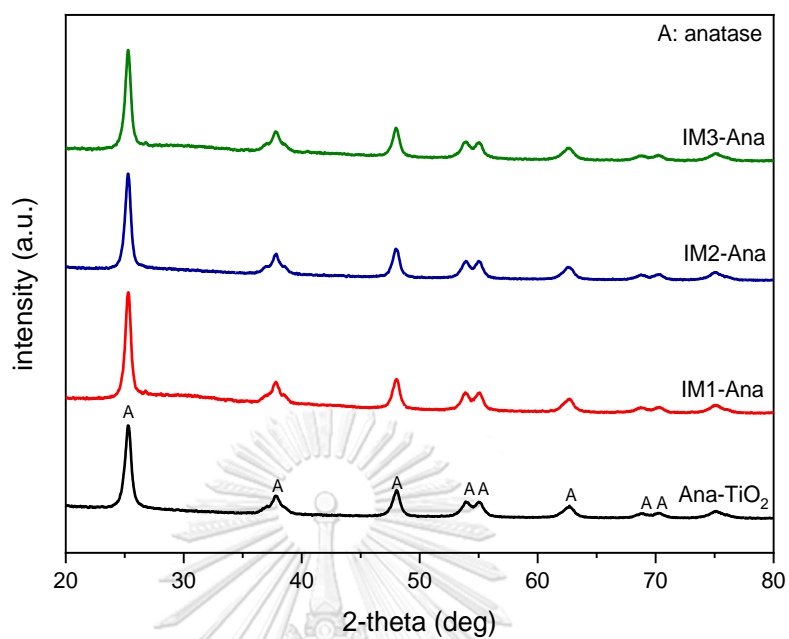


Figure 30 XRD patterns of Cu/Ana (IM) catalysts.

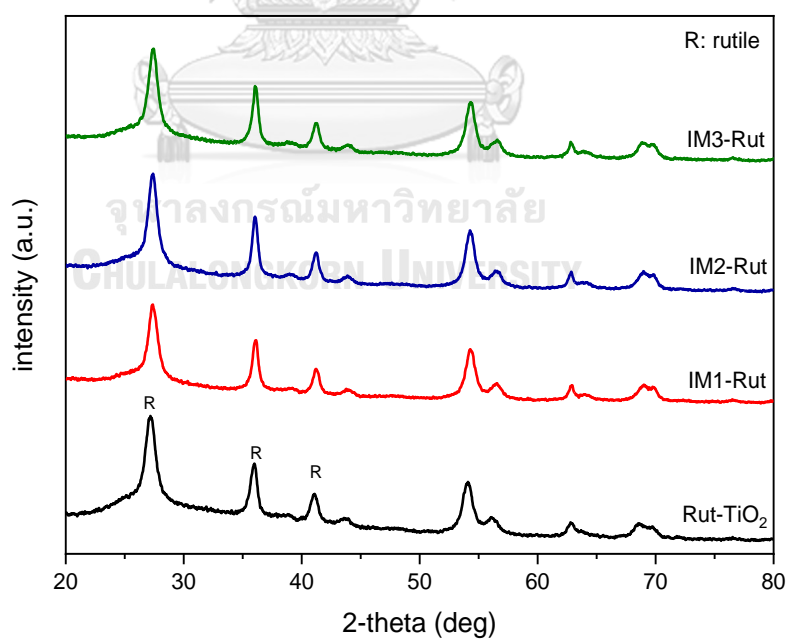


Figure 31 XRD patterns of Cu/Rut (IM) catalysts.

#### 4.2.2 Surface Area Measurement

This characterization techniques were to describe the specific surface area, pore volume, and pore size. The specific surface area refers to the activity of the photocatalysts due to photocatalytic reactions occur at the surface of the photocatalyst, when the high specific surface areas of photocatalysts will promote the activity of reaction which increased the production rate of methane.

The specific surface area of TiO<sub>2</sub> support and Cu deposited on TiO<sub>2</sub> prepared by incipient wetness impregnation method exhibited in **Table 7**. The BET surface area of Cu/P25 (IM) decreased from 54 to 51 m<sup>2</sup>/g when compare to pure P25-TiO<sub>2</sub> support because Cu particles blocked surface area of P25-TiO<sub>2</sub> and in the impregnation process, Cu particles agglomeration covered on the surface area and the catalysts via heat treatment at 400°C. In the case of Cu/Ana (IM), The BET surface area slightly decreased from 111 to 79 m<sup>2</sup>/g when compare to pure Ana-TiO<sub>2</sub> support. And Cu/Rut (IM), The BET surface area slightly decreased from 171 to 142 m<sup>2</sup>/g when compare to pure Rut-TiO<sub>2</sub> support. It could be seen that the surface area of all Cu/TiO<sub>2</sub> (IM) samples are different from the surface area of pure TiO<sub>2</sub> support.

**Table 7** Physical properties of the incipient wetness impregnated catalysts.

Catalyst	<sup>a</sup> Crystallite size (nm)		<sup>b</sup> Surface area (m <sup>2</sup> /g)	<sup>c</sup> band gap energy (eV)
	Anatase	Rutile		
P25-TiO <sub>2</sub>	20	23	54	3.21
IM1-P25	18	22	51	2.96
IM2-P25	18	22	52	2.55
IM3-P25	17	21	52	2.53
Ana-TiO <sub>2</sub>	20	-	111	3.23
IM1-Ana	17	-	80	3.14
IM2-Ana	19	-	81	3.01
IM3-Ana	18	-	79	2.83
Rut-TiO <sub>2</sub>	-	23	171	3.17
IM1-Rut	-	19	144	2.83
IM2-Rut	-	20	143	2.75
IM3-Rut	-	18	142	2.68

<sup>a</sup> Average crystallite size was determined by XRD using Scherrer equation.

<sup>b</sup> The BET surface area was determined by single point BET method.

<sup>c</sup> band gap energy was calculated by UV-visible absorption spectra.

#### 4.2.3 UV-vis spectrometer

The UV-vis absorption spectra of all the incipient wetness impregnated catalysts compare with pure TiO<sub>2</sub> supports are presented in **Figure 32-34** respectively. The absorption spectra of Cu modified TiO<sub>2</sub> catalysts can separate into three phases, including the sharp absorption band at wavelengths less than 400 nm, which were associated with the band structure of the original TiO<sub>2</sub> supports, the absorption band in 700–800 nm region, due to the Cu d-d transition, and an absorption tail in the 400–500 nm region, which was associated with the interfacial charge transfer (IFCT) phenomenon between TiO<sub>2</sub> valence band electrons and Cu(II) species.



The incipient wetness impregnated catalysts exhibited typical adsorption bands of  $\text{TiO}_2$  and Cu nanoparticles and the absorption peaks were increased with increasing of Cu loading content. That indicated the formation of Cu nanoparticles onto  $\text{TiO}_2$  and there is an interaction between Cu (II) species and the  $\text{TiO}_2$  support.

The band gap energy ( $E_{\text{bg}}$ ) of all the Cu/ $\text{TiO}_2$  catalysts were obtained from the extrapolation of Tauc plots of  $(h\nu\alpha)^{1/2}$  as a function of photon energy ( $h\nu$ ) and the obtained results are also shown in **Table 7**. It was investigated that increasing Cu doping content also reduced the band gap energy. The lowering of  $E_{\text{bg}}$  leads to Fermi level reducing, improving the photosensitivity of the catalysts and improving an absorption edge in the visible light region (400–700 nm).

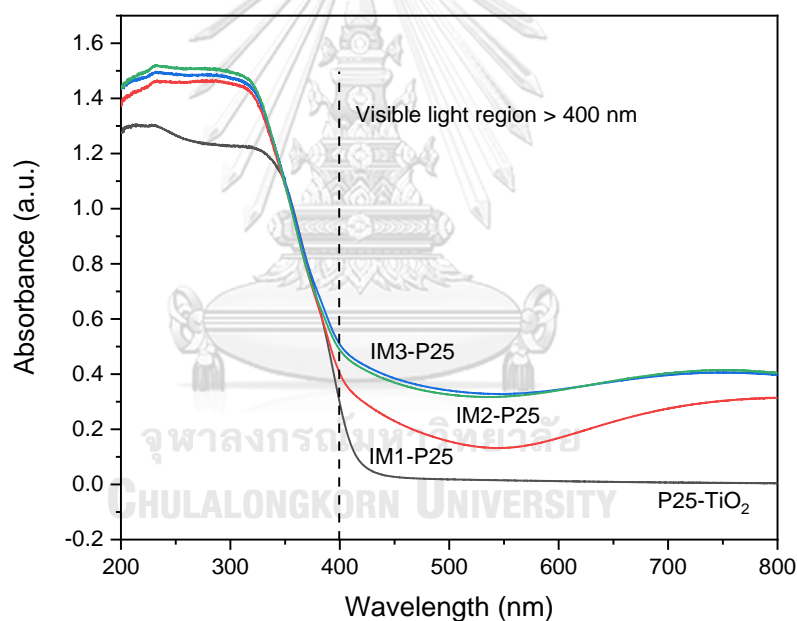


**Figure 32** The UV-Vis absorption spectra of Cu/P25 (IM) catalysts.

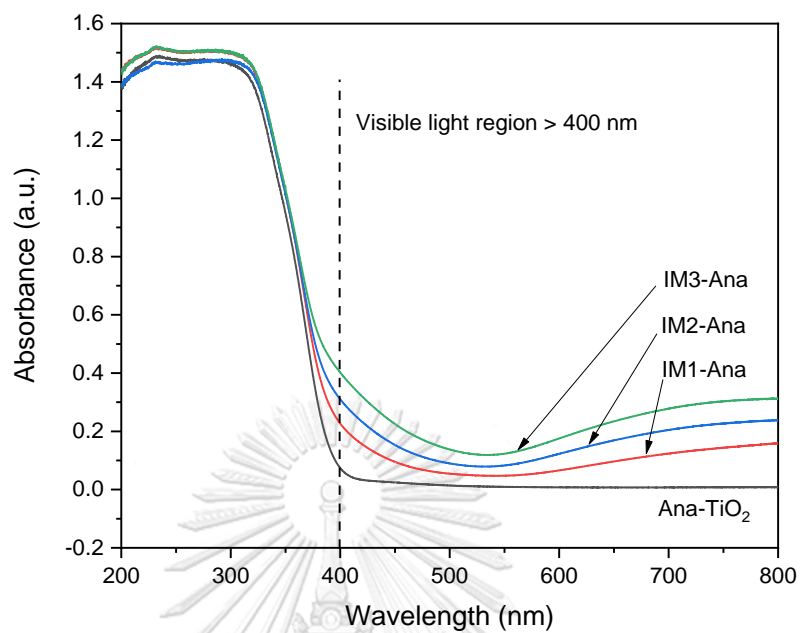


Figure 33 The UV-Vis absorption spectra of Cu/Ana (IM) catalysts.

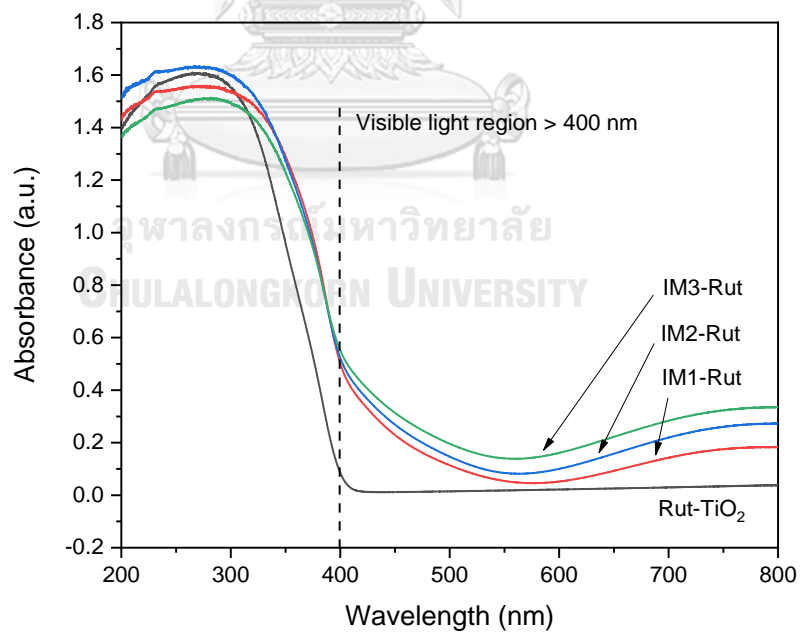
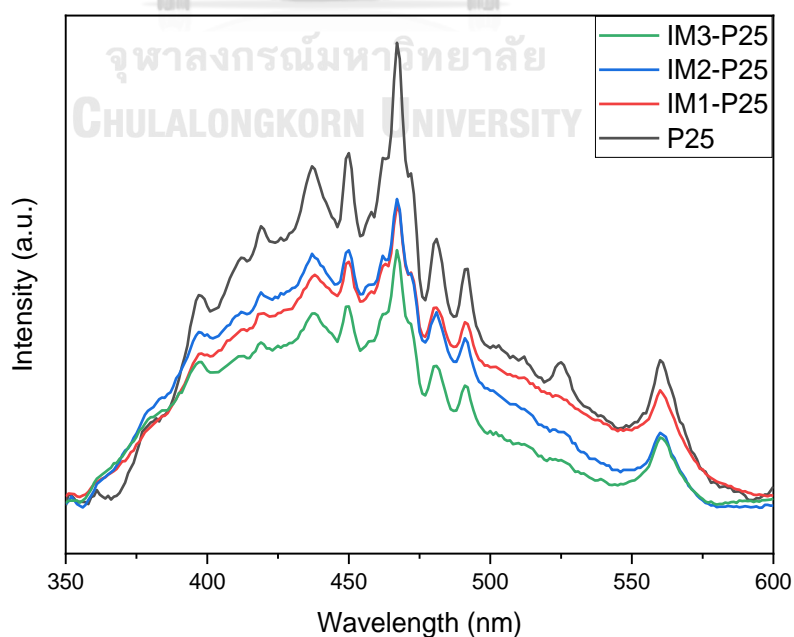


Figure 34 The UV-Vis absorption spectra of Cu/Rut (IM) catalysts.

#### 4.2.4 photoluminescence (PL)

photoluminescence (PL) is a technique for measured the electronic properties of semiconductor to determine the efficiency of photocatalysts such as charge carrier trapping, carrier lifetime and recombination of  $e^-h^+$  pairs. The PL emission spectra of all Cu/TiO<sub>2</sub> catalysts prepared by incipient wetness impregnation method are shown in **Figure 35-37**, respectively.

There are many peaks can be detected from PL consist of the signals at 436 nm was corresponded to the self-trapped electron localized on TiO<sub>6</sub> octahedral complex[63], and peaks at 469, 484, 492 nm have corresponded to the oxygen vacancies with two trapped electrons on TiO<sub>2</sub> surface [64, 65]. The emission spectra of the Cu modified TiO<sub>2</sub> was observed after Cu deposition, PL emission spectra decreased as Cu loading content increased. Except for Cu modified on rutile-TiO<sub>2</sub> support, Cu loading resulted in an increase of PL spectra except for IM2-Rut. The lower emission intensity due to the Cu nanoparticles trapped photoelectron from the conduction band of TiO<sub>2</sub> and retarded recombination of charge carrier process.



**Figure 35** The PL emission spectra of Cu/P25 (IM) catalysts.

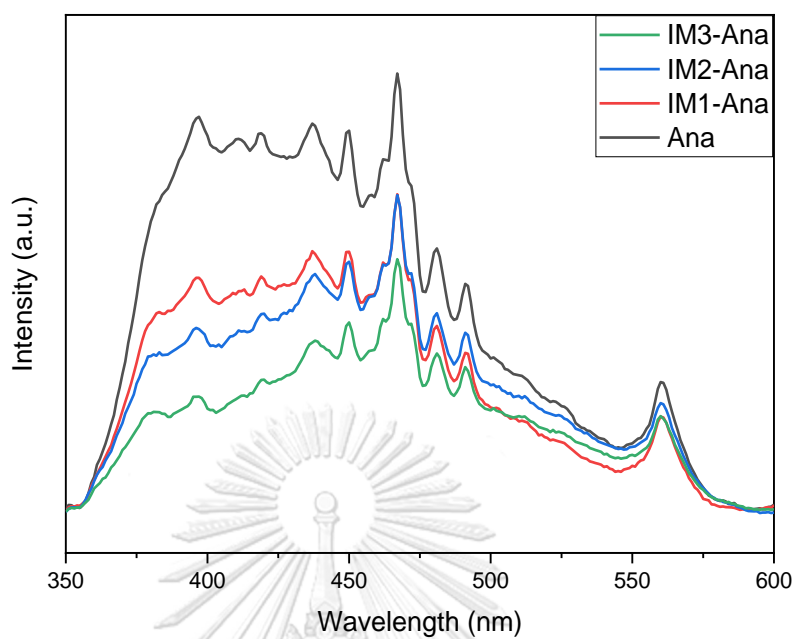


Figure 36 The PL emission spectra of Cu/Ana (IM) catalysts.

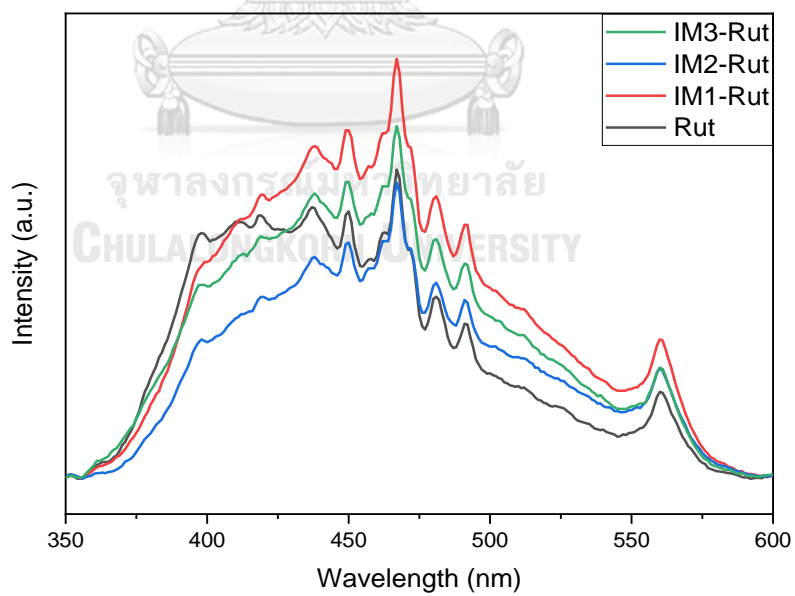
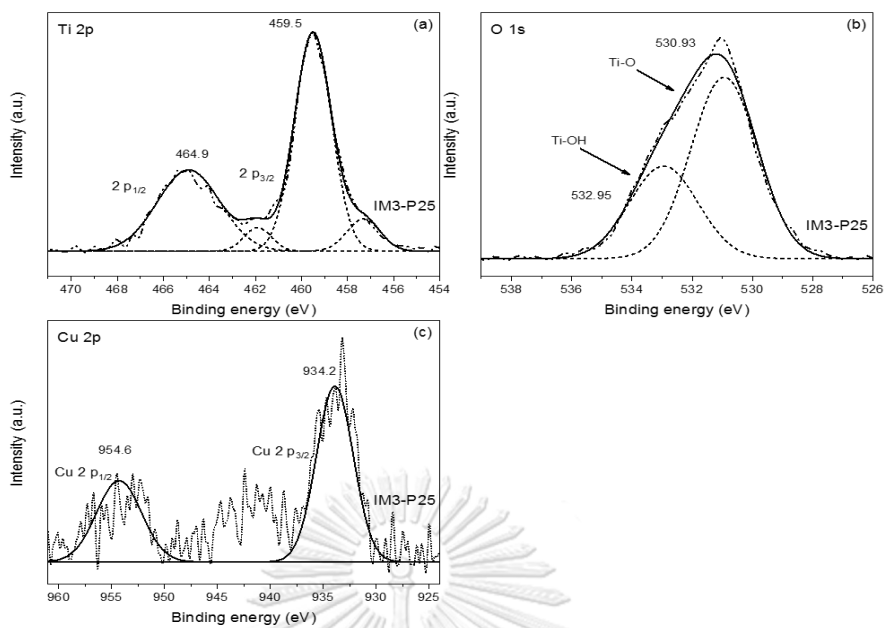


Figure 37 The PL emission spectra of Cu/Rut (IM) catalysts.

#### 4.2.5 X-ray photoelectron spectrometer (XPS)

X-ray photoelectron spectrometer (XPS) is a technique to determine the composition of the element on surface and electronic state. The XPS spectra of Ti 2p, O1s, and Cu2p of all Cu/TiO<sub>2</sub> catalysts prepared by incipient wetness impregnated method are shown in **Figure 38-40** respectively. For Cu/P25 (IM) catalysts, the peaks located at around 457.3 and 461.9 eV have corresponded to the Ti<sup>3+</sup>2p<sub>3/2</sub> and Ti<sup>3+</sup>2p<sub>1/2</sub>, respectively [66, 67], the other peaks at around 459.5 and 464.9 eV have corresponded to Ti<sup>4+</sup>2p<sub>3/2</sub> and Ti<sup>4+</sup>2p<sub>1/2</sub>, respectively [68-70]. In XPS spectra of O1s, the peak at 530.9 and 532.9 eV is corresponded as the Ti-O and OH- [71]. And XPS spectra of Cu2p, there are two peaks at around 934.2 and 954.6 eV, it is suggested that the Cu peaks around this area indicated to CuO [72].

For all Cu/TiO<sub>2</sub> (IM) catalysts, it is assigned that the characteristic peaks of Ti2p and O1s did not different after modified with Cu doping with incipient wetness impregnated method. However, catalyst compositions (%) of sputtered catalysts are shown in **Table 8**. It presented the amount of Cu increased in the order of P25 > anatase > rutile phase.



**Figure 38** The X-ray photoelectron spectra of IM3-P25 catalyst is simulated by Gaussian equation; XPS spectra of Ti2p (a), XPS spectra of O1s (b), and XPS spectra of Cu2p.

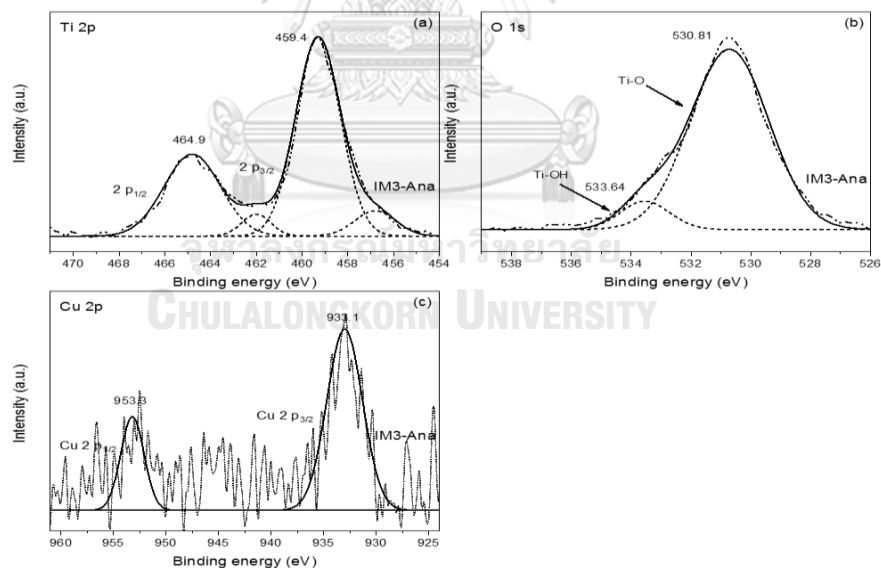


**Figure 39** The X-ray photoelectron spectra of IM3-Ana catalyst is simulated by Gaussian equation; XPS spectra of Ti2p (a), XPS spectra of O1s (b), and XPS spectra of Cu2p.

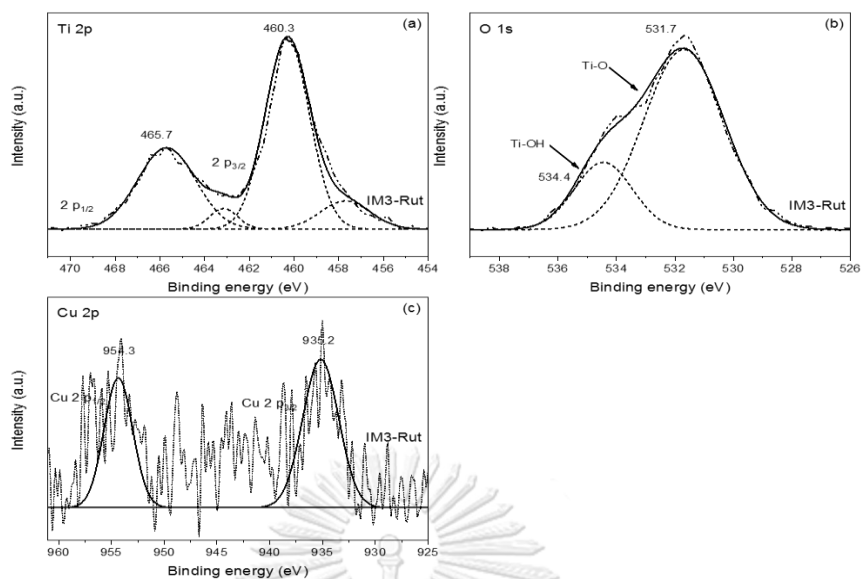


**Figure 40** The X-ray photoelectron spectra of IM3-Rut catalyst is simulated by Gaussian equation; XPS spectra of Ti2p (a), XPS spectra of O1s (b), and XPS spectra of Cu2p.

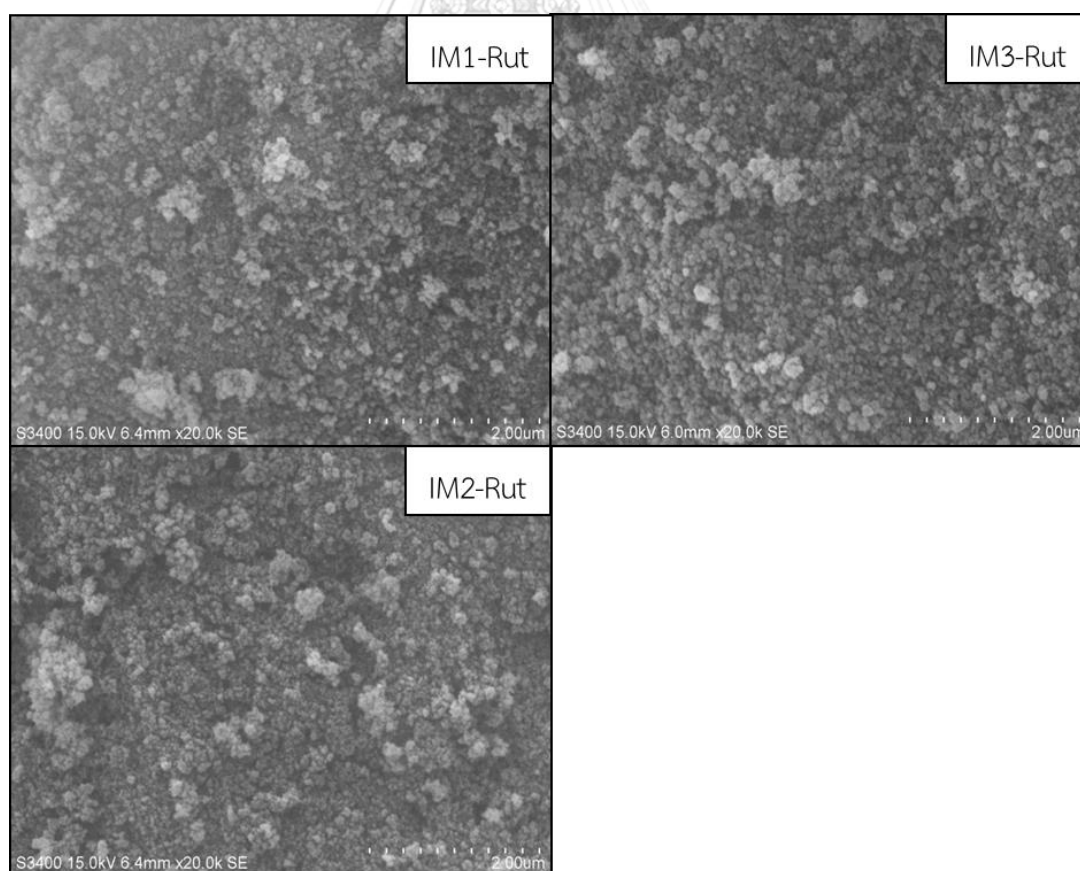
**Table 8** Catalyst compositions (%) of incipient wetness impregnated catalysts.

Catalyst	Catalyst compositions (%)			Catalyst compositions of Ti (%)	
	Cu <sup>+</sup>	Ti	O	Ti <sup>3+</sup>	Ti <sup>4+</sup>
IM3-P25	4.87	78.22	16.92	11.63	88.37
IM3-Ana	3.13	74.71	22.16	10.40	89.60
IM3-Rut	2.25	80.41	17.33	14.25	85.75

#### 4.2.6 Scanning electron microscopy and Energy Dispersive X-ray Spectroscopy (SEM-EDX)

**Figure 41** presented the morphology of Cu particles adhered onto all types of  $\text{TiO}_2$  support. The micrographs exhibited dispersion of Cu nanoparticles on Cu/P25 (IM), Cu/Ana (IM), and Cu/Rut (IM) respectively. It distinctly showed the agglomeration of spherical nanoparticles and the form of P25- $\text{TiO}_2$  supports is not much difference from modified with Cu nanoparticles and each other support, which prepared by incipient wetness impregnation method.

In addition, the EDX technique was used to reveal the amount of %wt. Cu covered on  $\text{TiO}_2$  surface are shown in **Table 9**. Amount of %wt. Cu on Cu-adhered onto  $\text{TiO}_2$  sample presented increasing of the Cu loading content. The amount of Cu increased in the order of P25 > rutile > anatase phase.





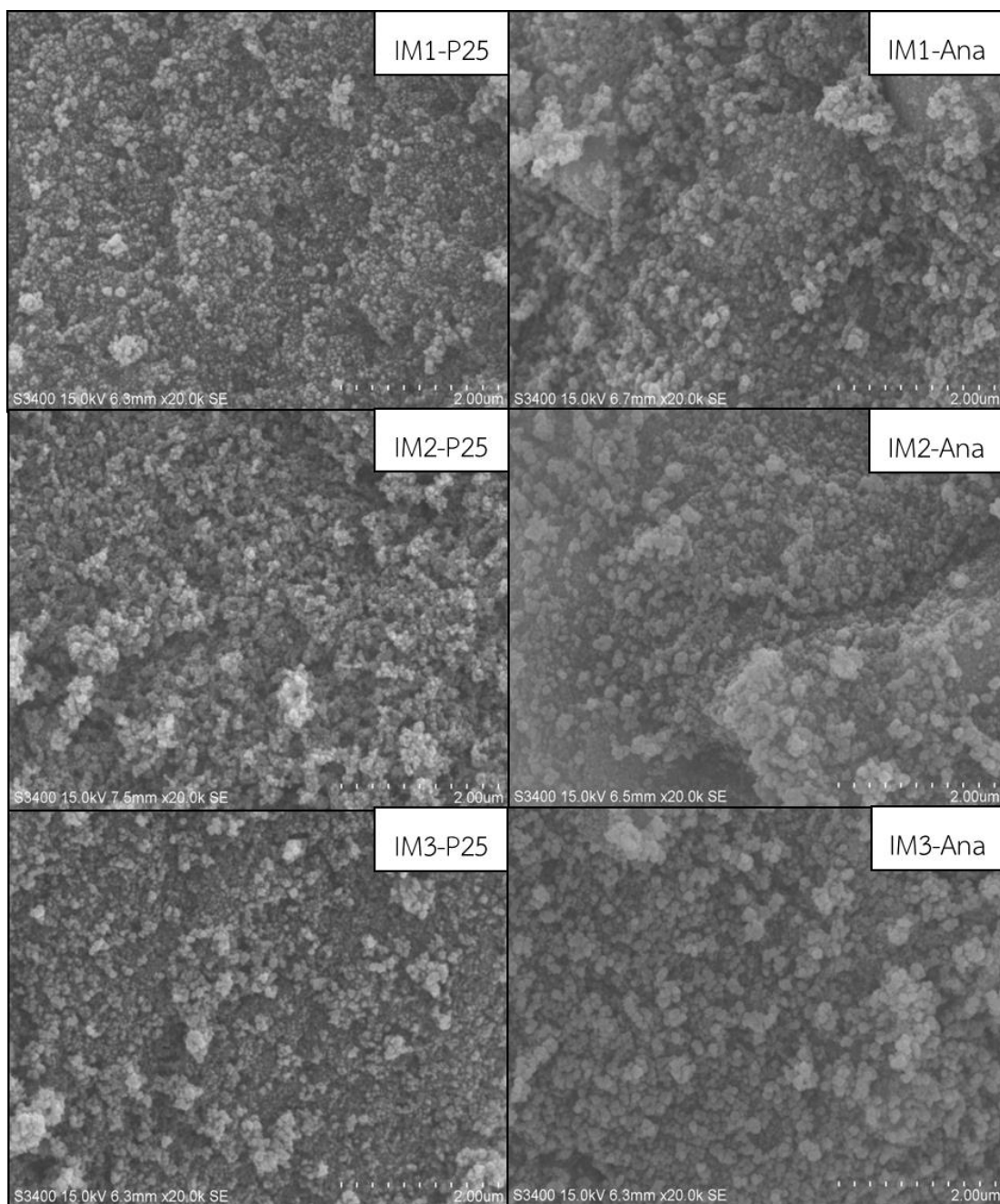


Figure 41 SEM of incipient wetness impregnated catalysts.

#### 4.2.7 Inductively coupled plasma (ICP)

The Cu doping content was measured by ICP techniques. ICP technique was used to reveal the amount of %wt. Cu in TiO<sub>2</sub> modified with Cu bulks. **Figure 42** clearly showed the amount of %wt. Cu in P25-TiO<sub>2</sub> modified with Cu samples higher was higher than those modified on other supports, including Rut-TiO<sub>2</sub> and Ana-TiO<sub>2</sub>, respectively. It can be seen that the Cu loading content of impregnated catalyst had a value near the sputtered catalyst.

Moreover, comparison of Cu doping content on all TiO<sub>2</sub> support measured by ICP and EDX techniques shows in **Table 9**. It can be seen that the Cu loading content measured by EDX technique was higher than the ICP technique. It demonstrated that Cu doping content covered on TiO<sub>2</sub> surfaces more than absorbed in TiO<sub>2</sub> pores.

**Table 9** Comparison of Cu doping content on TiO<sub>2</sub> support prepared by magnetron sputtering method.

Catalyst	Wt% of Cu	
	ICP	EDX
IM1-P25	0.68	3.42
IM2-P25	1.57	4.13
IM3-P25	2.47	5.40
IM1-Ana	0.34	1.11
IM2-Ana	0.70	2.71
IM3-Ana	1.40	3.60
IM1-Rut	0.57	2.66
IM2-Rut	1.23	3.43
IM3-Rut	2.11	4.58

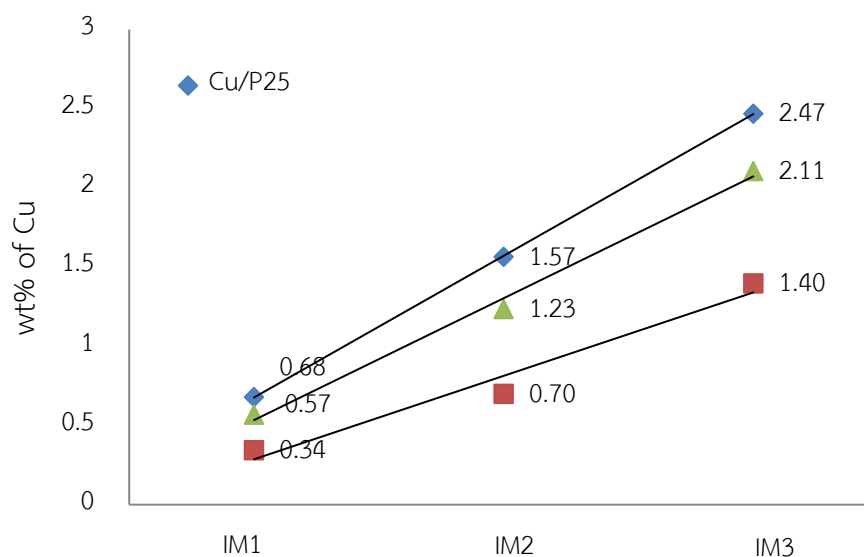


**Figure 42** %Wt. of Cu-adhered onto P25-TiO<sub>2</sub>, Ana-TiO<sub>2</sub>, and Rut-TiO<sub>2</sub> supports prepared incipient wetness impregnation method.

#### 4.2.8 Transmission electron microscopy (TEM)

The morphology and metal particles size of all the Cu/TiO<sub>2</sub> catalysts was determined by transmission electron microscopy. The TEM images of the Cu/TiO<sub>2</sub>(IM) catalysts are presented in **Figure 43-45**, respectively. The Cu/TiO<sub>2</sub> (IM) exhibited spherical Cu clusters and well dispersion. The spherical metal particles were the specific structure of the deposited metal prepared by using the incipient wetness impregnation method. An average Cu particles size of Cu/P25 (IM) equals 2.00 nm, Cu/Ana (IM) equals 1.68 nm and Cu/Rut (IM) equals 1.75 nm.

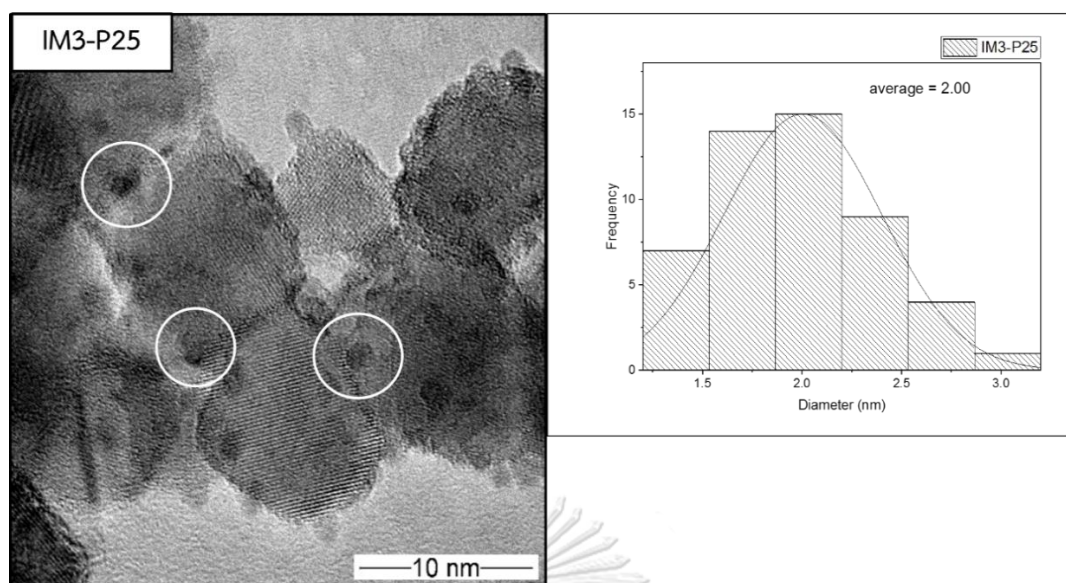


Figure 43 TEM and average Cu nanoparticle sizes of IM3-P25 catalyst.

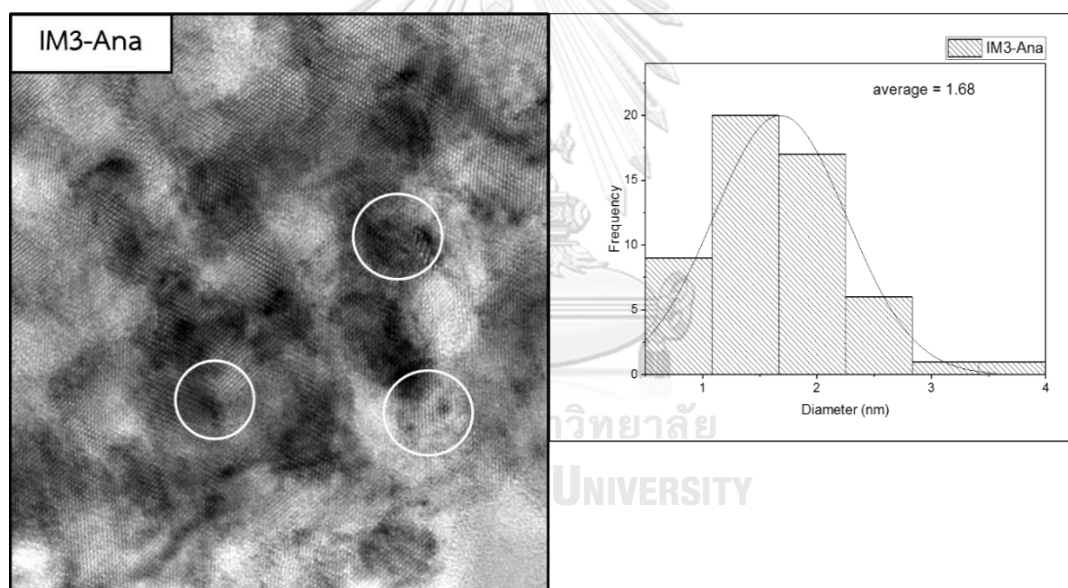
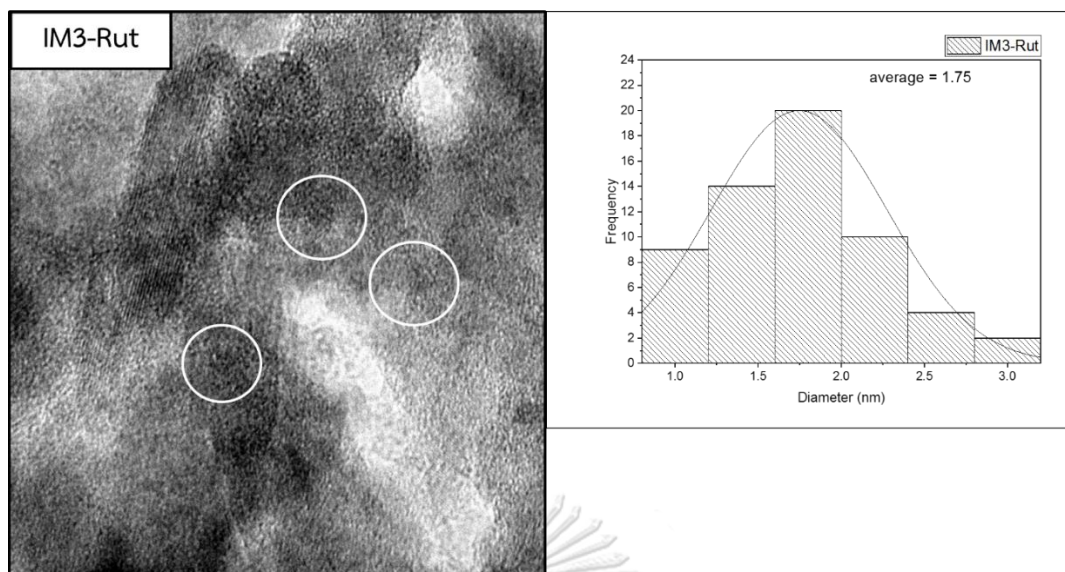


Figure 44 TEM and average Cu nanoparticle sizes of IM3-Ana catalyst.



**Figure 45** TEM and average Cu nanoparticle sizes of IM3-Rut catalyst.

#### 4.2.9 Photocatalytic activity of Cu/TiO<sub>2</sub> catalysts for photocatalytic reduction of CO<sub>2</sub> into methane.

The photocatalytic activity of all catalysts for photocatalytic reduction of CO<sub>2</sub> into methane under UV light is shown in **Figure 46**. For this experiment, methane was the main product obtained from all Cu/TiO<sub>2</sub> catalysts. The pure TiO<sub>2</sub> support showed relatively low activity under UV light irradiation. After doping with Cu on TiO<sub>2</sub> support, the photocatalytic activity of all incipient wetness impregnated catalysts increased the CH<sub>4</sub> production yield. A small amount of Cu doping content can improve the photocatalytic performance of TiO<sub>2</sub> due to Cu clusters trapped photoelectron and retarded recombination of charge carrier process. However, when increases of Cu doping content, it reduced band gap energy, when  $E_{bg}$  narrower it promoted the electron-hole recombination, the CH<sub>4</sub> production rate for Cu/TiO<sub>2</sub> decreased. An excess Cu loading higher than the optimum value could become recombination centers for electrons and holes pairs caused reducing of the catalytic activity

Consequently, the incipient wetness impregnation method is suitable for small amounts of Cu doping content. The CH<sub>4</sub> production of Three types of support increased in the order of rutile > P25 > anatase phase.

**Figure 47** showed the stability of SP3-P25 catalyst. The first round of the experiment showed the CH<sub>4</sub> production yield at 0.88. The stability of SP3-P25 catalyst slightly decreased after the second round and third round at 0.83 and 0.83, respectively.

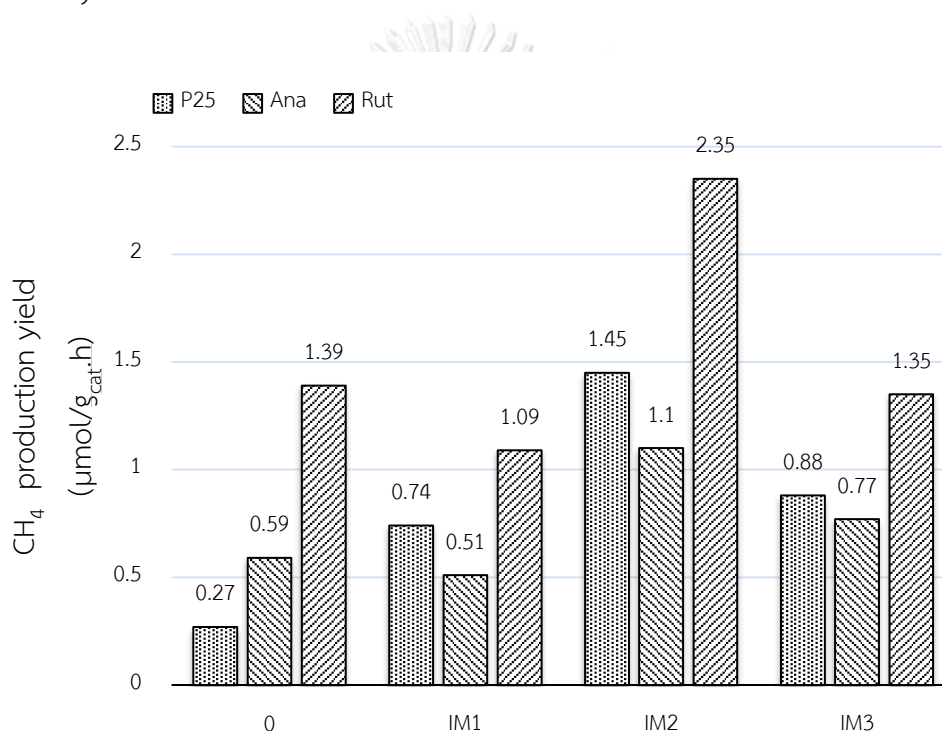


**Figure 46** CH<sub>4</sub> production yield of incipient wetness impregnated catalysts.

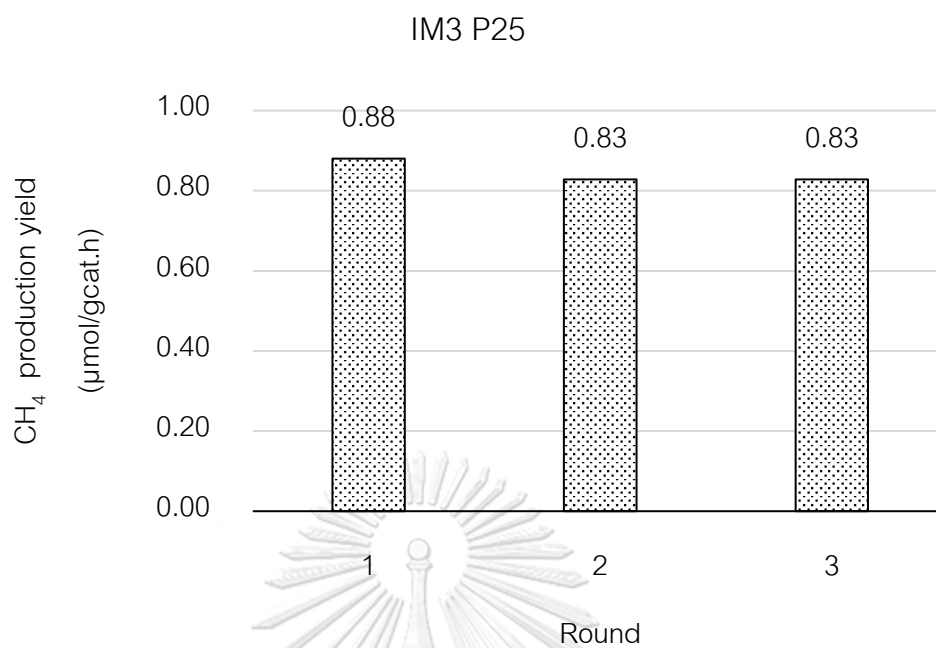


Figure 47 Stability of IM3-P25 catalyst.

### 4.3 Comparison between Cu/TiO<sub>2</sub> catalysts synthesized by magnetron sputtering method and incipient wetness impregnation method

The photocatalytic activity of Cu/TiO<sub>2</sub> catalysts for photocatalytic reduction of CO<sub>2</sub> and H<sub>2</sub>O into methane are shown the following.

For the Cu/TiO<sub>2</sub> catalysts were prepared by magnetron sputtering method exhibited methane production yield the higher than Cu/TiO<sub>2</sub> catalysts were prepared by incipient wetness impregnation method. From the UV-vis, BET, PL and XPS results, the band gap energy from UV-vis technique showed Cu/TiO<sub>2</sub> (IM) catalysts narrower band gap energy than Cu/TiO<sub>2</sub> (SP) catalysts due to Cu/TiO<sub>2</sub> (IM) catalysts via addition of metal precursor and heat treatment process caused strong interaction between Cu species and TiO<sub>2</sub> support more than Cu/TiO<sub>2</sub> (SP) catalysts via coating Cu target on TiO<sub>2</sub> surface. However, when  $E_{bg}$  narrower it can promote the electron-hole recombination, the CH<sub>4</sub> production yield for Cu/TiO<sub>2</sub> decreased. It can be seen from BET that Cu/TiO<sub>2</sub> (SP) catalysts showed higher surface area than Cu/TiO<sub>2</sub> (IM) catalysts due to the agglomeration of Cu nanoparticles in a pore of Cu/TiO<sub>2</sub> (IM) catalysts and agglomeration of TiO<sub>2</sub> pore from the heat treatment process. The higher surface area promoted the increasing of CH<sub>4</sub> production yield. The XPS spectra peaks of Cu/TiO<sub>2</sub> (IM) and Cu/TiO<sub>2</sub> (SP) catalysts exhibited a similar position in Ti2p<sub>3/2</sub> and Ti2p<sub>1/2</sub> peaks. But Cu2p<sub>3/2</sub> and Cu2p<sub>1/2</sub> peaks of Cu/TiO<sub>2</sub> (IM) catalysts were shifted to higher binding energy which indicated that there was a stronger interaction between Cu species and TiO<sub>2</sub> support. Comparison photocatalytic activity of TiO<sub>2</sub> support including P25-TiO<sub>2</sub>, Ana-TiO<sub>2</sub>, and RutTiO<sub>2</sub>. From PL emission spectra results, which showed the signals at 436 nm and peaks at 469, 484, 492 nm. The emission spectra of the TiO<sub>2</sub> supports decreased in the order of anatase > rutile > P25 phase as shown in **Figure 48**, but the result of rutile phase is better than P25 phase, it may appear from the higher surface area of rutile. The high surface area improved Cu dispersion and increased adsorption of CO<sub>2</sub> and H<sub>2</sub>O on the catalyst.



In order to investigate the stability of prepared catalysts, the Cu/TiO<sub>2</sub> catalysts prepared by both methods. The Cu/TiO<sub>2</sub> catalysts were tested repeatedly for three batches. It is clearly seen that the CH<sub>4</sub> production yield was lost slightly after the third batch. This suggests that the prepared Cu/TiO<sub>2</sub> catalyst by both methods is still active and can be used for long-term applications.

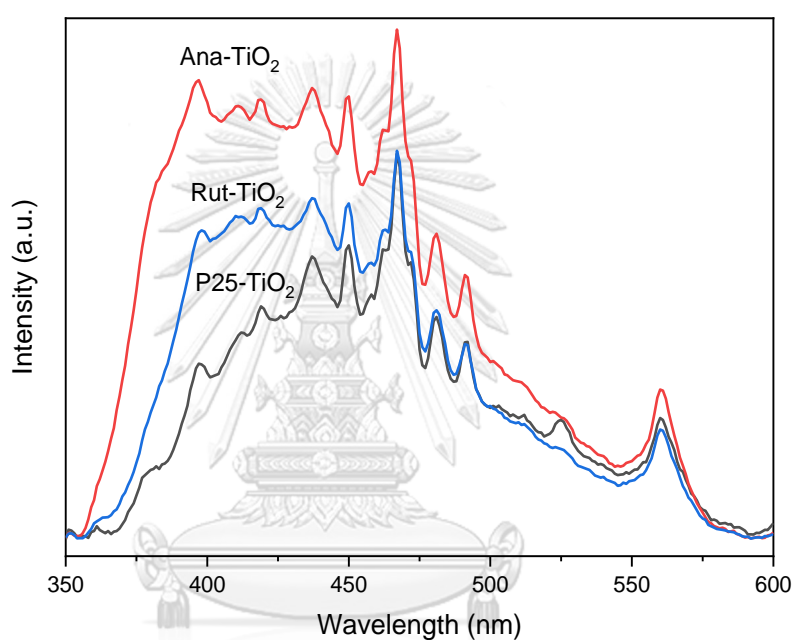


Figure 48 The PL emission spectra of TiO<sub>2</sub> catalysts.

## CHAPTER V

### CONCLUSIONS AND RECOMMENDATIONS

#### 5.1 Conclusions

The magnetron sputtering method has successfully been used to deposit CuO nanoparticles on the TiO<sub>2</sub> support. The Cu doping content increased linearly with extending sputtering time due to the constant Cu flux releasing in the sputtering process.

Considering the effect of preparation method, the sputtered catalysts exhibited higher photocatalytic activity than the pure TiO<sub>2</sub> supports and the impregnated catalysts. The copper species as a co-catalyst inhibited the recombination of electron-hole pairs which enhanced the efficiency of CO<sub>2</sub> photoreduction and increasing of the hydrocarbon production by trapping electron charge. Consequently, enhancement of photoexcited electron transfer by trapping electron leading to extend the lifetime of charge carriers in the process. Moreover, using copper species promoted selectivity of methane. However, an excess Cu loading higher than the optimum value could become recombination centers for electrons and holes pairs caused reducing of the catalytic activity.

The Cu/TiO<sub>2</sub> catalysts have a specific characteristic effect to reaction, sputtered catalysts presented irregular shaped Cu clusters on TiO<sub>2</sub> supports, whereas spherical clusters were obtained by impregnation. The UV-Vis spectra results presented the band gap energy from sputtered catalysts slightly decreased when increased the Cu sputtering time. Whereas the band gap energy from impregnated catalysts obviously decreased after increasing of Cu loading content due to stronger interactions between the Cu<sup>2+</sup> and the TiO<sub>2</sub> supports.

## 5.2 Recommendations

1. Characteristic of Cu nanoparticles supported on TiO<sub>2</sub> should be investigated by high-resolution analytical equipment such as high-resolution TEM.
2. Improvement of the process for continuous-flow in future.





APPENDIX

จุฬาลงกรณ์มหาวิทยาลัย  
**CHULALONGKORN UNIVERSITY**

## APPENDIX A

## CALCULATION FOR CATALYST PREPARATION

Reagent : Copper(II) nitrate trihydrate, 98%

Titanium (IV) oxide, 100%

The 1% Cu/TiO<sub>2</sub> catalyst prepared by incipient wetness impregnation method was shown.

Based on 2 g of TiO<sub>2</sub> prepared for 1% of Cu

Calculate percent:

$$\text{Weight Percent of Cu} = \frac{X \text{ g Copper}}{X \text{ g Copper} + 2 \text{ g Copper}} \times 100$$

$$0.01 = \frac{X}{X+2}$$

$$X = 0.0202 \text{ g of Cu}$$

Determine Cu for precursor:

$$X = [0.0202 \text{ g Cu}]$$

$$\left[ \frac{1 \text{ mol Cu}}{63.546 \text{ g Cu}} \right] \left[ \frac{241.6 \text{ g Cu(NO}_3)_2}{1 \text{ mol Cu(NO}_3)_2} \right] \left[ \frac{1 \text{ mol Cu(NO}_3)_2}{1 \text{ mol Cu}} \right] \left[ \frac{1}{0.98 \text{ purity}} \right]$$

$$X = 0.0784 \text{ g precursor}$$

## APPENDIX B

## CALCULATION OF THE CRYSTALLITE SIZE

Calculation of the crystallite size by Debye-Scherrer equation

The crystallite size can be calculated from  $2\theta$  profile analysis, the half-height width of diffraction peak using Debye-Scherrer equation.

From Scherrer equation:

$$D = \frac{k\lambda}{\beta \cos\theta}$$

Where

D = Crystallite size, Å

K = Crystalline-shape factor = 0.9

$\lambda$  = X-ray wavelength, 1.5418 Å for CuK $\alpha$

$\theta$  = Observed peak angle, degree

$\beta$  = X-ray diffraction broadening, radian

The X-ray diffraction broadening ( $\beta$ ) is the pure width of the powder diffraction, free of all broadening due to the experimental equipment. Standard  $\alpha$ -alumina is used to observe the instrumental broadening since its crystallite size is larger than 2000 Å. The X-ray diffraction broadening ( $\beta$ ) can be obtained by using Warren's formula.

From Warren's formula

$$\beta^2 = B_M^2 - B_S^2$$

$$\beta = \sqrt{B_M^2 - B_S^2}$$

Where  $B_M$  = Measured peak width in radians at half peak height  
 $B_S$  = Corresponding width of a standard material



## APPENDIX C

## CALCULATION OF THE BAND GAP FROM UV-VIS SPECTRA

The band gap ( $E_g$ ) of the sample was determined by the following equation:

$$E_g = \frac{hc}{\lambda} \quad (C.1)$$

Where  $E_g$  is a band gap (eV)

$h$  = Planks constant =  $6.63 \times 10^{-34}$  Joules sec

$C$  = Speed of light =  $3.0 \times 10^8$  meter/sec

$\lambda$  = Cut off wavelength (meters)

1 eV =  $1.6 \times 10^{-19}$  Joules (conversion factor)

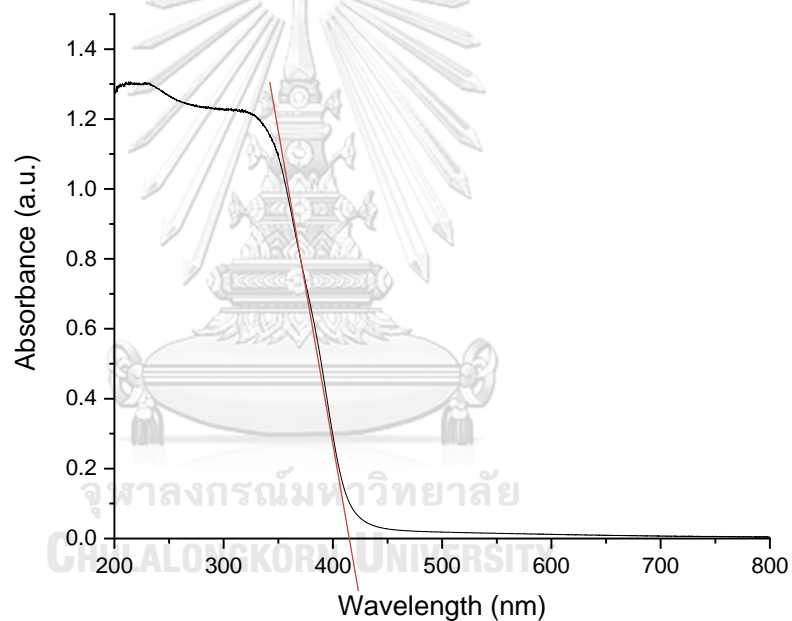


**Figure 49** UV-visible absorption characteristics of  $\text{TiO}_2$  (P25).

The spectra data recorded showed the strong cut off at 395 nm; where the absorbance value is a minimum.

Calculation:

$$E_g = \frac{(6.63 \times 10^{-34} \text{Joules} \cdot \text{sec})(3.0 \times 10^8 \text{meter/sec})}{(415 \times 10^{-9} \text{meters})(1.6 \times 10^{-19} \text{Joules})} = 2.99 \text{ eV}$$



## APPENDIX D

## CALCULATION FOR CATALYTIC PERFORMANCE

Calculation of CH<sub>4</sub> production rate of the catalysts are shown in this equation:

$$\text{CH}_4 \text{ production yield} = \left[ \frac{(\text{mole of CH}_4 \text{ production})(\text{total volume of CH}_4)}{(\text{weight of catalyst})(\text{reaction time})} \right] (\mu\text{mol/g}_{\text{cat}}\cdot\text{h})$$

The calibration curve of methane is shown in **Figure 50**

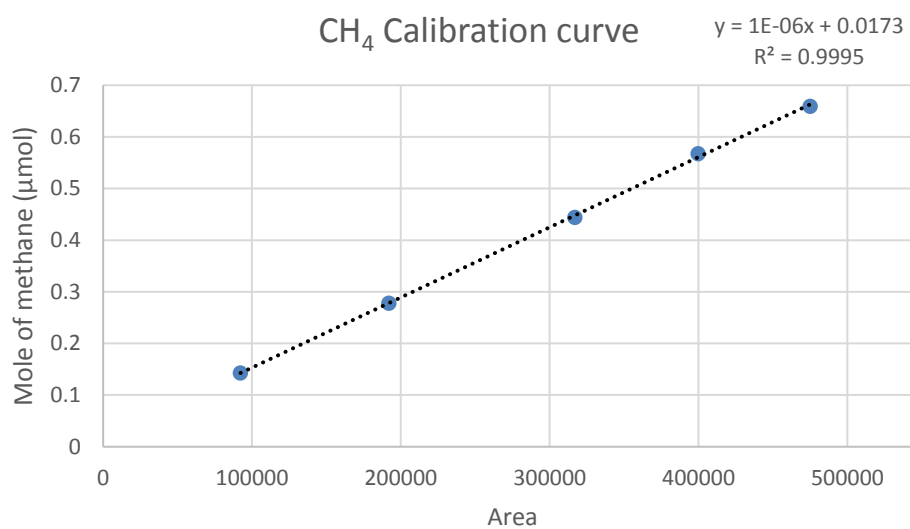


**Figure 50** The calibration curve of methane.

## REFERENCES

- [1] M. Takeuchi, Y. Sakamoto, and S. Niwa, "Study on CO<sub>2</sub> global recycling system," *Science of the total environment*, vol. 277, no. 1-3, pp. 15-19, 2001.
- [2] M. Tahir and N. S. Amin, "Recycling of carbon dioxide to renewable fuels by photocatalysis: Prospects and challenges," *Renewable and Sustainable Energy Reviews*, vol. 25, pp. 560-579, 2013.
- [3] T. Tamura, Y. Yakumaru, and F. Nishiwaki, "Experimental study on automotive cooling and heating air conditioning system using CO<sub>2</sub> as a refrigerant," *International Journal of Refrigeration*, vol. 28, no. 8, pp. 1302-1307, 2005.
- [4] P. D. Phuong and P. T. Nghia, "Method, chemical and automatic fire extinguishing system using liquified CO<sub>2</sub> to regulate the distribution of fire extinguishing agents," ed: Google Patents, 2005.
- [5] B. Kvamme, "Droplets of dry ice and cold liquid CO<sub>2</sub> for self-transport of CO<sub>2</sub> to large depths," *International Journal of Offshore and Polar Engineering*, vol. 13, no. 02, 2003.
- [6] N. Sivasankar, E. Cole, K. Teamey, and A. Bocarsly, "Electrochemical production of urea from NO<sub>x</sub> and carbon dioxide," ed: Google Patents, 2013.
- [7] G. W. Coates and D. R. Moore, "Discrete metal-based catalysts for the copolymerization of CO<sub>2</sub> and epoxides: discovery, reactivity, optimization, and mechanism," *Angewandte Chemie International Edition*, vol. 43, no. 48, pp. 6618-6639, 2004.
- [8] J. Kim *et al.*, "Methanol production from CO<sub>2</sub> using solar-thermal energy: process development and techno-economic analysis," *Energy & Environmental Science*, vol. 4, no. 9, pp. 3122-3132, 2011.
- [9] S. Gildemyn, K. Verbeeck, R. Slabbinck, S. J. Andersen, A. PrévotEAU, and K. Rabaey, "Integrated production, extraction, and concentration of acetic acid from CO<sub>2</sub> through microbial electrosynthesis," *Environmental Science & Technology Letters*, vol. 2, no. 11, pp. 325-328, 2015.
- [10] S. Bontemps and S. Sabo-Etienne, "Trapping formaldehyde in the homogeneous

- catalytic reduction of carbon dioxide," *Angewandte Chemie International Edition*, vol. 52, no. 39, pp. 10253-10255, 2013.
- [11] S. t. Neatu, J. A. Maciá-Agulló, P. Concepción, and H. Garcia, "Gold-copper nanoalloys supported on TiO<sub>2</sub> as photocatalysts for CO<sub>2</sub> reduction by water," *Journal of the American Chemical Society*, vol. 136, no. 45, pp. 15969-15976, 2014.
- [12] X. Liu, S. Inagaki, and J. Gong, "Heterogeneous molecular systems for photocatalytic CO<sub>2</sub> reduction with water oxidation," *Angewandte Chemie International Edition*, vol. 55, no. 48, pp. 14924-14950, 2016.
- [13] K. Wenderich and G. Mul, "Methods, mechanism, and applications of photodeposition in photocatalysis: a review," *Chemical reviews*, vol. 116, no. 23, pp. 14587-14619, 2016.
- [14] H. Yamashita, A. Shiga, S.-i. Kawasaki, Y. Ichihashi, S. Ehara, and M. Anpo, "Photocatalytic synthesis of CH<sub>4</sub> and CH<sub>3</sub>OH from CO<sub>2</sub> and H<sub>2</sub>O on highly dispersed active titanium oxide catalysts," *Energy conversion and management*, vol. 36, no. 6-9, pp. 617-620, 1995.
- [15] S. Neatu, J. Maciá-Agulló, and H. Garcia, "Solar light photocatalytic CO<sub>2</sub> reduction: general considerations and selected bench-mark photocatalysts," *International journal of molecular sciences*, vol. 15, no. 4, pp. 5246-5262, 2014.
- [16] S. Xie, Y. Wang, Q. Zhang, W. Deng, and Y. Wang, "MgO-and Pt-promoted TiO<sub>2</sub> as an efficient photocatalyst for the preferential reduction of carbon dioxide in the presence of water," *Acs Catalysis*, vol. 4, no. 10, pp. 3644-3653, 2014.
- [17] K. Iizuka, T. Wato, Y. Miseki, K. Saito, and A. Kudo, "Photocatalytic reduction of carbon dioxide over Ag cocatalyst-loaded ALa<sub>4</sub>Ti<sub>4</sub>O<sub>15</sub> (A= Ca, Sr, and Ba) using water as a reducing reagent," *Journal of the American Chemical Society*, vol. 133, no. 51, pp. 20863-20868, 2011.
- [18] Q. Zhai *et al.*, "Photocatalytic conversion of carbon dioxide with water into methane: platinum and copper (I) oxide co-catalysts with a core-shell structure," *Angewandte Chemie International Edition*, vol. 52, no. 22, pp. 5776-5779, 2013.

- [19] M. F. Kuehnel, K. L. Orchard, K. E. Dalle, and E. Reisner, "Selective photocatalytic CO<sub>2</sub> reduction in water through anchoring of a molecular Ni catalyst on CdS nanocrystals," *Journal of the American Chemical Society*, vol. 139, no. 21, pp. 7217-7223, 2017.
- [20] X. An, K. Li, and J. Tang, "Cu<sub>2</sub>O/reduced graphene oxide composites for the photocatalytic conversion of CO<sub>2</sub>," *ChemSusChem*, vol. 7, no. 4, pp. 1086-1093, 2014.
- [21] D.-S. Lee, H.-J. Chen, and Y.-W. Chen, "Photocatalytic reduction of carbon dioxide with water using InNbO<sub>4</sub> catalyst with NiO and Co<sub>3</sub>O<sub>4</sub> cocatalysts," *Journal of Physics and Chemistry of Solids*, vol. 73, no. 5, pp. 661-669, 2012.
- [22] S. Das and W. W. Daud, "A review on advances in photocatalysts towards CO<sub>2</sub> conversion," *Rsc Advances*, vol. 4, no. 40, pp. 20856-20893, 2014.
- [23] H. R. Kim, A. Razzaq, C. A. Grimes, and S.-I. In, "Heterojunction pnp Cu<sub>2</sub>O/S-TiO<sub>2</sub>/CuO: Synthesis and application to photocatalytic conversion of CO<sub>2</sub> to methane," *Journal of CO<sub>2</sub> Utilization*, vol. 20, pp. 91-96, 2017.
- [24] Y. Zhang, H. Ma, M. Yi, Z. Shen, X. Yu, and X. Zhang, "Magnetron-sputtering fabrication of noble metal nanodots coated TiO<sub>2</sub> nanoparticles with enhanced photocatalytic performance," *Materials & Design*, vol. 125, pp. 94-99, 2017.
- [25] M. A. Fox and M. T. Dulay, "Heterogeneous photocatalysis," *Chemical reviews*, vol. 93, no. 1, pp. 341-357, 1993.
- [26] J.-M. Herrmann, "Heterogeneous photocatalysis: fundamentals and applications to the removal of various types of aqueous pollutants," *Catalysis today*, vol. 53, no. 1, pp. 115-129, 1999.
- [27] H. Gu, Z. Wang, and Y. Hu, "Hydrogen gas sensors based on semiconductor oxide nanostructures," *Sensors*, vol. 12, no. 5, pp. 5517-5550, 2012.
- [28] N.-G. Park, J. Van de Lagemaat, Frank, and AJ, "Comparison of dye-sensitized rutile-and anatase-based TiO<sub>2</sub> solar cells," *The Journal of Physical Chemistry B*, vol. 104, no. 38, pp. 8989-8994, 2000.
- [29] X. Liu, J. Fang, Y. Liu, and T. Lin, "Progress in nanostructured photoanodes for dye-sensitized solar cells," *Frontiers of materials science*, vol. 10, no. 3, pp. 225-237, 2016.

- [30] J. Moma and J. Baloyi, "Modified Titanium Dioxide for Photocatalytic Applications," in *Photocatalysts-Applications and Attributes*: IntechOpen, 2018.
- [31] S. Bagheri, N. Muhd Julkapli, and S. Bee Abd Hamid, "Titanium dioxide as a catalyst support in heterogeneous catalysis," *The Scientific World Journal*, vol. 2014, 2014.
- [32] W. Kangwansupamonkon, V. Lauruengtana, S. Surassmo, and U. Ruktanonchai, "Antibacterial effect of apatite-coated titanium dioxide for textiles applications," *Nanomedicine: Nanotechnology, Biology and Medicine*, vol. 5, no. 2, pp. 240-249, 2009.
- [33] Q. Zhang, Y. Li, E. A. Ackerman, M. Gajdardziska-Josifovska, and H. Li, "Visible light responsive iodine-doped TiO<sub>2</sub> for photocatalytic reduction of CO<sub>2</sub> to fuels," *Applied Catalysis A: General*, vol. 400, no. 1-2, pp. 195-202, 2011.
- [34] Y. Ma, X. Wang, Y. Jia, X. Chen, H. Han, and C. Li, "Titanium dioxide-based nanomaterials for photocatalytic fuel generations," *Chemical reviews*, vol. 114, no. 19, pp. 9987-10043, 2014.
- [35] D. T. Cromer and K. Herrington, "The structures of anatase and rutile," *Journal of the American Chemical Society*, vol. 77, no. 18, pp. 4708-4709, 1955.
- [36] W. H. Baur, "Atomabstände und bindungswinkel im brookit, TiO<sub>2</sub>," *Acta Crystallographica*, vol. 14, no. 3, pp. 214-216, 1961.
- [37] J. Yu, C. Y. Jimmy, W. Ho, and Z. Jiang, "Effects of calcination temperature on the photocatalytic activity and photo-induced super-hydrophilicity of mesoporous TiO<sub>2</sub> thin films," *New Journal of Chemistry*, vol. 26, no. 5, pp. 607-613, 2002.
- [38] T. Toyoda and I. Tsuboya, "Apparent band-gap energies of mixed TiO<sub>2</sub> nanocrystals with anatase and rutile structures characterized with photoacoustic spectroscopy," *Review of scientific instruments*, vol. 74, no. 1, pp. 782-784, 2003.
- [39] K. Y. Jung, S. B. Park, and H. D. Jang, "Phase control and photocatalytic properties of nano-sized titania particles by gas-phase pyrolysis of TiCl<sub>4</sub>," *Catalysis Communications*, vol. 5, no. 9, pp. 491-497, 2004.
- [40] Y. Paz, "Application of TiO<sub>2</sub> photocatalysis for air treatment: Patents' overview," *Applied Catalysis B: Environmental*, vol. 99, no. 3-4, pp. 448-460, 2010.

- [41] J. Kim, I. Cho, I. Kim, C. Kim, N. H. Heo, and S. Suh, "Manufacturing of anti-viral inorganic materials from colloidal silver and titanium oxide," *Revue Roumaine De Chimie*, vol. 51, no. 11, p. 1121, 2006.
- [42] A. Fujishima, T. N. Rao, and D. A. Tryk, "TiO<sub>2</sub> photocatalysts and diamond electrodes," *Electrochimica acta*, vol. 45, no. 28, pp. 4683-4690, 2000.
- [43] J. Chen, S.-c. Kou, and C.-s. Poon, "Hydration and properties of nano-TiO<sub>2</sub> blended cement composites," *Cement and Concrete Composites*, vol. 34, no. 5, pp. 642-649, 2012.
- [44] S. Guo, Z. Wu, and W. Zhao, "TiO<sub>2</sub>-based building materials: above and beyond traditional applications," *Chinese Science Bulletin*, vol. 54, no. 7, pp. 1137-1142, 2009.
- [45] E. Quagliarini, F. Bondioli, G. B. Goffredo, A. Licciulli, and P. Munafò, "Self-cleaning materials on architectural heritage: compatibility of photo-induced hydrophilicity of TiO<sub>2</sub> coatings on stone surfaces," *Journal of Cultural Heritage*, vol. 14, no. 1, pp. 1-7, 2013.
- [46] T. W. Woolerton, S. Sheard, E. Reisner, E. Pierce, S. W. Ragsdale, and F. A. Armstrong, "Efficient and clean photoreduction of CO<sub>2</sub> to CO by enzyme-modified TiO<sub>2</sub> nanoparticles using visible light," *Journal of the American Chemical Society*, vol. 132, no. 7, pp. 2132-2133, 2010.
- [47] L. G. Devi and R. Kavitha, "A review on non metal ion doped titania for the photocatalytic degradation of organic pollutants under UV/solar light: role of photogenerated charge carrier dynamics in enhancing the activity," *Applied Catalysis B: Environmental*, vol. 140, pp. 559-587, 2013.
- [48] A. Dhakshinamoorthy, S. Navalon, A. Corma, and H. Garcia, "Photocatalytic CO<sub>2</sub> reduction by TiO<sub>2</sub> and related titanium containing solids," *Energy & Environmental Science*, vol. 5, no. 11, pp. 9217-9233, 2012.
- [49] H. Yoshida, "Heterogeneous photocatalytic conversion of carbon dioxide," in *Energy Efficiency and Renewable Energy Through Nanotechnology*: Springer, 2011, pp. 531-559.
- [50] S. Navalon, A. Dhakshinamoorthy, M. Álvaro, and H. Garcia, "Photocatalytic CO<sub>2</sub>

- reduction using non-titanium metal oxides and sulfides," *ChemSusChem*, vol. 6, no. 4, pp. 562-577, 2013.
- [51] M. I. Litter, "Heterogeneous photocatalysis: transition metal ions in photocatalytic systems," *Applied catalysis B: environmental*, vol. 23, no. 2-3, pp. 89-114, 1999.
- [52] W. Siripala, A. Ivanovskaya, T. F. Jaramillo, S.-H. Baeck, and E. W. McFarland, "A  $\text{Cu}_2\text{O}/\text{TiO}_2$  heterojunction thin film cathode for photoelectrocatalysis," *Solar Energy Materials and Solar Cells*, vol. 77, no. 3, pp. 229-237, 2003.
- [53] J. Wang, S. He, Z. Li, X. Jing, M. Zhang, and Z. Jiang, "Microemulsion synthesis of copper oxide nanorod-like structures," *Colloid and Polymer Science*, vol. 287, pp. 853-858, 2009.
- [54] M. Tahir and N. S. Amin, "Advances in visible light responsive titanium oxide-based photocatalysts for  $\text{CO}_2$  conversion to hydrocarbon fuels," *Energy Conversion and Management*, vol. 76, pp. 194-214, 2013.
- [55] K. Li, X. An, K. H. Park, M. Khraisheh, and J. Tang, "A critical review of  $\text{CO}_2$  photoconversion: catalysts and reactors," *Catalysis Today*, vol. 224, pp. 3-12, 2014.
- [56] N. Sasirekha, S. J. S. Basha, and K. Shanthi, "Photocatalytic performance of Ru doped anatase mounted on silica for reduction of carbon dioxide," *Applied Catalysis B: Environmental*, vol. 62, no. 1-2, pp. 169-180, 2006.
- [57] T. Inoue, A. Fujishima, S. Konishi, and K. Honda, "Photoelectrocatalytic reduction of carbon dioxide in aqueous suspensions of semiconductor powders," *Nature*, vol. 277, no. 5698, p. 637, 1979.
- [58] J. Van de Loosdrecht *et al.*, "Calcination of Co-based Fischer-Tropsch synthesis catalysts," *Topics in catalysis*, vol. 26, no. 1-4, pp. 121-127, 2003.
- [59] E. Poels, J. Dekker, and W. Van Leeuwen, "Hydrothermal sintering of the active phase in alumina supported fixed bed nickel catalysts during reduction," in *Studies in Surface Science and Catalysis*, vol. 63: Elsevier, 1991, pp. 205-214.
- [60] Y. Li, W.-N. Wang, Z. Zhan, M.-H. Woo, C.-Y. Wu, and P. Biswas, "Photocatalytic reduction of  $\text{CO}_2$  with  $\text{H}_2\text{O}$  on mesoporous silica supported  $\text{Cu}/\text{TiO}_2$  catalysts,"

*Applied Catalysis B: Environmental*, vol. 100, no. 1-2, pp. 386-392, 2010.

- [61] D. Liu *et al.*, "On the impact of Cu dispersion on CO<sub>2</sub> photoreduction over Cu/TiO<sub>2</sub>," *Catalysis Communications*, vol. 25, pp. 78-82, 2012.
- [62] H. W. Nasution, E. Purnama, S. Kosela, and J. Gunlazuardi, "Photocatalytic reduction of CO<sub>2</sub> on copper-doped Titania catalysts prepared by improved-impregnation method," *Catalysis Communications*, vol. 6, no. 5, pp. 313-319, 2005.
- [63] H. Khan and D. Berk, "Effect of a chelating agent on the physicochemical properties of TiO<sub>2</sub>: characterization and photocatalytic activity," *Catalysis letters*, vol. 144, no. 5, pp. 890-904, 2014.
- [64] P. Verma and S. K. Samanta, "Degradation kinetics of pollutants present in a simulated wastewater matrix using UV/TiO<sub>2</sub> photocatalysis and its microbiological toxicity assessment," *Research on Chemical Intermediates*, vol. 43, no. 11, pp. 6317-6341, 2017.
- [65] Y. Jiang, Z. Yang, P. Zhang, H. Jin, and Y. Ding, "Natural assembly of a ternary Ag-SnS-TiO<sub>2</sub> photocatalyst and its photocatalytic performance under simulated sunlight," *RSC Advances*, vol. 8, no. 24, pp. 13408-13416, 2018.
- [66] N. R. F. Machado and V. S. Santana, "Influence of thermal treatment on the structure and photocatalytic activity of TiO<sub>2</sub> P25," *Catalysis Today*, vol. 107, pp. 595-601, 2005.
- [67] G. Wang, L. Xu, J. Zhang, T. Yin, and D. Han, "Enhanced photocatalytic activity of powders (P25) via calcination treatment," *International Journal of Photoenergy*, vol. 2012, 2012.
- [68] K. Imamura, S.-i. Iwasaki, T. Maeda, K. Hashimoto, B. Ohtani, and H. Kominami, "Photocatalytic reduction of nitrobenzenes to aminobenzenes in aqueous suspensions of titanium (IV) oxide in the presence of hole scavengers under deaerated and aerated conditions," *Physical Chemistry Chemical Physics*, vol. 13, no. 11, pp. 5114-5119, 2011.
- [69] R. Bhosale, R. Hyam, P. Dhanya, and S. Ogale, "Chlorate ion mediated rutile to anatase reverse phase transformation in the TiO<sub>2</sub> nanosystem," *Dalton Transactions*, vol. 40, no. 43, pp. 11374-11377, 2011.



- [70] K. Imamura, K. Hashimoto, and H. Kominami, "Chemoselective reduction of nitrobenzenes to aminobenzenes having reducible groups by a titanium (IV) oxide photocatalyst under gas-and metal-free conditions," *Chemical Communications*, vol. 48, no. 36, pp. 4356-4358, 2012.
- [71] A. Naldoni *et al.*, "Effect of nature and location of defects on bandgap narrowing in black TiO<sub>2</sub> nanoparticles," *Journal of the American Chemical Society*, vol. 134, no. 18, pp. 7600-7603, 2012.
- [72] H.-J. Choi and M. Kang, "Hydrogen production from methanol/water decomposition in a liquid photosystem using the anatase structure of Cu loaded TiO<sub>2</sub>," *International Journal of Hydrogen Energy*, vol. 32, no. 16, pp. 3841-3848, 2007.
- [73] H. Wang, Y. Li, X. Ba, L. Huang, and Y. Yu, "TiO<sub>2</sub> thin films with rutile phase prepared by DC magnetron co-sputtering at room temperature: Effect of Cu incorporation," *Applied Surface Science*, vol. 345, pp. 49-56, 2015.
- [74] W. Hui, S. Guodong, Z. Xiaoshu, Z. Wei, H. Lin, and Y. Ying, "In-situ synthesis of TiO<sub>2</sub> rutile/anatase heterostructure by DC magnetron sputtering at room temperature and thickness effect of outermost rutile layer on photocatalysis," *Journal of Environmental Sciences*, vol. 60, pp. 33-42, 2017.



จุฬาลงกรณ์มหาวิทยาลัย  
**CHULALONGKORN UNIVERSITY**

## VITA

**NAME** Nantiya Jantarasorn

**DATE OF BIRTH** 26 December 1993

**PLACE OF BIRTH** Rayong

**INSTITUTIONS ATTENDED** The Bachelor's Degree in Chemical Engineering from Department of Chemical Engineering, Faculty of Engineering, Burapha University, Chonburi, Thailand in June 2016.  
Master's Degree study in Chemical Engineering at Department of Chemical Engineering, Faculty of Engineering, Chulalongkorn University, Bangkok, Thailand in 2016 and cooperated with the center of excellence on catalysis and catalytic reaction engineering research group.

**HOME ADDRESS** 10/76 M.2, Noen Phra, Muang Rayong, Rayong, 21000